Study of the Cavity Wall Background in the SNO Detector

by

Matthieu Dayon

A thesis submitted to the Department of Physics and Astronomy

in conformity with the requirements for

the degree of Master of Science

Queen's University

Kingston, Ontario, Canada

September, 1999

To my parents

Abstract

The background signal produced by the cavity wall in the SNO cavity was calculated using the SNOMAN Monte Carlo program. The results obtained were compared with previously made calculations and measurements and were found to agree reasonably well in the high-energy region. A proposal for a set of two cavity wall calibration sources for the SNO detector follows this analysis. The proposed design consists of a thin walled (0.5 mm thick) cylindrical stainless steel canister, 2 feet tall and 4 inches in diameter filled with norite or shotcrete. A curium/lithium compact neutron source would be placed at its center. To permit the extraction of the undesired neutron capture gamma ray signal from the steel, a set of stainless steel covers would have to be made that could be slid over the existing canister wall. Such sources would produce signals that would be clearly detected by the SNO detector, making possible the measurement of the cavity wall background.

Acknowledgements

Over the course of my stay at Queen's, as a master student with SNO, I have had the good fortune to get in contact with scores of wonderful people, all of which I would like to thank. I will however only mention here those persons I have had closest relations with. First and foremost, I want to extend my most sincere thanks to my supervisor, Professor Barry Robertson, for his guidance, support and incites. I would also like to convey my gratitude to my colleagues who have, in uncountable occasions, helped me with research related and unrelated problems: Mark Boulay, Lorne Erhardt, André Hamer, Annie Hsu, Chris Jillings, Ed Korpach, Bryce Moffat, and, in his own special way, Paul Miyagawa. To all these very fine individuals, I send a thousand thanks.

Table of Contents

Vita 117

List of Tables

List of Figures

Chapter 1

Introduction

The Sudbury Neutrino Observatory (SNO) is what is generally called a second generation solar neutrino experiment. Its main purpose is to measure the flux of neutrinos generated by the fusion of boron (^{8}B) in the core of our Sun. Though this solar neutrino flux is very large, the weak nature of the interactions by which they can be observed makes them extremely difficult to detect and event rates are very low. This makes the SNO detector very vulnerable to background events. Neutrons and gamma rays from external sources are very likely to mimic a neutrino interaction if they find their way inside the detector. Amongst these backgrounds, the one produced by the surrounding wall is especially important because it can give birth to relatively high-energy gamma rays. It is most important to get a clear understanding of this external flux if solar neutrino information is to be extracted from this experiment. This thesis presents calculations estimating the strength of this wall background signal and explores the possibility of making a calibration source that could be used to measure it.

1.1 Neutrinos and Solar Neutrinos

Of all the fundamental particles that are known to exist, neutrinos are perhaps the most elusive ones. Our ignorance is mostly due to the fact that they only interact through the weak force, which makes them extremely hard to detect. Indeed, they were discovered only some 27 years ago, by Cowan and Reines [1], after Pauli [2] hypothesized their existence in a desperate attempt to save the law of conservation of energy in nuclear β-decay.

To this date, very little is known about these leptons. From a measurement of the Z^0-width, physicists have inferred that there should be in fact three flavors for neutrinos with mass below 45 GeV [3]. This agrees with the discovery of only three types of neutrinos, namely, the electron-neutrino (ν_e), the muon-neutrino (ν_μ) and the tau-neutrino (ν_τ). They are all included as part of the standard model of particle physics which treats them as massless particles with no magnetic moment. However the validity of such a statement is still unsure. Scores of experiments have tried to characterize neutrinos. Some kinematical tests include the study of β-decay, pion decay, and tau decay. Other experiments are investigating processes that the present standard model does not contain. They include the search for magnetic moments by looking at $\nu_e e \longrightarrow \nu_e e$ and $\nu_\mu e \longrightarrow \nu_\mu e$ scattering [4] [5], double β-decay, and neutrino oscillation. Detection of supernova neutrinos (SN1987) and atmospheric neutrinos (coming from the interaction of primary cosmic rays with the earth atmosphere) have also been of great value in understanding the physics of these particles. Until now, only upper limits have been found for neutrino magnetic moments and masses. However, the interest in neutrino physics has not ceased from increasing. This is due in part to the fact that understanding the neutrinos is fundamental to both elementary particle physics and astrophysics.

Neutrinos are of interest to the astrophysicists who try to understand the origin and destiny of our universe. Because they are so numerous, neutrinos, if they were to be even slightly massive, could account for some of the missing mass in our universe and play a major role in saying whether it will end in a "big crunch" or not. They also attract the attention of the astrophysicists interested in stellar evolution. Being produced at the heart of stars, and because they can escape it with minimal interaction, neutrinos can be used as probes to study the core of our Sun and verify our solar models. By turning this argument around, it should be possible to learn something about neutrinos, if the Sun's dynamic is well understood.

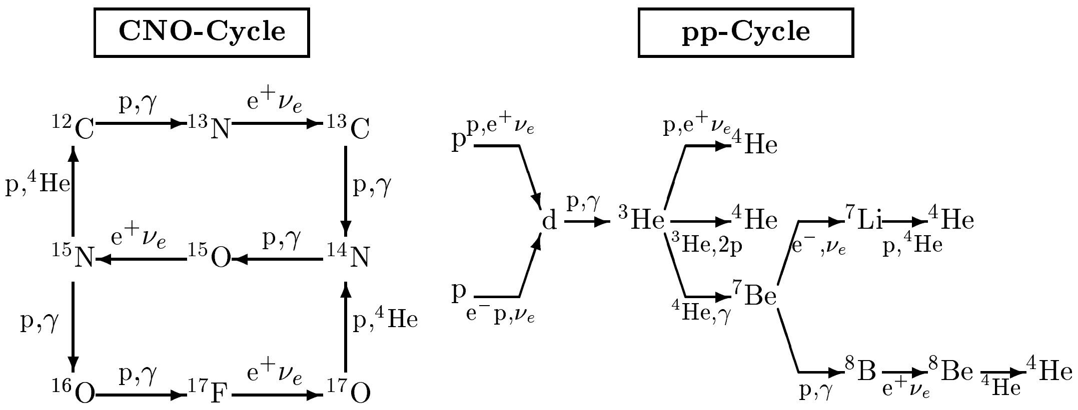

Figure 1.1: Energy generation in the Sun via pp and CNO cycles. The pp-chain dominates but generates less energetic neutrinos than the CNO cycle. On earth, the pp-neutrino flux averages around 6.0×10^{10} neutrinos per cm^2 per second while CNO neutrinos have a rate of about 1.0×10^9 neutrinos per cm^2 per second.

Very early in the history of nuclear physics, it had been realized that stars were getting their energy from nuclear fusions. A typical young star like our Sun would "burn" protons, *i.e.*, convert protons into ^{4}He nuclei (α-particles). This is done in two ways, the pp-chain and the carbon-nitrogen-oxygen (CNO) chain, as shown in figure 1.1. All the reactions are exothermic. The net result is the same for both pp- and CNO-cycles

$$4\ p \longrightarrow {}^4\mathrm{He} + 2\ \nu_e + 26.73\ \mathrm{MeV} \tag{1.1}$$

Because there is a shortage of heavier elements in young stars, the pp-chain dominates. Figure 1.2 shows a simplified layout of this chain of reactions with the neutrino energies associated with each step. It can be seen that most of the neutrinos produced come from the primary pp-reaction and have low energies (E$_\nu \leq 0.42$ MeV). Higher energy neutrinos come with much lower fluxes.

The internal dynamics of the Sun has been extensively studied. Because of the close proximity of the Sun to the Earth, precise measurements of solar parameters have been possible. Given the observed values for the Sun's age, radius, mass, geometry, luminosity spectrum, and surface chemical composition, it has been possible to develop a model of

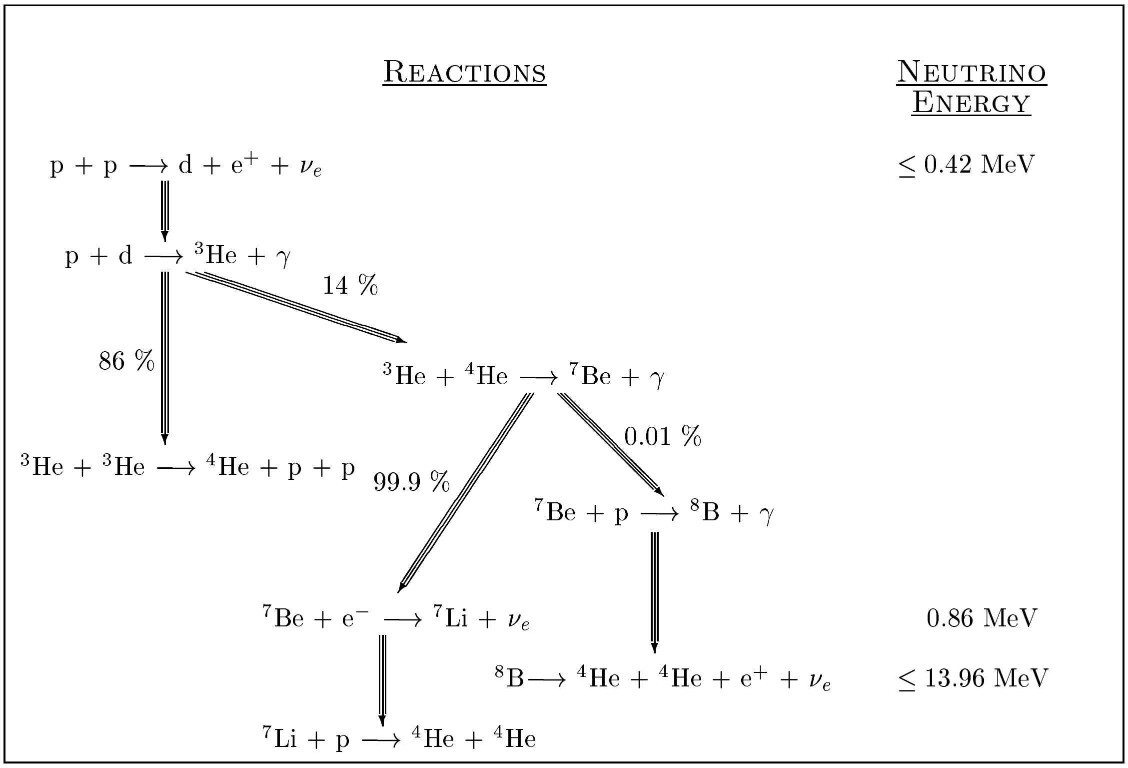

Figure 1.2: (Simplified) Chain reactions in the Sun with neutrino energies, rates and branching ratios. All the reactions shown have a positive Q-value.

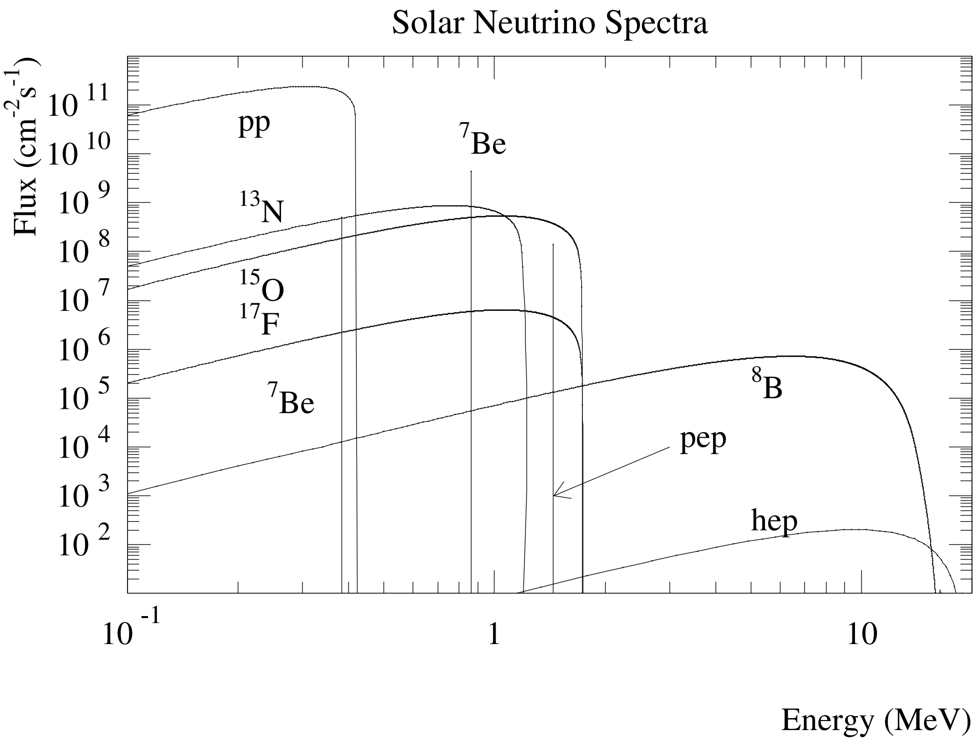

Figure 1.3: Solar neutrino flux spectra as a function of energy. The fluxes are at a distance of one astronomical unit from the Sun. The fluxes for the pep and ^{7}Be neutrinos are in units of cm^{-2}s^{-1}. The others are in units of cm^{-2}s^{-1}MeV^{-1}. This diagram is based on Figure 1.1 of Ref. [7]. The pep neutrinos shown on this figure come from the reaction $p+e^-+p \longrightarrow {}^2\mathrm{H}+\nu_e$ (a variant of the pp chain) while the hep neutrinos come from the reaction $^3\mathrm{He}+p \longrightarrow {}^4\mathrm{He}+e^+ + \nu_e$.

the interior of the Sun: the so-called standard solar model (SSM). It is driven by the basic equations of stellar evolution, namely, (i) mass conservation, (ii) hydrostatic equilibrium (gas and radiation pressure balance gravity), (iii) energy balance, and (iv) energy transport (mostly from radiation and convection). It is furthermore constrained by recent analyses of the sound speed profile in the solar interior obtained by helioseismological measurements [6]. However, some parameters are adjustable, and are cause for small uncertainties. Figure 1.3 gives the best estimate of what the neutrino flux from each reaction is on Earth.

1.2 Solar Neutrino Experiments to Date

At present, results from five neutrino experiments are available, namely the chlorine-experiment, the two gallium experiments, GALLEX and SAGE, and two water Čerenkov experiments, the Super-Kamiokande detector and its precursor, Kamiokande.

The Chlorine Experiment

The first solar neutrino experiment by R.Davis started in 1968 and is still running today [8] [9]. This landmark experiment, located in the Homestake mine in South Dakota, detects solar neutrinos with energies above 814 keV by the reaction

$$\nu_e + {}^{37}\mathrm{Cl} \longrightarrow e^- + {}^{37}\mathrm{Ar}. \tag{1.2}$$

This experiment consists of 615 tons of *perchloroethylene* (C_2Cl_4) under about 4000 meter water equivalent (m.w.e.) of shielding. Such a detector is mostly sensitive to ^{8}B and ^{7}Be neutrinos, with small contributions due to pep, ^{13}N and ^{15}O neutrinos. The unit for neutrino flux used in such an experiment is the SNU (Solar Neutrino Unit), defined as

$$1 \text{ SNU} = 10^{-36} \text{ captures per target per atom per second} \tag{1.3}$$

The averaged result is found to be [10]

$$2.55 \pm 0.25 \text{ SNU} \tag{1.4}$$

while theory predicts 7.7 $\pm$ 1.2 SNU [11]. This discrepancy is the origin of what is called the solar neutrino problem: fewer neutrinos are measured than what the theory predicts.

The Gallium Experiments

In order to understand better the details of this solar neutrino problem, two experiments were run using ^{71}Ga as the target material. These are GALLEX and SAGE. The reaction is

$$\nu_e + {}^{71}\mathrm{Ga} \longrightarrow e^- + {}^{71}\mathrm{Ge}. \tag{1.5}$$

which has a threshold of 233 keV, low enough to detect pp- neutrinos. GALLEX used 30 tons of gallium in a 110 ton $GaCl_3$ solution, while SAGE used 57 tons of metallic gallium. Both used different extraction techniques to count the ^{71}Ge nuclei produced, making their respective results totally independent. The results from these two experiments are [12] [13]

$$76.4 \pm 6.3 \text{ (stat.) } ^{+4.5}_{-4.9} \text{ (sys.)} \quad \text{SNU} \qquad \text{(GALLEX)} \tag{1.6}$$

$$66.6^{+6.8}_{-7.1} \text{ (stat.) } ^{+3.8}_{-4.0} \text{ (sys.)} \quad \text{SNU} \qquad \text{(SAGE)} \tag{1.7}$$

when the theoretical predictions are 137^{+8}_{-7} SNU [11]. Here again, observation is in disagreement with the theory. Although both results detect many fewer neutrinos than predicted by theory, they agree extremely well.

Real Time Water Čerenkov Detectors

The chlorine experiment and the two gallium experiments are radiochemical detectors. The observation of a neutrino interaction can only be deduced after counting the number of daughter nuclei produced (^{37}Ar or ^{71}Ge). For this reason, these three experiments cannot give any information other than the absolute flux of electron-neutrinos. The Super-Kamiokande detector, and its predecessor Kamiokande, are real-time detectors. They use water as a target for electron neutrinos. An interacting neutrino, elastically scattering off an electron, is detected by the Čerenkov light produced by the recoiling electron. This process can be detected in real time and energy and directional information can be obtained. Kamiokande used 3 kilotons of light water, with a fiducial volume (volume actually used to extract data) of 680 tons, while Super-Kamiokande consists of 50 kilotons of which 22.5 kilotons is used as fiducial volume. With a threshold of 6.5 MeV for Super-Kamiokande and 7.5 MeV for Kamiokande, these experiments are only sensitive to ^{8}B solar neutrinos. The measured fluxes are [14]

$$\Phi(^8\text{B}) = (2.80 \pm 0.19 \text{ (stat.) } \pm 0.33 \text{ (sys.)}) \times 10^6 \text{ cm}^{-2}\text{s}^{-1} \qquad \text{(Kamiokande)} \tag{1.8}$$

$$\Phi(^8\text{B}) = (2.44 \pm 0.06 \text{ (stat.) } ^{+0.09}_{-0.07} \text{ (sys.)}) \times 10^6 \text{ cm}^{-2}\text{s}^{-1} \qquad \text{(Super-Kamiokande)} \tag{1.9}$$

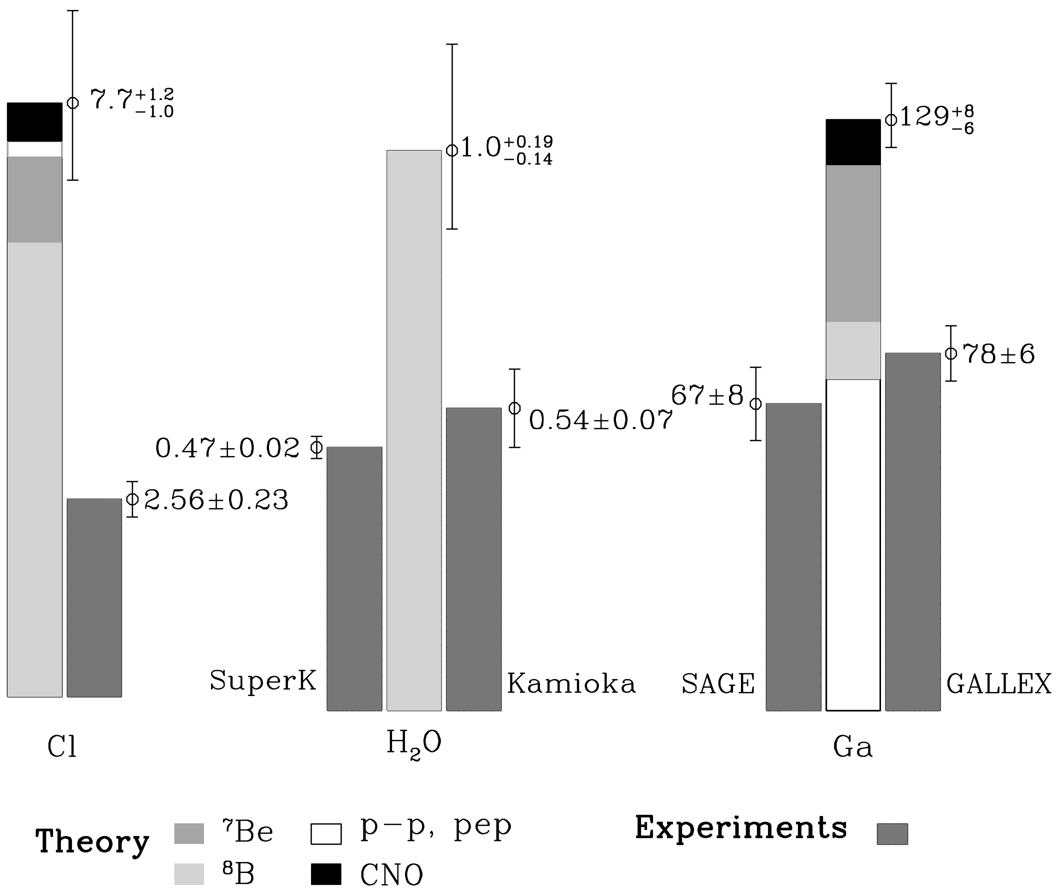

Figure 1.4: Solar neutrino fluxes observed by experiments and the detailed expected fluxes according to the standard solar model [11]. The theoretical and measured rates for the two radio-chemical experiments are expressed in SNU while the measured results of the two Kamiokande detectors are given as fractions of the predicted rate. (Taken from [15])

where the standard solar model calls for a flux of $(5.2 \pm 1.0) \times 10^6$ cm^{-2}s^{-1}.

A summary of the results from these experiments and their theoretical predictions is given in figure 1.4. This figure also shows what the contributing neutrino sources are expected to be.

1.3 Possible Solutions to the Solar Neutrino Problem

The discrepancy between the measured fluxes and the predictions of the standard solar model points to three subdivisions to the so-called solar neutrino problem. The first and original question was raised by the chlorine experiment which saw fewer neutrinos than expected. This was confirmed by the four other experiments. The second problem is found when a comparison of the observations from the chlorine experiment and the two water Čerenkov detectors is made. All three are primarily sensitive to ^{8}B solar neutrinos, yet the discrepancy between results and predictions is larger for the chlorine than it is for the other two experiments. This might suggest that the deficit depends somehow on the neutrino energy since the chlorine experiment detects neutrinos with energies as low as 0.8 MeV. Lastly, the measurements from the gallium experiments only leaves room for the predicted flux of pp- neutrinos, and could suggest a depletion of ^{7}Be neutrinos.

Astrophysical Solutions

In order to solve these problems, the first step is to look back at our model for the Sun and see if it can be corrected to account for the observations. For example, an option would be to assume a lower temperature for the Sun's core. This would have the effect of reducing the number of high energy neutrinos produced. This could solve the first solar neutrino problem. A reduction to 96 % of the BP standard solar model [11] value for the core temperature could explain the Super-Kamiokande results. However, it would increase both the ^{7}Be and pp-neutrino fluxes . As mentioned before in presenting the third solar neutrino problem, this goes against the results found by the two gallium experiments.

The model cannot simply try to totally suppress the amount of ^{7}Be in the Sun. The predictions for the presence of this element are very solid. Indeed, ^{7}Be is the only conceivable source of ^{8}B in the Sun, the same ^{8}B that is source to the neutrinos observed by the Kamiokande experiments.

The recently made helioseismological measurements, added to the already existing, well known, boundary conditions of the sun, highly constrain the solar models and prevent any major tinkering that could lead to an astrophysical solution to the problem.

Finally, it turns out that the second solar neutrino problem is independent of any solar model. There is no astrophysical scenario which could distort the ^{8}B neutrino spectrum to bring agreement to both chlorine and water Čerenkov experiments.

For this reason, physicists have turned their attention towards other explanations implying new physics.

Neutrino Oscillation

At the moment, the preferred solution lies in the idea of neutrino oscillation. It is a process by which a neutrino of a given flavor could "oscillate" and change into a neutrino of different flavor. This is similar to the CKM-mixing found in the quark sector. Such oscillations could occur either in vacuum or in matter (called the MSW-effect) [16] [17]. This would not affect the overall flux of neutrinos from the Sun but would change the relative amount of each neutrino type reaching the earth. An electron-neutrino born in the core of the Sun would "oscillate out" of the electron-flavor, making it undetectable by all five experiments. The MSW-effect is particularly attractive because its energy dependence could suppress the intermediate energy neutrinos completely, slightly reduce those with high energies, and leave the low energy ones unaffected. This means that it could explain the third solar neutrino problem by having all of the beryllium neutrinos change flavor. However, it should be said that this is a process that can only occur if neutrinos are to have a nonzero mass. This would also be a reaction in which the lepton number would change. These two points are going against the present hypothesis of the standard model of particle physics.

Other Solutions

Other solutions to the solar neutrino problem have been proposed. If neutrinos were to have a magnetic moment, a result similar to the MSW-effect would be seen and neutrinos would there again change flavor. Such a process also requires neutrinos to be massive. For this reason, such a spin-flavor induced precession could occur in addition to the MSW-effect.

1.4 Future Solar Neutrino Experiments

In order to distinguish between all the hypothesized solution and investigate more thoroughly the crucial ^{7}Be region, a series of new experiments are under construction or development that should shade light on the matter and help solve the solar neutrino problem.

Borexino

Borexino is an experiment that has been designed to investigate the region around 862 keV where ^{7}Be neutrinos are created. It consist of a 300 tons scintillator detector located in the Gran Sasso Laboratory in Italy (where GALLEX was situated as well). Neutrinos with energies above 450 keV will be detected by scattering off electrons. The expected rate is 50 events per day according to the standard solar model, or only 10 a day if the MSW-effect turns out to be existent. It should come into operation around 2001 [18].

ICARUS

The ICARUS proposal [19] [20] calls for the use of 5 kilotons of ultra-pure liquid argon to detect ^{8}B solar neutrinos through neutrino-electron scattering (at a threshold of about 5 MeV) and the reaction

$$\nu_e + {}^{40}\mathrm{Ar} \longrightarrow e^- + {}^{40}\mathrm{K}^* \tag{1.10}$$

(with a threshold of 5.9 MeV). The detector would be placed in the Gran Sasso Laboratory as well. In order to get such a large mass detector in place, the approach has been to consider building a series of 600-ton detectors installed next to one another. A proposal for a first module was recently approved. Working on principles similar to that of bubble chambers, it will be able to record with very high efficiency and spatial accuracy tracks left by any ionizing event. Still in its development phase, no definite time scale has been set for this experiment yet.

HELLAZ

HELLAZ [21] is a proposed experiment that would be able to detect pp-neutrinos in real time. It would consist of 6 tons of helium under high pressure at liquid nitrogen temperature under a pressure of 5 bars. Under these conditions some 2 $\times 10^{30}$ electrons will be present to serve as targets for the $\nu_x + e^- \longrightarrow \nu_x + e^-$ scattering reaction. The recoiling electrons identifying a neutrino interaction will be recorded by looking for the trail of ionization electrons produced. With this set up, HELLAZ would study an energy region dominated by the pp- and ^{7}Be neutrinos. Like ICARUS, HELLAZ is at a stage of development and research. While a test module is currently being used, it is not sure when the full scale experiment could start.

1.5 The Sudbury Neutrino Observatory

The Sudbury Neutrino Observatory (SNO) is a real-time solar neutrino experiment located in the Creighton Mine, near Sudbury, in Ontario [22] [23]. It consist of 1000 tons of heavy water viewed by 9522 light sensors. It detects neutrinos through three channels, one of which is flavor independent, and two of which are only sensitive to electron-neutrinos. From this comes its analytic power, as it will give a model independent test of the oscillation hypothesis. SNO should be able to distinguish between the different oscillation scenarios with a high confidence level. With a threshold around 5 MeV, ^{8}B neutrinos are observed. Data taking started in the second trimester of 1999.

Chapter 2

Neutrino Events and Backgrounds in SNO

Over the past fifteen years, a number of experimental particle physics projects needing low backgrounds have been built. They range from dark matter search to proton decay investigation, double-beta decay to muon physics experiments. In all cases, because of very low event rates, their practical feasibility relies critically on reducing to a minimum the external backgrounds. For this to be achieved, the detectors used in these projects have been buried deep underground and carefully designed to stay out of reach of the sources of undesirable signals. SNO is such an experiment. This chapter will first present the three reactions by which neutrinos are detected in SNO. This will then allow a description of the backgrounds to be made. The emphasis will be placed on those fluxes which are of external origin. In particular, the high-energy component of these signals will be highlighted. Such a discussion will be given at the same time as a careful description of the geometry of the detector and its shielding features.

2.1 Neutrino Detection

As mentioned in the introduction, the SNO detector will detect incoming neutrinos through three main channels, namely the weak neutral current (NC), the weak charged current (CC) and electron elastic scattering (ES). Figure 2.1 shows the Feynman diagrams for these reactions. A neutrino of any type can disintegrate the deuteron present in the heavy water through the neutral current reaction

$$\nu_x + d \longrightarrow p + n + \nu_x \qquad (Q = -2.22 \text{ MeV}). \tag{2.1}$$

The threshold for this reaction is 2.223 MeV. To be detected, the resulting neutron must be absorbed. One way this can happen is by having the neutron be moderated in the heavy water before being radiatively captured on deuterium, releasing a 6.25 MeV gamma ray. This gamma ray will Compton scatter an electron which in turn will produce Čerenkov light detected by the photomultiplier tubes (PMTs). Such a process has a relatively low efficiency (about 23%). To increase the number of detected events, 2500 kg of $MgCl_2$ could be added to the heavy water. Neutrons capturing on ^{35}Cl would liberate 8.6 MeV in the form of a cascade of gamma rays. This would bring the capture probability to 83%. An other option would be deploy in the vessel an array of ^3He proportional counters (called NCDs for Neutral Current Detectors). These would detect 45% of the neutrons produced by reaction 2.1. The decision whether to use the salt or the NCD technique (both mutually exclusive) has not been taken yet. The detector will likely be run with one and then the other.

The second channel for neutrino detection is through the weak charged current

$$\nu_e + d \longrightarrow p + p + e^- \qquad (Q = -1.44 \text{ MeV}). \tag{2.2}$$

These events will be detected through the Čerenkov light produced by the electron traveling in the water. It should be noted that this reaction is flavor-specific. Only the electron-type neutrinos will undergo this inverse β-decay on deuterium.

Finally, an incoming neutrino can scatter off an atomic electron present in the water

$$\nu_x + e^- \longrightarrow \nu_x + e^-. \tag{2.3}$$

Once again, the recoiling electron will be a source of detectable Čerenkov radiation. This is the reaction observed in light water detectors like Super-Kamiokande. The cross-section

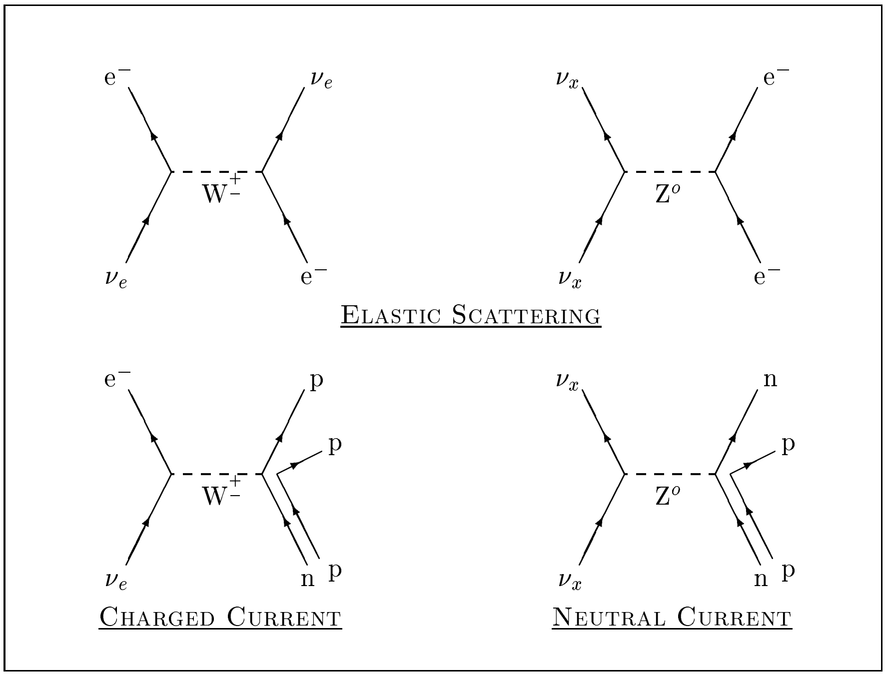

Figure 2.1: Feynman diagrams of the three reactions by which neutrinos are detected in SNO.

for this interaction is dependent on the neutrino energy, but there is no minimal energy threshold as such. It is the background levels that will set the effective threshold.

In a perfectly clean environment, it would be possible to detect Čerenkov photons from all CC and ES electrons. But in practice, one is limited by external signals producing light that the PMTs will detect. Figure 2.2 gives the signal expected to be measured by SNO in a year (in the case where salt has been added to the heavy water). Here, the horizontal axis represents the number of PMTs hit ("NHit") which is a representation of the energy released by the original interaction (the more energetic the scattering, the more Čerenkov photons will be emitted and the more PMTs will record light; this NHit to energy scale is a linear one). Also shown in the figure are the expected rates for the major backgrounds. Indeed, neutrino interactions are not the only processes able to cause PMT firing. Any reaction that can generate light should be investigated as a potential background signal that could be misinterpreted as being a neutrino event. Figure 2.2 shows that the three neutrino reactions are detected over a relatively wide energy range, starting with very few PMT hits. However, at low energies, these signals have to compete against others, undesirable but much stronger. This figure should make it clear that it is these backgrounds that will dictate what the threshold of the SNO detector will be. For this reason, maximum reduction of these non-neutrino fluxes has been a main concern in designing the detector.

2.2 SNO Shielding and Backgrounds

Ever since the SNO project's conceptual phase, it has been kept in mind that the reduction of background fluxes was the one most important factor that would dictate whether or not a neutrino flux measurement would be feasible or not. Indeed, due to the very low rate at which ^{8}B neutrinos are expected to be detected and because their energies will not go over 20 MeV, such a signal would be weaker, by several orders of magnitude, than the many signals from radioisotopes naturally present in ordinary laboratories. For this reason, the location, shape, and material composition of the detector have been the subject of careful

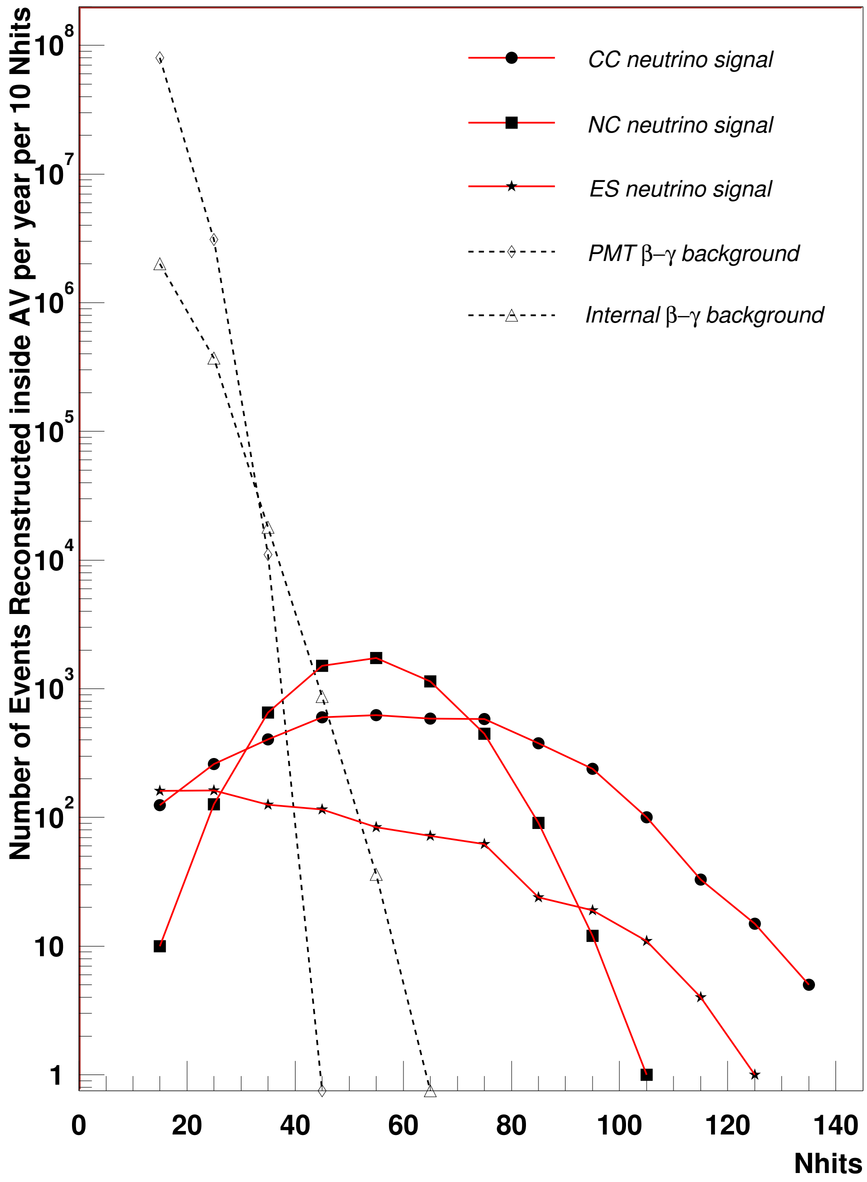

Figure 2.2: Backgrounds and Signals in the SNO Detector, reconstructed inside the D_2O per year per 10 NHits bin. The x-axis unit is NHits (the number of PMT hits). The CC energy spectrum assumes a neutrino flux equal to $1/3$ of the SSM value while the NC energy spectrum assumes the full SSM rate and salt has been added to the heavy water. The three neutrino spectra have been taken from [24]. The two β/γ backgrounds are from the more recent analysis found in [25].

selection.

2.2.1 Location and Geometry of the SNO detector

Stars and other astrophysical sources emit large amounts of highly energetic particles such as protons, electrons and helium nuclei. Some of these will impinge on the earth, enter the atmosphere and interact with air molecules, creating showers of secondary particles. The resulting radiation reaching the ground includes leptons and hadrons (protons and neutrons). Their flux at sea level is of the order of hundreds of particles per meter square per second. At these rates, any low activity experiment is inconceivable. To reduce these signals to an acceptable level, the detectors must be shielded. The hadronic component of the cosmic radiation can be eliminated easily with minimal protection. However, the leptons, mostly muons and neutrinos produced by the decay of charged mesons in the upper atmosphere, are much more penetrative and difficult to eliminate.

Atmospheric neutrinos typically have GeV energies making them easily distinguishable from their solar counterparts. They are also much less numerous. For these reasons, they do not really constitute a background to SNO. Cosmic ray muons however are more problematic and their flux can only be reduced by having them go through a massive layer of material, calling for an underground location for the experiment. A cavity has been excavated in the Creighton Mine, near Sudbury, Ontario, to house the SNO detector, some 1000 meters away from mining activity. Located 6800 feet under the surface of the earth (with shielding properties equivalent to 6000 meters of water), a count of less than a hundred cosmic rays a day is expected.

The heavy water (D_2O) that makes the core of the detector is contained in a spherical acrylic vessel (AV) crowned with an acrylic chimney. This assembly is immersed in light (ordinary) water. The Čerenkov light from the neutrino interactions will be recorded by an array of 9522 PMTs facing the D_2O region, and placed on a spherical support structure (PMT Support Structure or PSUP).

The vessel has a radius of 6 meters while the PMTs are located 8.5 meters from its center. The cavity itself is barrel-shaped with a waist diameter of 21.4 meters. The surrounding rock is norite, a rock very similar to granite in composition. The surface of the walls is covered with a fast setting concrete called shotcrete. A layer of about 15 centimeter of this material was spread. At the interface between shotcrete and water, there is an 8 millimeter thick polyurethane liner. Figure 2.3 shown a cross section of the SNO detector.

2.2.2 Internal and PMT Backgrounds

With the cosmic ray flux reduced to an acceptable level, the next problem to be addressed was that of radiation sources close to or within the D_2O. Various radioisotopes are found naturally in ordinary material. By generating gamma rays, alpha particles, neutrons or electrons, they can mimic the very neutrino interactions that SNO is trying to detect. The practicality of shielding against such events is limited. The main course of action is to get very high purity levels in the materials used in the detector. Through complex reverse osmosis and other techniques, the D_2O and H_2O placed in the detector are made extremely pure, making it possible to reach the very stringent requirements. In particular, for the D_2O, these design limits have been set to 4.5 $\times 10^{-14}$ g/g for U and 3 $\times 10^{-15}$ g/g for Th concentration [26].

Similarly, the acrylic, the salt additives and the ^{3}He neutron detectors had to be carefully treated so that they wouldn't be too important a source of radiation.

In the water as in all other materials, one of the processes most likely to occur and mimic a neutrino interaction is the so-called β/γ decay. Through this reaction, a radioisotope (mostly ^{214}Bi and ^{208}Th coming from the uranium and thorium decay chains) will β-decay to a daughter nuclei in an excited state which will almost immediately liberate, upon de-excitation, a gamma ray. The combined signals from these two particles could be recorded by SNO as coming from a single, more energetic event. Also, the gamma ray, if energetic enough, could photodisintegrate deuteron and thus become a background to the

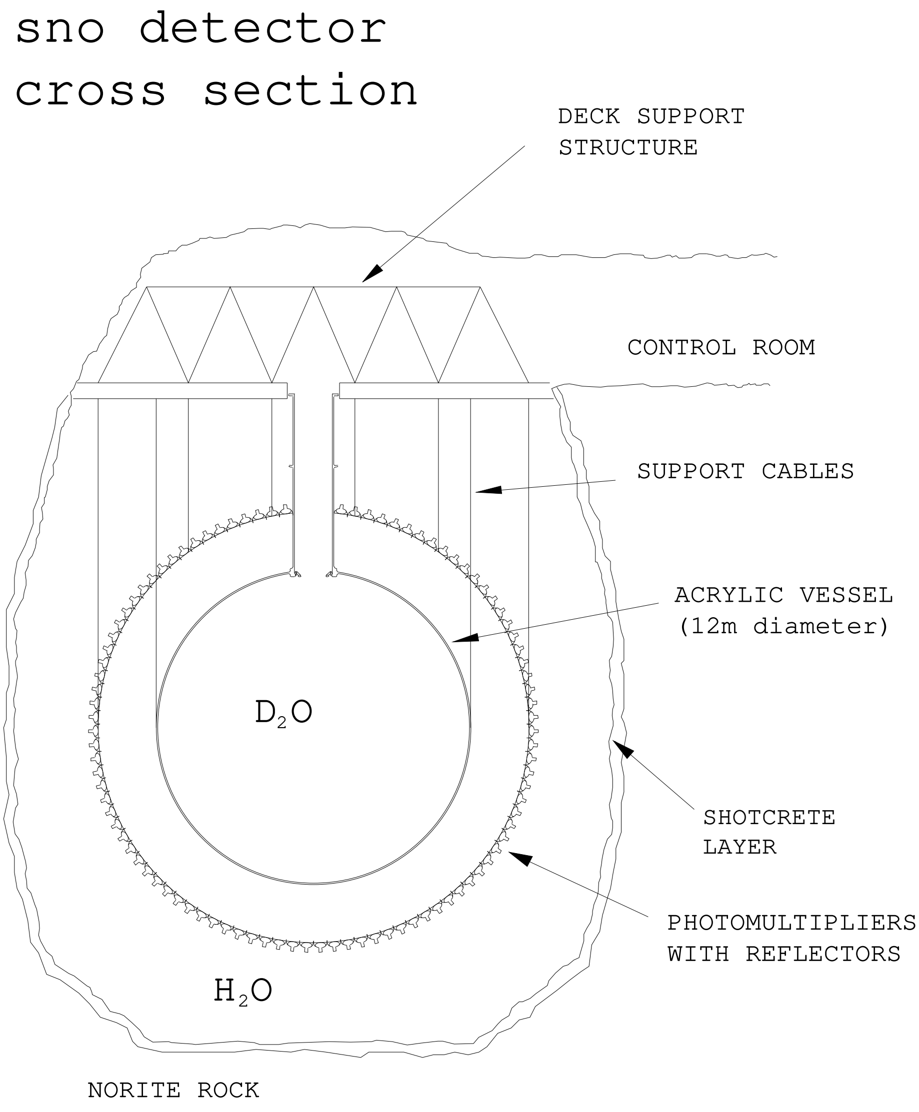

Figure 2.3: Cross Section of the SNO detector.

NC reaction.

Following the same guidelines of purity, the PMTs were specially manufactured. Schott Glaswerke produced for SNO a borosilicate glass with U and Th impurity levels of less than 40 ppb. Still, the PMTs had to be placed a safe distance away from the D_2O. The light water between the PSUP and the AV is used as a shield, stopping the electrons and attenuating the gamma rays before they reach the center of the detector.

Such careful design brings down to an acceptable level what would otherwise have been a background stronger than the actual signal to be measured. Figure 2.2 shows what the spectrum due to these PMT and internal β/γ backgrounds. At low energies their presence is still felt and they will make any measurement below approximately 6 MeV impossible.

2.2.3 Cavity Wall Background

An other background, not shown in figure 2.2, is that of the wall. This is the one on which the present work is focusing. Because the norite rock cannot be purified in the same way all the components of the detector could, it is a relatively strong source of radiation. By having a sufficiently thick shield these radiations can be attenuated before they get to the D_2O region.

Light Water and Shotcrete Shielding

Any radiation leaving the norite body will have to go through a significant amount of material before entering the inner region of the detector. Between the back of the PSUP and the wall, at waist level, there is more than a meter and a half of light water. Between, this water and the rock itself, some 15 cm of shotcrete provides some further radiation attenuation.

Water is a cheap and readily available. Also, as alluded to before, it can be purified to very high levels and therefore provide a "clean" shield. Fast neutrons are expected to leave the rock. These are most efficiently slowed down by materials containing hydrogen. This makes water one of the best neutron shields. Thanks to their water content, concretes make relatively good neutron shields too. The factor by which the neutron flux is attenuated is given by [27]

$$A_n = \exp\left(-\Sigma_R t\right) \tag{2.4}$$

where t is the shield thickness and Σ_R is the macroscopic removal cross section for the material in question. For water, Σ_R is 0.103 cm^{-1}, for concrete it is 0.092 cm^{-1}. For the present configuration with 1.5 meters of water and 15 centimeters of shotcrete, a total attenuation factor of 4.9×10^{-8} is found.

Calculations of the neutron flux from the wall in the SNO cavity, as well as some preliminary measurements, have been made. These will be presented in the next chapter. Sufficient for now is it to say that with these rates and the attenuation above, the number of neutrons entering the AV (and likely to be a background to the NC-signal) is negligible.

Once brought to thermal energies, the neutrons will most likely capture on hydrogen, thereby releasing a 2.223 MeV gamma ray. The shields should also effectively prevent any gamma ray from reaching the D_2O, should it be from rock origin or otherwise.

As gamma rays pass through matter, they interact in various ways, depending on their energy, with the atoms present in the material. At high energies, the main contribution to the cross section comes from Compton scattering and pair production. The strength of these two effects increase with the atomic number Z of the material. This is clearly understandable from the fact that the heavier the element, the more electrons it will have for the gamma ray to Compton interact with, and the stronger the magnetic field around the nucleus, causing pair production. For this reason, although hydrogen was an excellent moderator for neutrons, it will do poorly at attenuating gamma rays. The attenuation factor for gamma rays takes the form [28]

$$A_\gamma = \exp\left[-(\mu/\rho)(\rho t)\right] \tag{2.5}$$

where the quantity μ/ρ is called the mass attenuation coefficient and has units of cm^2/g. The parameter ρ is the density and t is the thickness of the shielding material. One therefore expects shotcrete, with its higher density, to provide a better barrier against gamma rays than water for the same pathlength of material.

The mass attenuation coefficient increases with decreasing energy: the lower the gamma ray energy the larger the cross-section and the stronger the attenuation. This says that a 2 MeV gamma ray starting in the wall at the boundary between norite and shotcrete will be attenuated by a factor of roughly 1/4 before entering the water and further attenuated by a factor of 7.6×10^{-6} before reaching the back of the PMTs.

Natural Radioactivity in the Rock

The rock is host to a variety of radioisotopes susceptible of generating radiation. However, only a handful of processes will give rise to these high energy gamma rays of interest to the present discussion.

By far, the most common way by which high energy gamma rays are produced is by the neutron capture process. This is an exothermic reaction in which a neutron is captured by a nucleus and where the binding energy is released in the form of one or more gamma rays. The cross-section for such a reaction is dependent on the energy of the incoming neutron: the faster it moves, the lower the chance of getting absorbed. For this reason, most of the captures occur for neutrons with thermal energies. Those with higher velocities will first lose their energy by scattering. However, such scattering processes, as well as the absorption reactions, will themselves be different from one target element to the next. Even the energy of the released gamma rays when radiative captures occur varies from nucleus to nucleus. For example, iron and manganese are two strong neutron absorber which lead to the emission of high energy gamma rays whereas oxygen and carbon will capture neutrons a thousand times less effectively and will never produce gamma rays with energies in excess of 4 MeV. A clear characterization of the neutron capture induced gamma ray spectrum in the wall therefore requires a very detailed knowledge of the elemental composition of norite and shotcrete. An in-depth study of how neutrons propagate is also needed given that, with their large diffusion length, these particles can migrate tens of centimeters before being captured. This geometry-dependent problem is a complex one which will be presented more thoroughly in the next chapter.

Every material contains traces of certain isotopes. Some of these isotopes, namely ^{238}U, ^{235}U and ^{232}Th, will produce neutrons by spontaneous fission. This channel is not the most important source of neutrons but is the the easiest to calculate. With its half-life of $T_{1/2}^{\mathrm{s.f.}} = 8.18 \times 10^{15}$ years, ^{238}U is the predominant contributor ($\mathrm{T}_{1/2}^{\mathrm{s.f.}} > 10^{21}$ years for ^{232}Th and $\mathrm{T}_{1/2}^{\mathrm{s.f.}} = 1.9 \times 10^{17}$ years for the low abundance ^{235}U). On average, 2.4 ± 0.2 neutrons are emitted per fission event [29] [30]. This translates into 3.72×10^5 neutrons per year per gram of uranium. The shape of the neutron energy spectrum follows very closely a Maxwellian distribution of the form [31]

$$N(E) = \text{Const.}\ \sqrt{E}\ \exp\left(-\frac{E}{\tau}\right). \tag{2.6}$$

Here the normalization constant would be 0.452 and the "temperature" τ would be 1.3 MeV.

But more important than fission, neutrons are created by α-particles. These helium nuclei which are generated when radioisotopes undergo α-decay are typically liberated with energies of a few MeV. They will collide with nuclei in the host material and some will have sufficient momentum to penetrate the coulomb barrier of the light elements. In most cases, this nuclear interaction will liberate a neutron. Depending on the energy of the α-particle and the abundance of light elements in the material, the neutron yield varies between 10^{-6} and 10^{-9} neutron per α-particle [32]. This very low rate of production is compensated by the large quantity of α-particles typically released, the final result being that more neutrons are produced in this way than by spontaneous fission of ^{238}U. Norite and shotcrete that are found in the wall will contain traces of certain isotopes among which ^{238}U and ^{232}Th. Both of these elements decay through the emission of α- and β-particles to lead as shown in figure 2.4. When the two chains are in secular equilibrium, eight α-particles are produced per ^{238}U decay and six are produced per ^{232}Th decay. Table 2.1 lists the α-particles with

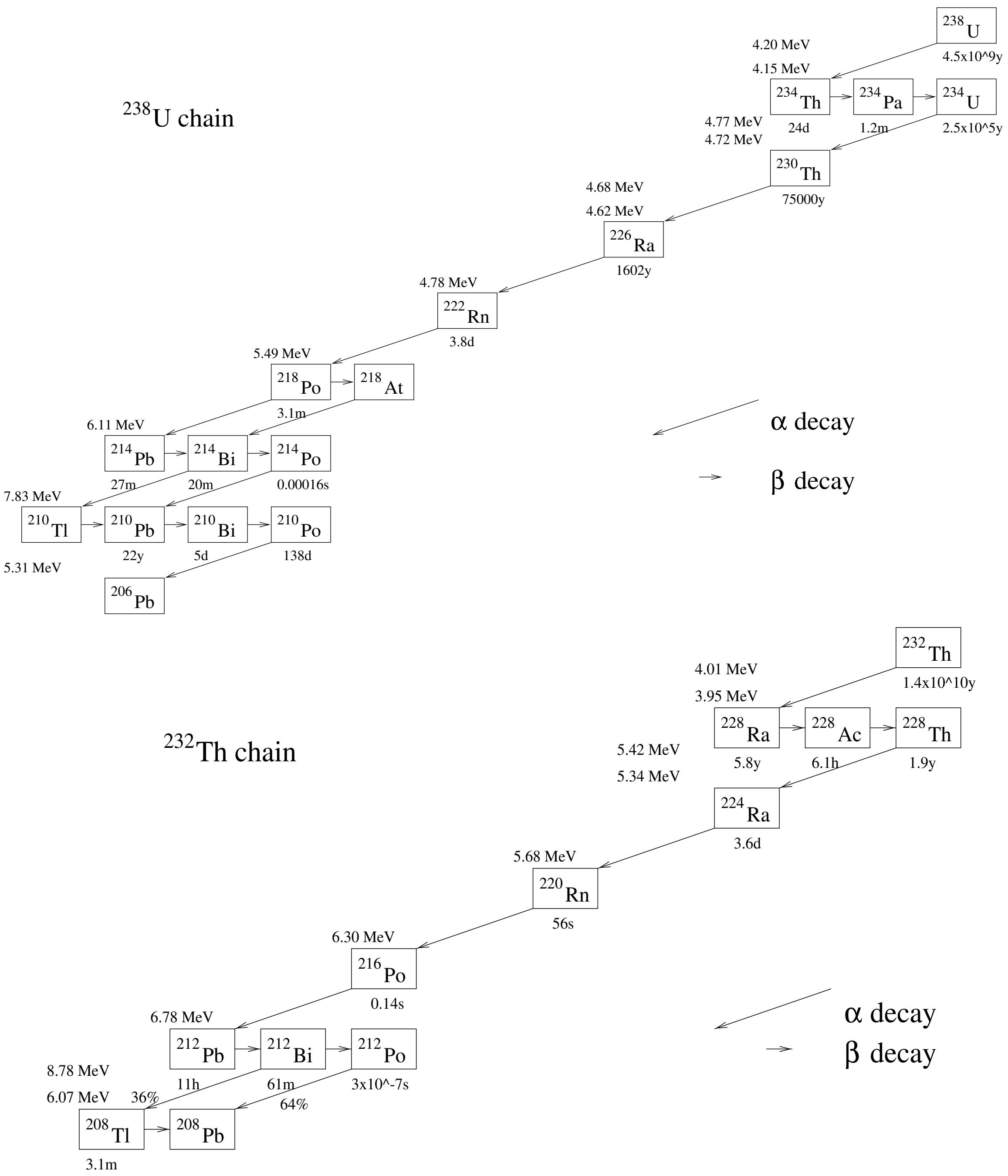

Figure 2.4: The Decay Chain for ^{238}U and ^{232}Th: these two radioactive elements decay through a series of α- and β-particle emissions to lead.

^{238}U Decay Chain			^{232}Th Decay Chain		
Nucleus	α-particle Energy (MeV)	Intensity per ^{248}U Decay	Nucleus	α-particle Energy (MeV)	Intensity per ^{232}Th Decay
^{238}U	4.196	0.77	^{232}Th	4.016	0.77
	4.149	0.23		3.957	0.23
^{234}U	4.777	0.725	^{228}Th	5.423	0.727
	4.724	0.275		5.341	0.267
				5.210	0.0036
^{230}Th	4.688	0.763		5.172	0.0018
	4.621	0.234			
			^{224}Ra	5.686	0.94
^{226}Ra	4.785	0.9445		5.449	0.0555
	4.602	0.0555			
			^{220}Rn	6.288	0.9993
^{222}Rn	5.490	0.999		5.747	0.0007
	4.987	0.001			
			^{216}Po	6.779	1.00
^{218}Po	6.003	1.000			
			^{212}Bi	6.090	0.0979
^{214}Po	7.687	0.9999		6.051	0.2516
	6.904	0.0001		5.769	0.0060
				5.625	0.0005
^{210}Po	5.305	1.000		5.607	0.0039
			^{212}Po	8.784	0.64

Table 2.1: ^{238}U and ^{232}Th Decay Chain α-Particles (taken from [34])

at least 0.01% emission probability. The α-decay half-life for ^{238}U is $T_{1/2} = 4.47 \times 10^9$ years, which is shorter compared to $T_{1/2} = 1.40 \times 10^{10}$ years of ^{232}Th [33]. However, the fact that higher-energies α-particles are produced by ^{232}Th and because, in most material, including norite and shotcrete, the concentration of ^{232}Th is greater than that of ^{238}U, the (α,n) yield of the two chains are comparable. These rates together with the radioactivity levels in norite and shotcrete are listed in table 2.2 and element by element details can be found in Appendix A.

The shape of the energy spectrum of the neutrons produced in this way depends on

Isotope	Norite		Shotcrete	
	Concentration (ppm)	Neutron production (n/y/cm^3)	Concentration (ppm)	Neutron production (n/y/cm^3)
Th	5.10	8.13	2.4	0.99
U	1.10	3.51	1.2	1.05
U-fission		1.19		1.03
Total		12.83		3.07

Table 2.2: Radioactivity levels and neutron production rates in the wall due to uranium and thorium decay chains

both the composition and the ^{238}U and ^{232}Th contamination of the material. By using a thick target neutron yield model and solving the kinematic of the three body problem using a method developed by Hess [35], Heaton calculated this spectrum for norite and various types of concretes [32]. This work was performed as part of the preliminary research and development effort put in place at the time the SNO project was proposed and relied on information available then. Measurements of norite rock samples have shown an average concentrations of 1.2 ppm uranium and 3.3 ppm of thorium. The concentration of these two isotopes in the norite rock was later measured by direct gamma counting [36]. New values of (1.10 $\pm$ 0.09) ppm uranium and (5.10 $\pm$ 0.48) ppm thorium were found. It is expected that these new proportions will have an effect on the shape of the neutron spectrum. The thorium chain produces more energetic α-particles than uranium which in turn will likely create more energetic neutrons through (α,n) reactions. However, because the repercussion this would have on the spectral shape will not be very profound, the lengthy calculations performed by Heaton were not repeated for the new concentrations. The neutron energy spectrum found for the old values of uranium and thorium concentration were scaled to meet the new levels. To this was added the spontaneous fission contribution to get the total neutron energy spectrum for norite which was used in the calculations presented in this thesis. It is shown in figure 2.5.

The radioactivity contamination in shotcrete was also measured by direct gamma counting [37], from samples collected at various heights. For this shielding material, concentrations of (1.188 $\pm$ 0.034) ppm uranium and (2.39 $\pm$ 0.13) ppm thorium were found. Though less active than norite, it will also produce some neutrons. Shotcrete itself was not among the concretes studied by Heaton. However, by comparing the results found for other shielding materials, and from composition arguments, it has been possible to construct the energy spectrum for neutrons produced in shotcrete, again, without going through the calculations done before by Heaton. This spectrum, which includes the spontaneous fission component, is shown in figure 2.6. The shape difference between the spectrum of figures 2.5 and 2.6 can be explained mostly from an elemental composition difference. The high-energy tail appearing for norite and absent from the shotcrete spectrum can be explained by the magnesium content of each material. One of magnesium isotopes, ^{25}Mg (with a 10% natural abundance), has a significantly positive Q-value which will allow the release of neutrons with energies above 6 MeV. Norite contains about 3% (weight) of magnesium while shotcrete has less than 0.1%.

The polyurethane liner will produce virtually no neutrons. Its contamination levels were measured at the Ultra Low Background detector at the University of Guelph to be less than 0.003 ppm uranium and less than 0.009 ppm thorium [38].

Although the result of an α-particle colliding with a light element nucleus will most likely be the liberation of a neutron, there are other possible channels that need to be investigated. The (α,p) reaction where a proton is expelled instead of a neutron is of little interest to the present discussion. Much more relevant are the (α,nγ) and (α,pγ) processes. These occur when the collision brings the daughter nucleus into an excited state which it will leave, thus getting to the ground-state, by emitting a gamma ray. A good understanding of the rates at which such reactions take place is crucial since this could turn out to be a significant source of high-energy gamma rays. This point was first raised by Pomansky [39], who estimated that the rate and energies of gamma rays produced in this way could be comparable to that

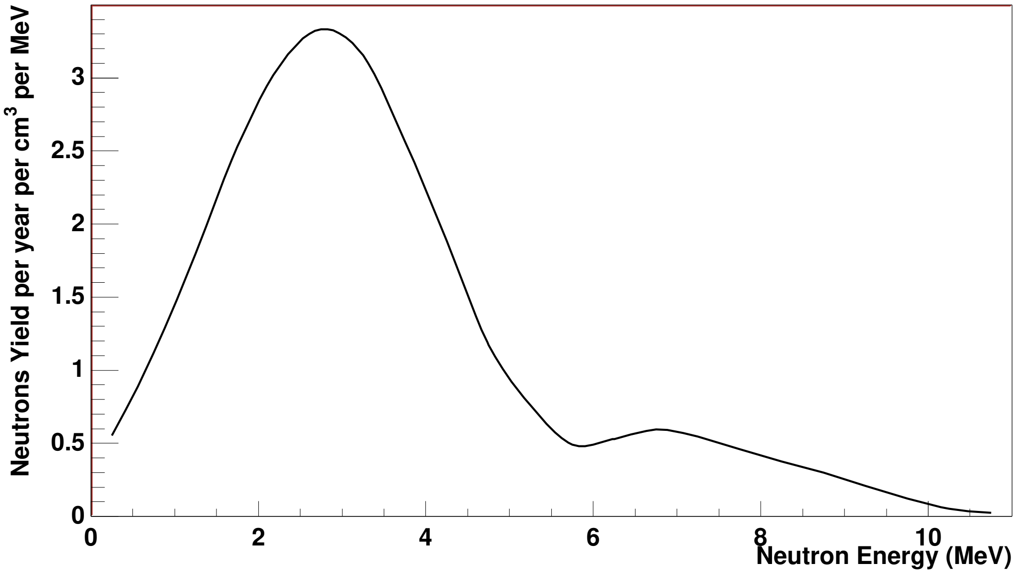

Figure 2.5: Calculated Neutron Spectrum for Norite (for 1.1 ppm ^{238}U and 5.1 ppm ^{232}Th but using the spectral shape found for concentrations of 1.1 ppm ^{238}U and 3.3 ppm ^{232}Th).

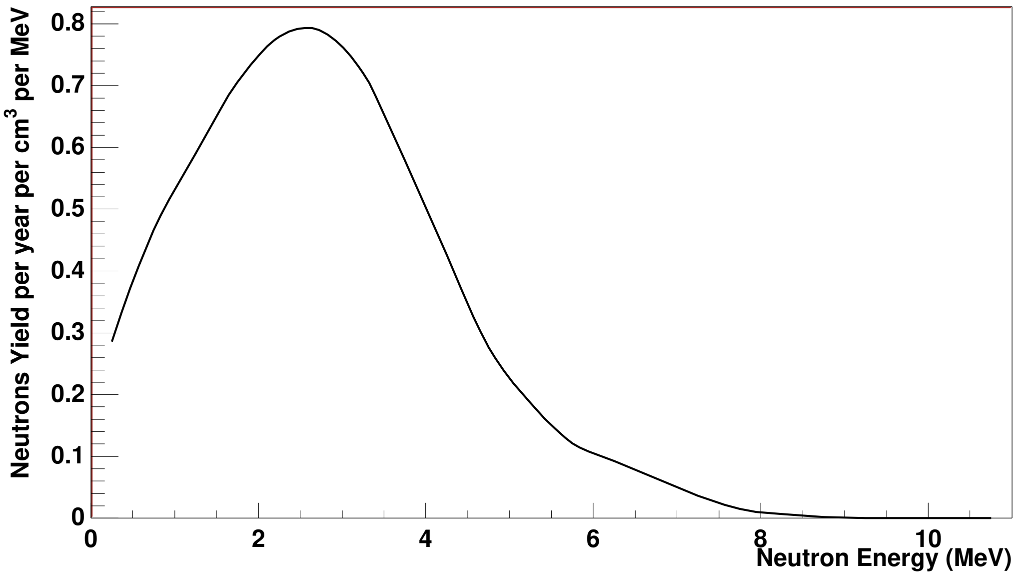

Figure 2.6: Neutron Spectrum for Shotcrete (with 1.2 ppm ^{238}U and 2.4 ppm ^{232}Th).

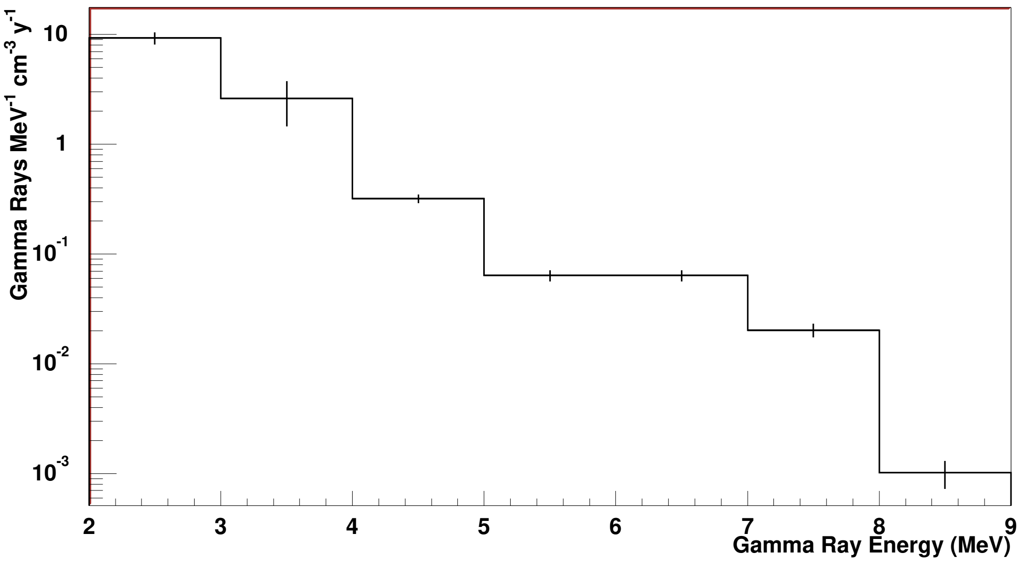

Figure 2.7: Direct α-induced gamma ray spectrum in norite constructed by Heaton [40] for 1.13 ppm ^{238}U and 5.35 ppm ^{232}Th concentrations.

from neutron captures in underground environment. This theoretical prediction has been investigated by Heaton [40], who constructed the direct gamma ray spectrum for granite and norite from measurements of α-induced thick-target gamma ray yields. The granite results found are far below what Pomansky predicted. Figure 2.7 shows this spectrum in norite.

The spontaneous fission process mentioned previously is accompanied by the generation of several gamma rays. These however are very weak. The average energy of these particles is around 1 MeV and the total energy liberated in this way per fission is approximately 8 MeV [41]. The chances of producing a 4 MeV gamma ray are less than a percent. Given a rate of 0.50 spontaneous fission per gram per year in norite, such a source of gamma rays turns out to be a full order of magnitude weaker than the direct α-induced gamma ray flux presented above and can therefore be safely omitted from the present analysis.

2.2.4 Cosmic Ray Background

With a detector as "clean" as SNO, where every material used in the construction was tested for purity and low radioactivity levels, the sources of background that were originally the weakest are likely to take on a prominent role. In looking for high energy gamma ray sources attention should be turned back to these cosmic rays against which the SNO detector was said to be so well shielded. Because of the fact that these cosmic rays are so energetic, the few that do pass through the cavity or near it could become a major background of their own.

For SNO, the overburden is mostly composed of norite rock having a density ranging from 2.8 to 3.0 g/cm^3. If one assumes an average density of 2.9 g/cm^3 for the rock and does not take into account the presence of ore bodies in various location, which may have very different properties [42], nor the presence of mine drifts, SNO is found to be located at a depth of 6000 m.w.e., making it one of the deepest laboratory in the world. A semi-empirical formula has been found that gives the flux of cosmic ray muons in an underground location as a function of depth [43]. Applied to SNO, it predicts a rate of 72 ± 5.8 muons per day entering the PSUP. Of these, half will enter the D_2O region. From the data collected to this day by SNO, a preliminary rate of 72.6 ± 3.6 muons per day has been found [44].

As a cosmic ray muon passes through the rock, the detector or the shielding, it may inelastically scatter with atoms and lead to the production of a variety of particles, such as pions, neutrons, gamma and beta rays, or radioactive nuclei. If such a production occurs within the PSUP, passage of the muon will leave a characteristic PMT hit pattern. If the track passes within the water of the outer volume, outward looking PMTs (OWLs) will record its presence. In many cases this will be used to veto events that will immediately follow and could be interpreted as background from a spallation product. It is expected that a muon-^{16}O collision will generate such radioactive nuclei as ^{8}B, ^{12}B and ^{12}N which are high-energy β-emitters (13 to 16 MeV endpoint energies) [22]. Because of their relatively short half-lives, ranging between 10 and 800 ms, these should be identified with a high efficiency and should not be cause of concern.

For these interactions that do not occur within the detector, but in the rock surrounding it, the option of vetoing out cosmic ray-induced background could become virtually impossible. However, the remote location at which these reactions would take place would call for the spallation products to travel through a thick shielding before reaching the core of the detector. The main concern is with neutrons. With their multi-GeV energies, the cosmic ray muons can produce extremely fast neutrons. The cross-section for such a reaction in rock is known [45] and can be used to get an estimate of its rate at the SNO depth. Radcliffe calculated that some 5×10^{-14} neutrons/(g s) would be produced in the rock [46]. Because these neutrons are created with extremely high energies, some will be able to get through the detector's shielding and into the D_2O region. Radcliffe's calculations forecast a mere 0.5 to 40 neutrons per year at the acrylic vessel.

As very energetic muons pass through the rock they will also produce bremsstrahlung radiations, gamma rays that could enter the detector. Very little investigation has been done on this particular question. Only a preliminary analysis has been done on the subject for the case of an air filled detector. However, because some of the gamma rays will have energies in the range of hundreds of MeV, these could account for an additional background of its own.

Chapter 3

Understanding the Cavity Wall Background

With a clear understanding of how background events are generated, calculations can be performed which will provide estimates of how much these will affect the ability of SNO to measure the solar neutrino flux. It is expected that virtually all the background signals originating from the cavity wall will be due to gamma rays produced in norite and shotcrete. The rate at which gamma rays are produced is established by how many neutrons and α-particles are created and how they move and interact in the various materials. By considering all this information, and armed with the right instruments, one should be able to make predictions about the gamma ray flux coming from the wall. Back in the days when SNO was on the drawing board, such calculations were already being made. Later, following changes from the original design and the acquisition of new information, Skensved and Robertson [24], using Monte Carlo computations, estimated the strength of various background signals including that of the cavity wall. This work was done in 1994, at a time when the detector was being assembled. Five years later, SNO is finished building, and data taking has started. At this point, a detailed estimate of the wall background's spectral shape is needed. Various computational tools were considered to do this analysis. The two most promising ones are presented in section 3.1 of this chapter. Following this introduction, this section describes the analysis performed, presents the results obtained, and provides a comparison with previous estimates and measurements.

3.1 Available Tools

Making predictions about the flux of gamma rays from the rock relies for the most part on understanding where neutrons are captured. Much information about the production rate and energy of these particles was worked out by Heaton, as presented in chapter 2. With these available, attention was focused towards understanding the transport and capture of neutrons traveling through the various materials in the wall. A choice had to be made as to the technique that would be used for this analysis. The neutron diffusion theory, and the random statistical sampling method, commonly known as the Monte Carlo technique, are two instruments that could address the issues at hand.

3.1.1 The Diffusion Theory

The diffusion theory relies on solving the diffusion equation found in many areas of physics. This equation is based on Fick's law which was originally used to describe the change in concentration of a solution in chemistry. Applied here, it states that neutrons will flow out of high neutron density regions into areas of low density. By substituting Fick's law into an equation of continuity, the diffusion equation of the form

$$D\nabla^2\phi - \Sigma_a\phi + S = \frac{1}{v}\frac{\partial\phi}{\partial t} \tag{3.1}$$

is obtained, where D is a medium-dependent parameter called the diffusion coefficient. The parameter Σ_a is the neutron macroscopic absorption cross section (which may vary with position), ϕ is the neutron flux (in neutrons/cm^2 s), v is the neutron speed and S the source term describing the rate and position of neutron production. Equation 3.1 can only be used with a constant v (monoenergetic neutrons). In the present case, the neutrons studied are very energetic and will lose their energy through scattering to be brought to thermal energies. This is a highly polyenergetic problem that can only be addressed by a series of these equations laid side by side, each dealing with neutrons from a certain energy group. This is the idea behind the group diffusion method. Such a technique will modify Equation 3.1 to account for neutrons transferring from one energy group to an other. The new diffusion equation for the g^{th} group, assuming a total of N such group, would look like

$$D_g \nabla^2 \phi_g - \Sigma_{ag}\phi_g + S_g - \sum_{h=g+1}^{N} \Sigma_{g\to h}\ \phi_g + \sum_{j=1}^{g-1} \Sigma_{j\to g}\ \phi_g = \frac{1}{v_g}\frac{\partial \phi_g}{\partial t} \tag{3.2}$$

where $\Sigma_{g\to h}$ and $\Sigma_{j\to g}$ are called the group transfer cross-sections and are a measure of how much neutrons, through scattering collisions, are transfered from one group to an other.

Even for the time-independent scenario, where the right-hand side could be simplified to be zero, the diffusion equation turns out to be a complicated one. Very few geometries will admit an analytical solution. Also, because of the three-dimensional nature of the problem, equation 3.1 should in fact be looked at as being three separate equations. The problem is made even more complex with the introduction of the group diffusion method; the more energy groups one uses to do the analysis, the more equations have to be solved. Finally, the various parameters that need to be supplied in these equations have to be constructed from experimental data. Because this analytic tool has been used extensively in designing nuclear reactor, parameters for materials such as plutonium, uranium, beryllium, and a few others can be found in the literature [47]; however, no accurate numbers are available for norite or shotcrete.

3.1.2 The Monte Carlo Method

A significantly different approach to the problem would be to use the Monte Carlo method. By modeling a physical system by a finite number of events, also called "histories", it is possible to get insights as to the behavior of that system. In the present case, this technique would consist of looking at the histories of neutrons, starting with their generation at a source point and ending with their capture. In the event of radiative captures, modeling could extend to the propagation of the generated gamma rays. By studying a statistically significant number of such histories taking place in a geometry similar to that of the wall, it would be possible to simulate the gamma ray and neutron fluxes coming out of the cavity walls. If random statistical sampling is to be used, the physical processes described has to be well understood. Scattering and capture cross-sections for neutrons as a function of energy have been measured experimentally for virtually all the elements of the periodic table [48]. This provides a firm basis on which neutron transport and interactions can be calculated.

Because a large number of histories needs to be generated to get a statistically significant sample, the Monte Carlo method turns out to be very computationally demanding. In the past, this proved to be a primary limitation, but modern-day computers have become fast enough to conceivably generate millions of histories in reasonable amounts of time. However, even with that many events being generated, this may still not give statistically meaningful information about very rare outcomes. Large uncertainties are to be expected for such candidates [49]. This should be borne in mind whenever the Monte Carlo technique is to be used.

This random statistical sampling method was developed with the advent of the first computers during the second world war. Ever since, its use has been steadily increasing. It is now widely used in far-ranging fields of science, in particular in nuclear and particle physics. These two disciplines perform experiments which have grown so complex that the Monte Carlo approach is required to bring meaning to the data they generate. By comparing simulated results and actual measurements, physicists look for inconsistencies which would imply new physics. The SNO experiments also works along these lines. A computer program called SNOMAN (for SNO Monte carlo and ANalysis) has been written by the collaboration to address this reality [50].

3.1.3 SNOMAN

Given the complexity of the SNO detector, it is not surprising to find its associated Monte Carlo code to be a large and intricate construct. Since its birth in 1991 [51], SNOMAN has not ceased to grow. It was designed to simulate the behavior of the detector to various classes of signals including solar neutrinos, calibration sources and backgrounds. Every signal in SNO can be pictured as a series of interactions and particle motions. These, called respectively vertices and tracks in the Monte Carlo jargon, need to be modeled accurately if any reliable information is to come out of this computer program. SNOMAN was designed to simulate such transport and interaction stages for photons (and gamma rays), electrons (and positrons), muons, neutrinos and neutrons. However, no framework has been put in place to deal with α-particles. Though these particles indirectly play a most important role in the gamma ray generation processes in the wall, their absence from the Monte Carlo program is not detrimental. As mentioned before, by making use of Heaton's work, SNOMAN could be used as a tool to study the behavior of the neutrons and gamma rays they generate.

The algorithms and data tables used to model neutron transport were taken from the well-known MCNP (Monte Carlo N-Particle) transport code developed at the Los Alamos National Laboratory [52]. Over the energy range from 10^{-5} eV to 20 MeV, the most likely neutron interactions, (n,n), (n,2n), (n,3n), (n,γ), (n,α) or (n,fission), to name but a few, are typically covered. When a particle that SNOMAN doesn't know how to transport is generated by neutron collision (α-particles, fission products, etc.), it is simply recorded as having been produced. More problematic is the subject of gamma rays created by radiative capture. The program needs to be provided with data tables stating the probabilities and energies with which these particles will come out. Until recently, SNOMAN only simulated outgoing gamma rays for (n,γ) reaction taking place on ^{1}H, ^{2}H, ^{35}Cl, ^{58}Ni, ^{60}Ni or ^{62}Ni target nuclei. This sample proved to be sufficient to simulate events taking place inside the heavy water. However, in order to use SNOMAN to study the neutron capture in the rock and the shielding, additional routines had to be written to accommodate additional targets. This task was performed by McGregor who provided the code with the capacity for dealing with radiative captures of some twenty new isotopes [53].

With SNOMAN already existing, especially with its latest improvement in terms of neutron radiative capture, but also because of its versatility, it was felt that the Monte Carlo technique would prove to be a more powerful tool than the neutron diffusion theory. It was therefore used intensively in studying background generation processes in the wall. The results presented in this thesis were found using version 3.0185 of SNOMAN, with the added custom routines mentioned above.

3.2 Modeling the Wall

3.2.1 Geometry

To determining the number of gamma rays entering the D_2O region, one must first of all get an estimate of the flux leaving the wall. This can be found by modeling the wall in the Monte Carlo environment. SNOMAN is defined with a strict geometry, that of the detector. It also allows for certain elements, like calibration sources and NCDs, to be placed in certain regions. A certain medium is attributed to every part of the detector: acrylic for the vessel, glass for the PMT envelope, and so on. With a set geometry and material composition, the program can simulate the propagation and interaction of particles in this virtual detector.

The SNOMAN code is in constant evolution. When this study started, the geometry of the wall was improperly defined as being a bare norite wall. This was in no way problematic for studies done on the physics going on inside the core of the detector (solar neutrino flux simulations for example). But, for the present work, an alternative had to be found. The wall structure was modeled by creating a new "calibration source"-type element for the detector. Limited to simple geometries, a cylinder, 3 meters in radius, was used. Placed at the center of the detector, it was made of three layers parallel to the bases. The first one, norite, was some 8 meters thick. The second, shotcrete, was made 15 cm thick. And finally, the top layer consisted of a thin sheet of 8 mm of polyurethane. The actual wall surface is uneven and slightly curved, but it was assumed that taking flat walls as a model would prove to be a sufficiently good approximation.

This geometry does not simulate every constituent making up the wall. An important omission was the steel structure inside the wall. While the cavity was being excavated, 3 meter long steel bars called reenforcement bars were forced inside the norite wall to hold in place a steel mesh that covered the whole surface. This technique extensively used in mines keeps rubble from falling off and relieves some of the strain applied on the wall. These were not removed when the shotcrete layer was sprayed on. Though this frame only constitute a small fraction of the wall surface, it could play a role in the production of high-energy gamma ray. This is because steel is made of elements like iron, nickel, chromium and manganese, all of which have a high probability of emitting high-energy gamma rays upon neutron capture.

Building a complex steel meshing geometry inside the cylindrical structure described above was not feasible. However, placing a fourth layer, 4 mm thick, between the rock and the concrete was possible. The idea followed was to weight the results from Monte Carlo runs done with that extra steel thickness and runs done without. Nothing could be done easily however to account for the reenforcement bars but increase the volume of the mesh to account for that part of these bars located in the shotcrete. An effective steel coverage of 5% of the surface of the wall was used as the ratio.

The cavity was excavated in the shape of a barrel. But the surface was left very uneven, with bumps and depressions reaching sometimes a few tens of centimeters. When this surface was covered with shotcrete, irregularities were filled to provide a smoother wall with protuberances averaging at most a dozen of centimeters. This implied putting more shotcrete in some region than others. The 15 cm of concrete used in the model was an estimate of the effective average thickness. In order to put some error limits on such a simulation, two other wall models were simulated. One included only 10 cm of shotcrete while the other had 20 cm of shotcrete.

In all cases, to isolate these wall-like blocks from the influence of any other elements, the media assigned to every other parts of the detector were all changed to water or air, depending whether water-fill or air-fill configuration was studied.

3.2.2 Neutron Production

Simulations of (n,γ) reactions were started with the generation of neutrons in shotcrete and norite. Events taking place very deep inside the rock should have no influence over the actual neutron and gamma ray fluxes entering the cavity. Indeed, in the rock, a neutron with a few MeV of energy will migrate on average a mere 10 cm before reaching thermal velocities. Such a neutron will then travel half a meter to a meter, on average, before getting captured. For this reason, only reactions taking place in the first 2.5 meters of rock were modeled. Similarly, because the gamma ray attenuation length in the rock is on the order of 5 to 14 cm (depending on energy), this approach was also used in simulating direct α-induced gamma ray.

The neutron production rates described in section 2.2.3 were used in the Monte Carlo simulations. For each run, the fate of every neutron was recorded. Those getting radiatively captured triggered the release of gamma rays that would in turn be tracked. By identifying which of them reached the surface, the gamma ray flux coming out of the wall was obtained.

3.2.3 Direct Gamma Ray Production

Gamma rays from direct α-capture were also simulated. Gamma rays were created in the norite according to the spectrum constructed by Heaton and shown previously in figure 2.7. These rates were calculated for concentrations of 1.13 ppm ^{238}U and 5.35 ppm ^{232}Th. These contamination levels are on the order of 5% above the numbers presented in table 2.2. Results presented later will in fact show that this slight over-estimation will not be noticeable and that these direct α-induced gamma rays contribute only to second order to the overall flux from the wall. Because the spectrum for this channel in shotcrete has never been calculated, no modeling of (α,nγ) or (α,pγ) gamma rays have been included in the simulation of the concrete shielding. Given that the results found for norite, and because, from a compositional point of view shotcrete is expected to produce fewer such gamma rays than the rock, this omission will again prove to be of no significant effect.

3.3 Results

Once this framework was properly set and the neutron and gamma ray production rates were established, numerical computation was left to SNOMAN and results were reaped.

3.3.1 Neutron Flux

The first information provided by the simulation was the detail of where neutrons are captured. Investigating where neutrons, which started in the wall, end their journeys gives what is called the neutron capture density, in units of neutrons per year per cm^3. This quantity is plotted as a function of location in the wall or the water with a linear scale in figures 3.1 and with a logarithmic scale in figure 3.2. The x-axis of these plots represents the relative position within the water or block used in the simulation. The $x = 400$ cm line indicates the position of the polyurethane liner between the wall and the water, while the line at $x = 385$ cm denotes where the norite-shotcrete interface (and the steel mesh) was located.

Figure 3.1 reveals information on what happens to neutrons. Though they are uniformly produced inside norite ($x < 385$ on the graph), neutrons are seen to capture with a varying density depending on the depth. This feature is due to the geometry of the wall. This also explains the non-uniformity of capture in shotcrete. Peaks can be noticed at both shotcrete interfaces. This is due to the fact that shotcrete has a low capture cross-section. It will act mostly as a moderator, slowing down fast neutrons. The thermal macroscopic absorption cross-section varies greatly from one material to the next. For norite, $\Sigma_A = 0.014$ cm^{-1}, for shotcrete, $\Sigma_A = 0.009$ cm^{-1}, while for steel it is $\Sigma_A = 0.260$ cm^{-1} and for water it is $\Sigma_A = 0.022$ cm^{-1}. This means that while many of the fast neutrons from norite will

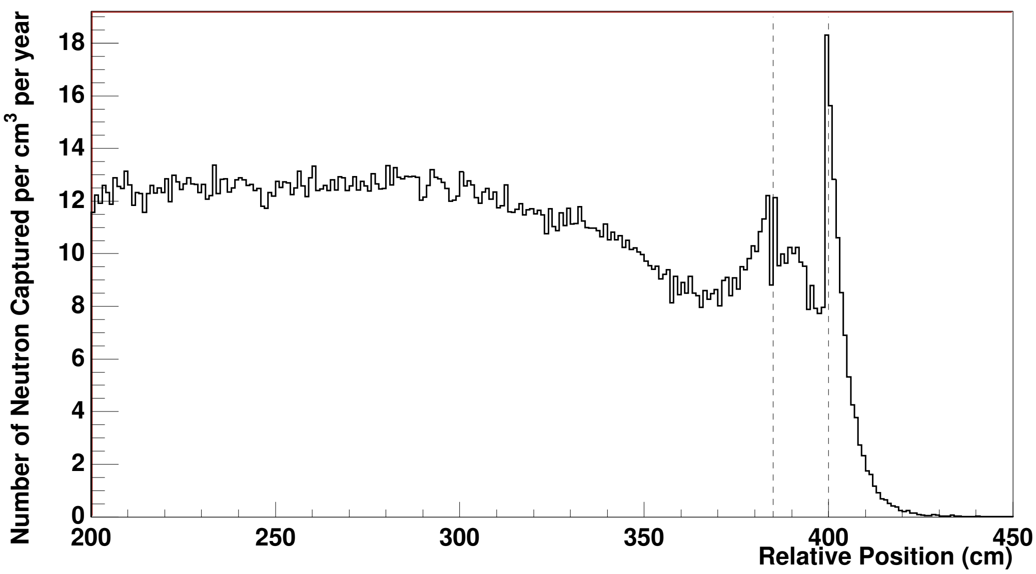

Figure 3.1: Neutron capture density in the wall for a water-filled cavity (linear scale). Norite is located at $x < 385$ cm, shotcrete is between $x = 385$ cm and $x = 400$ cm, water is found for $x > 400$ cm, the steel mesh is at $x = 385$ cm, and the polyurethane liner is at $x = 400$ cm.

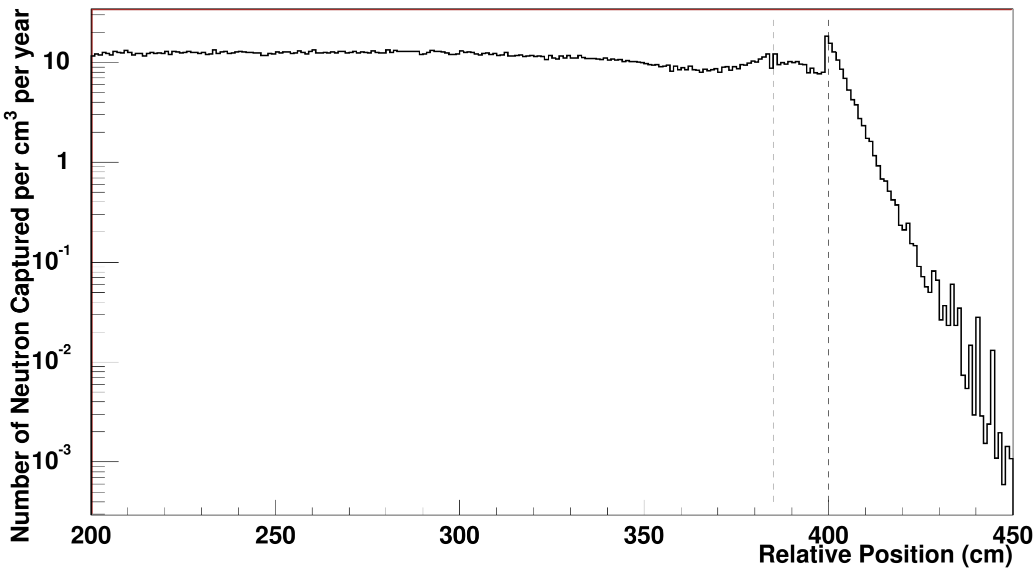

Figure 3.2: Neutron capture density in the wall for a water-filled cavity (logarithmic scale). Apart from the change in the y-axis, this figure is the same as Figure 3.1.

slow down to thermal energies in the concrete, they will have time to leave it before getting captured, but these will be stopped after traveling only a few centimeters in materials with higher capture cross-sections.

Water acts as a reflector. This means that many neutrons leaving the wall will be redirected towards it. In this way, a neutron of rock origin may very likely go through a thickness of norite, through the shotcrete shield, in the water, then back across the shotcrete to get captured in norite or in the steel mesh. Some also, on such a way back, will get captured in the concrete. Without water to reflect the neutrons, the capture density appears different, as shown in figure 3.3. The size of the norite and steel peaks are reduced by 10% and many fewer neutrons end up being captured in shotcrete. The simulation did not try to follow the history of neutrons past one meter from the wall. Some of these neutrons roaming in the cavity will end-up getting captured in the wall on other side while others will likely be absorbed by whatever material could be present in the cavity at that

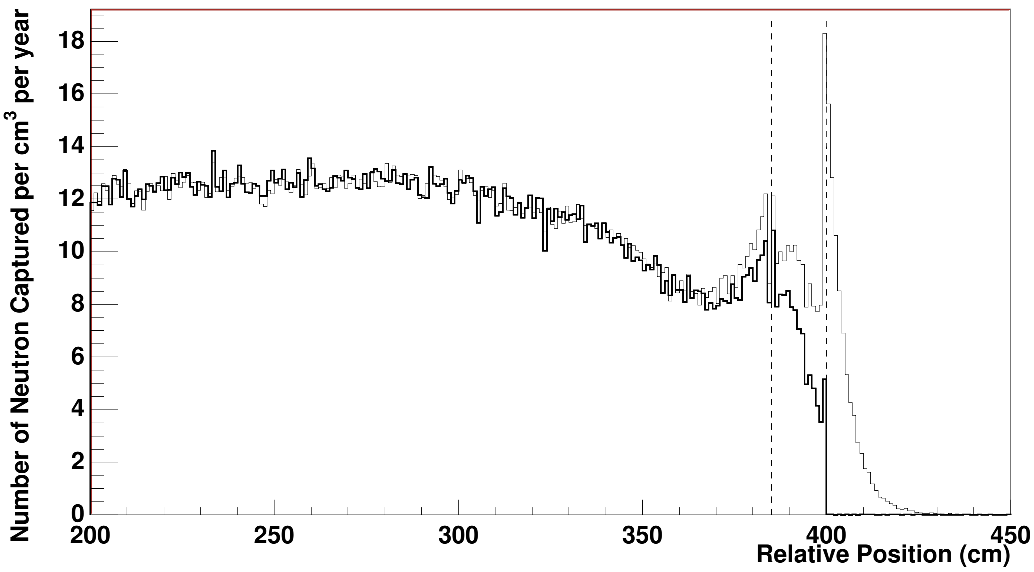

Figure 3.3: Neutron capture density in the wall for both air-filled (thick solid line) and water-filled (thin solid line) cavities. Norite is located at $x < 385$ cm, shotcrete is between $x = 385$ cm and $x = 400$ cm, air or water is found for $x > 400$ cm, the steel mesh is at $x = 385$ cm, and the polyurethane liner is at $x = 400$ cm.

time. As a result, one should expect the gamma ray spectra from the wall to be different when the cavity is filled with air than when it is filled with water.

Polyurethane is a polymer. Its oxygen, hydrogen, and carbon composition (the latest being very similar to oxygen in terms of neutron capture) will make it behave almost exactly like water. It will act as a reflector and its hydrogen will capture many neutrons as seen by the peak at $x = 400$ cm in figure 3.1.

In the water-filled configuration, many neutrons will get captured outside the wall, in the water. It has been said before that effectively all neutrons escaping the wall will be stopped by the water shielding before reaching the core of the detector. Such a claim can now be confirmed by SNOMAN. Figure 3.2 shows the exponential fall-off of the neutron capture density in water for increasing distance from the wall. However, it is difficult to draw any quantitative conclusion from this. The statistical limitation that the Monte Carlo technique encounters when investigating rare events can be seen here. Only an extremely small fraction of the neutrons will get past 25 cm of water. This causes the histogram to show an apparent discontinuity past that point.

The question of the number of neutrons from the wall getting to the detector is better addressed by reckoning the number of neutrons leaving the wall per unit time and using the neutron attenuation formula (equation 2.4). Using SNOMAN simulations, it was found that 1.0×10^{-5} neutrons per cm^2 escape the wall every second to enter the water. These will have to cross at least 1.75 meters of water shielding before reaching the back of the PMTs. An attenuation factor of 1.5×10^{-8} is associated with such a thickness. When scaled to the whole cavity, this says that fewer than 30 neutrons of wall origin will enter the PSUP volume every year. This is negligible compared to other sources of neutrons in that area (mostly from α-capture on light elements in the PMT glass).

If no shotcrete shielding had been installed at all, simulations say that instead of a flux of 1.0×10^{-5}, it would be 1.2×10^{-5} neutrons per cm^2 that would leave the wall and enter the water every second. The decision of putting in a layer of shotcrete could not really be justified on the basis that it would simply reduce the neutron flux by 20%. The real reason for having such a shield becomes evident when one looks at gamma ray fluxes from the wall.

3.3.2 Gamma Ray flux

Understanding where neutrons capture is especially relevant to the study of gamma ray fluxes. The capture density accounts for all the ways in which neutrons can be absorbed. But the majority of neutrons will be captured through the (n,γ) process. If this reaction occurs far away from the surface, chances are, the gamma ray will be attenuated before it can enter the water. Also, a neutron captured in norite is more likely to produce a high-energy gamma ray than a similar neutron captured in shotcrete. The calculated gamma ray spectrum per neutron capture for both materials is shown in figure 3.4. This is due to the difference in their intrinsic composition (given in Appendix A). In particular, norite has a

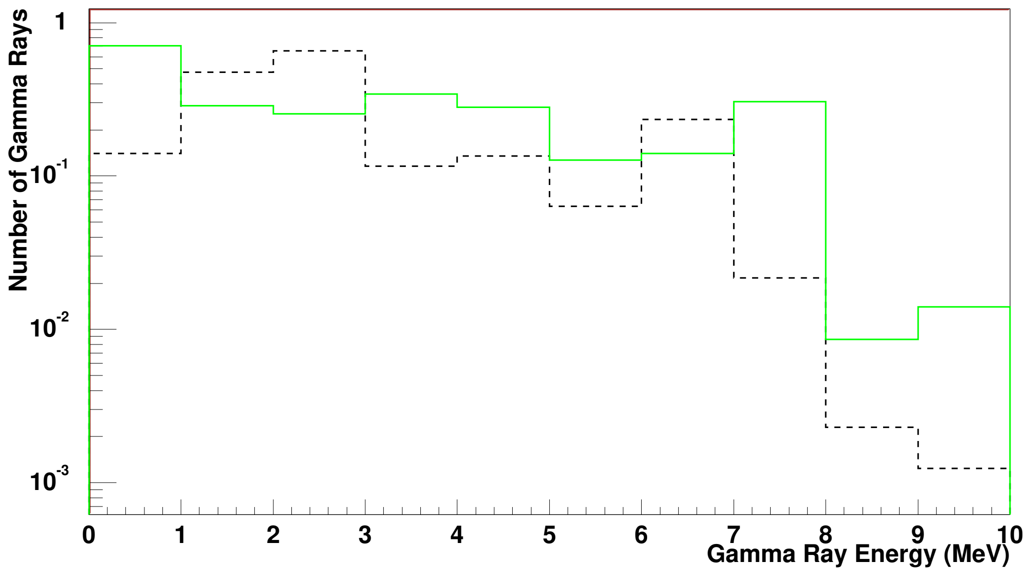

Figure 3.4: Gamma ray spectrum per neutron capture for norite (solid line) and shotcrete (dashed line) as given by SNOMAN. It is seen that norite is more likely to produce high-energy gamma rays than shotcrete. It can also be noticed that the integral flux per capture is greater than one, saying that generally each radiative neutron capture releases more than one gamma ray.

non-negligible iron and magnesium content.

The norite spectrum in figure 3.4 is that given by SNOMAN. It has also been worked out by Earle and Wong [54] as part of the preliminary calculations in support of the SNO project, in 1987. Both are plotted on figure 3.5 and are seen to disagree slightly. The difference between the two spectra is only due to the use of different elemental compositions. The numbers used by this early analysis relied on preliminary elemental concentration assays. While, for example, the presently accepted concentration of iron is 6.2% weight, these older numbers assumed an iron concentration of 7.1%. This difference would explain the higher numbers found by Earle and Wong in the 8 to 10 MeV bins. However, even if the detail numbers are not the same, both spectra have the same order of magnitude.

Following a radiative capture, at least one gamma ray is released. But, depending on the element on which the capture occurs, many gamma rays may come out in a cascade.

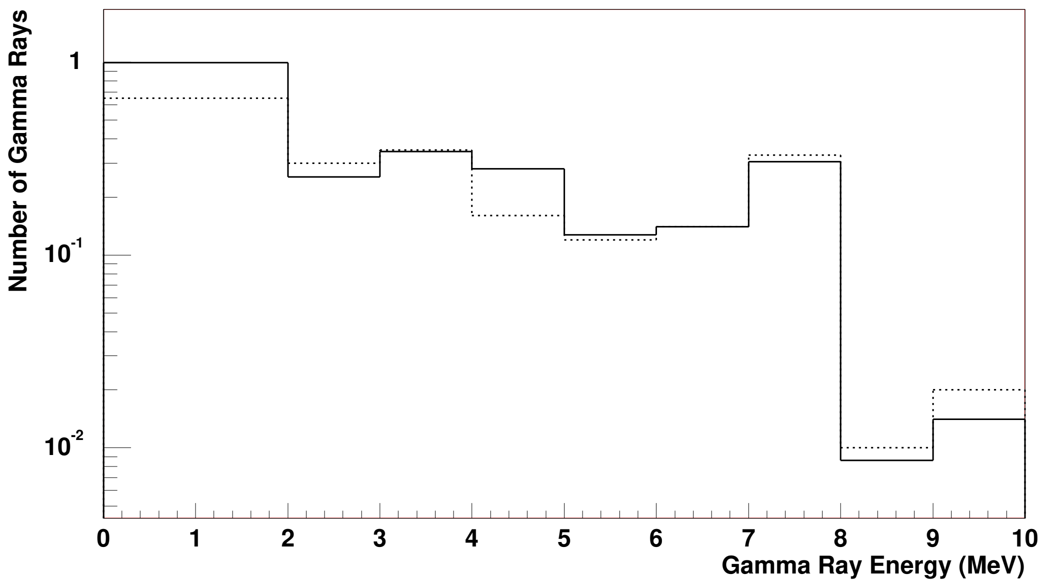

Figure 3.5: Gamma ray spectrum per neutron capture for norite according to SNOMAN (solid line) and Earle and Wong (dash line). The rates between 0 and 2 MeV have been summed into a single bin.

In norite, an average of 2.5 gamma rays are expected to come out of norite for each (n,γ) reaction. It was found that, depending on the location, this radiative process leads to the generation of some 6.0 to 8.0 gamma rays per cm^3 per year with energy greater than 5 MeV. This rate is much larger than that of gamma rays coming from direct α-capture, predicted by Heaton to be 0.15 gamma rays per year per cm^3 above 5 MeV.

Figure 3.6 shows the overall gamma ray flux coming out of the cavity walls in the case of a water-filled detector as calculated using this analysis. Only the high-energy end of this spectrum contains valuable information. This is because, by simulating the (n,γ) reactions in both norite and shotcrete, and the direct α-induced gamma rays in norite, virtually all the gamma rays with more than 5 MeV of energy were taken into account. However, a large number of reactions can release low-energy gamma rays, none of which have been accounted for in the calculations. These includes such sources as the decays of ^{238}U and ^{232}Th daughters (like ^{208}Tl, ^{212}Bi, ^{214}Bi, ^{228}Ac or ^{234}Pa), the decay of ^{40}K (a potassium

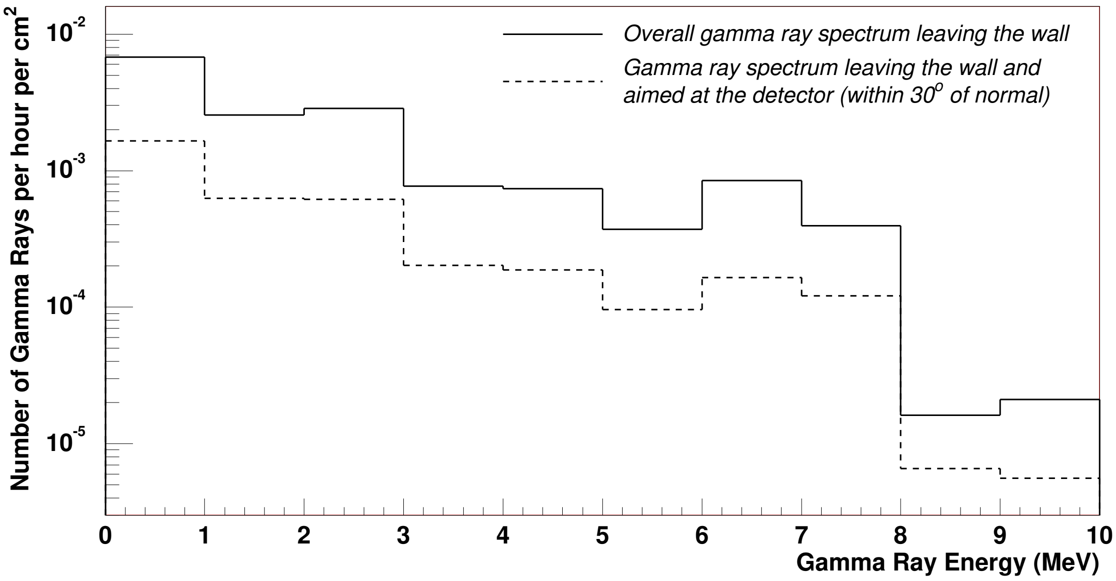

Figure 3.6: Gamma ray flux leaving the wall per cm^2 in a water-filled detector. Only the high-energy end of this spectrum is expected to accurately describe the actual flux.

isotope with a natural abundance at the 0.01% level), and the spontaneous fission of ^{238}U. The gamma rays released in these processes will typically have energies averaging between 0 and 3 MeV. The high-end tail of their distribution might be found to reach such energies as 4 or 5 MeV, but one would expect the rates of such events to be well below that of radiative neutron and α-captures. Also shown in figure 3.6 is the spectrum of gamma rays that are heading for the SNO detector. The magnitude of this second spectrum, which only includes those gamma rays leaving the wall with an angle smaller than 30^o from the wall normal, is on average a factor of 4 below that of the overall spectrum. This solid angle corrected flux will be used in calculations presented later in this chapter.

It is of interest to compare the "full wall" result of figure 3.6 with what such a flux would have been if the shotcrete shielding had not been laid. This unshielded configuration has been investigated and is shown in figure 3.7. On the same figure have also been drawn the fluxes for 10 and 20 cm thick shotcrete layers.

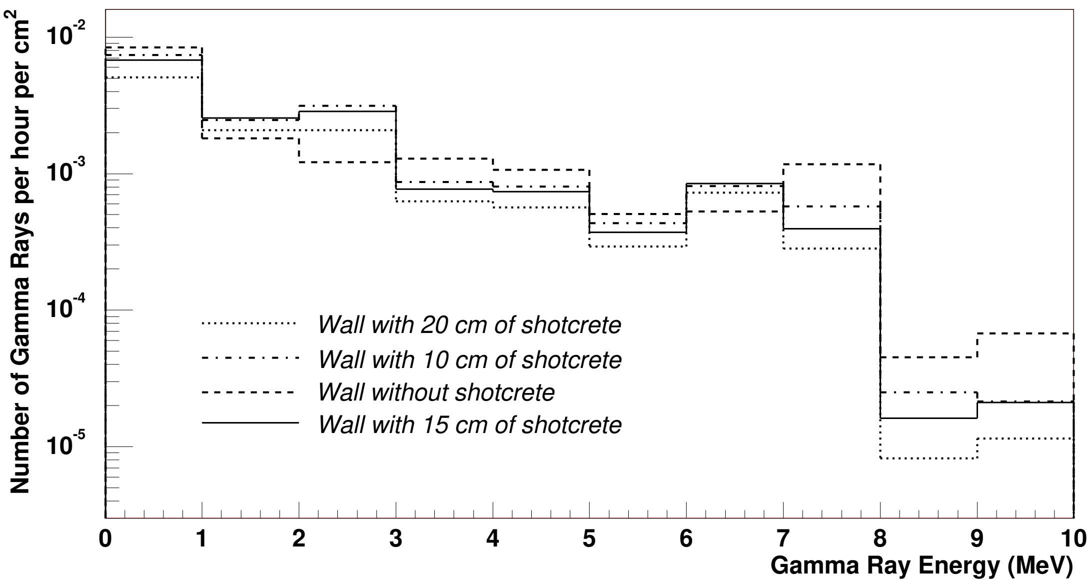

Figure 3.7: Gamma ray flux leaving the wall in a water-filled detector for various wall configurations.

The neutron capture density landscape with and without shotcrete are expected to be dissimilar. Gamma rays produced in both cases will have to cross different materials before entering the water and will therefore be attenuated differently. As a result, it was not surprising to find that their respective outgoing gamma ray spectra are not equal. Indeed, an unshielded wall gives out about three times more gamma rays with energies above 7 MeV than its shielded equivalent. This shows explicitly the raison d'être of the shotcrete layer.

The actual thickness of shotcrete that was placed on the walls is not known with certainty. Some areas have been covered with more shotcrete than others. Figure 3.7 provides information about the possible repercussion this could have on the gamma ray flux leaving the wall. This figure indicates that such wall thickness variations will only change the rates by a small factor.

It has been noted that steel has a very high absorption cross section compare to norite, shotcrete and water, and that the gamma rays released from neutron radiative captures in

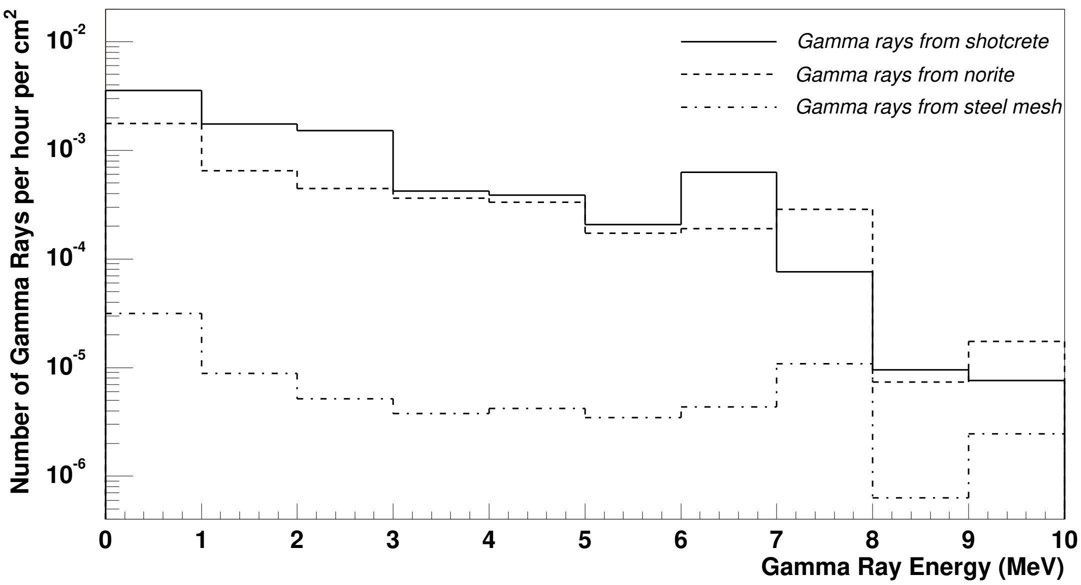

Figure 3.8: Gamma ray spectra from various origin leaving the wall in a water-filled detector.

it can have very high energies. It was therefore first though that the presence of a steel mesh in the shotcrete, next to the norite body, would account for a major increase of the high-energy gamma ray flux from the wall. Figure 3.8 shows that this fear was not justified and that the gamma ray yield from steel is significantly smaller than that of shotcrete and norite. The largest steel contribution is found at high-energies where it represents 9% of the outgoing gamma rays. This can be understood by the fact that the relative volume of steel is by far smaller than that of the other two materials. Also, because the steel is not located too close to the water interface, it is not exposed to a high flux of thermal neutrons, as can be seen in figure 3.1.

Knowing the gamma ray flux leaving the cavity wall and directed at the detector core, it is possible to find out how many of these gamma rays will find their way inside the D_2O region as well as how many will cause interactions that will be reconstructed inside the AV. To reach the heavy water volume, gamma rays have to pass through, and be attenuated by, the water shielding and the PMTs and their support structure. The effect of the water

Gamma Ray Energy (MeV)	Wall without shotcrete shielding (day^{-1})	Wall with a 10 cm shotcrete shielding (day^{-1})	Wall with a 15 cm shotcrete shielding (day^{-1})	Wall with a 20 cm shotcrete shielding (day^{-1})
3 – 4	9.7×10^{-4}	7.8×10^{-4}	6.3×10^{-4}	5.2×10^{-4}
4 – 5	8.4×10^{-3}	7.4×10^{-3}	6.0×10^{-3}	4.9×10^{-3}
5 – 6	1.9×10^{-2}	1.9×10^{-2}	1.6×10^{-2}	1.5×10^{-2}
6 – 7	7.3×10^{-2}	1.1×10^{-1}	8.8×10^{-2}	9.3×10^{-2}
7 – 8	3.9×10^{-1}	2.5×10^{-1}	1.7×10^{-1}	1.2×10^{-1}
8 – 9	2.1×10^{-2}	1.4×10^{-2}	2.0×10^{-2}	1.4×10^{-2}
9 – 10	1.1×10^{-1}	3.8×10^{-2}	3.2×10^{-2}	1.9×10^{-2}

Table 3.1: Gamma ray flux of wall origin entering the AV (with energy above 3 MeV) for a water-filled detector. The rates are given for various wall configurations. Since only gamma rays from (n,γ), (n,nγ) and (n,pγ) were taken into account, only rates above 5 MeV will likely describe the full flux, while those below 5 MeV will only represent lower limits.

shielding can be found by making use of equation 2.5. This attenuation calculation could be done with SNOMAN, but because of the important thickness of water, as many as a few billion events would have to be generated to get statistically acceptable results. However, the attenuation provided by the PSUP, the PMT bases and the PMTs themselves is best found using SNOMAN which has every individual parts modeled. Therefore, finding the number of gamma rays entering the D_2O consisted of first finding the attenuation due to the whole water body (from the cavity wall to the AV and applying solid angle corrections), and from there, Monte Carlo modeling the passage of the remaining particles through the PSUP assembly.

Because of the barrel shape of the detector, not all gamma rays will have to cross the same thickness of water. The waist region, being closer to the PSUP, will account for most of the background. The approximation was made that 80% of the overall signal seen by SNO will have come from this area [55]. Therefore, the effective wall surface used in the calculations was 8×10^6 cm^2.

The results from this analysis for the various configurations presented before are listed in table 3.1. Only gamma rays with energies above 3 MeV were the subjects to this set of calculation.

More important than the number of gamma rays which actually enter the heavy water is the number of events from wall gamma ray origin which reconstruct inside the heavy water region. SNO records the PMT-hit timings and patterns from which event positions are deduced. Mainly because of scattering, reactions that occurred within the light-water region can sometime be fitted as though having taken place inside the D_2O. By taking the above gamma ray fluxes, and modeling the interaction of these gamma rays in the detector, the Monte Carlo provided a measure of how many reconstructed events due to gamma rays from the wall are to be expected inside the AV. This calculation was done is a way similar to that presented above when finding the number of gamma rays entering the heavy water. Using equation 2.5, the gamma ray attenuation provided by the layer of water between the wall and a virtual sphere of radius 700 cm (centered around the AV) was calculated. The PSUP and PMT assembly structure attenuation factor was found using SNOMAN. This gave the number of gamma rays left 1 meter from the AV. These "survivors" were then modeled in a last SNOMAN simulation that would record any PMT hit these gamma rays would induce. In the end, only those events which reconstructed inside the 600 cm radius of the AV were kept.

The result of this analysis, expressed in terms of the number of PMT hit, a so-called NHit spectrum, of events reconstructing inside the AV, is shown is figure 3.9. Only the part of this plot above "50 NHits" was plotted given that this study only dealt with gamma rays with high energies. Indeed, according to the estimate that some 8.5 PMTs will fire for every MeV of energy of the event registered, a 50 NHits signal would be synonymous to a 5.9 MeV event. On figure 3.9 are also plotted the results for different shielding configurations. These will give a measure of the uncertainty coming from the possible shotcrete thickness variation. However, the results observed above 80 NHits suffer from the characteristic Monte Carlo limitation of statistical accuracy. The irregularities in that region are only due to statistical fluctuations.

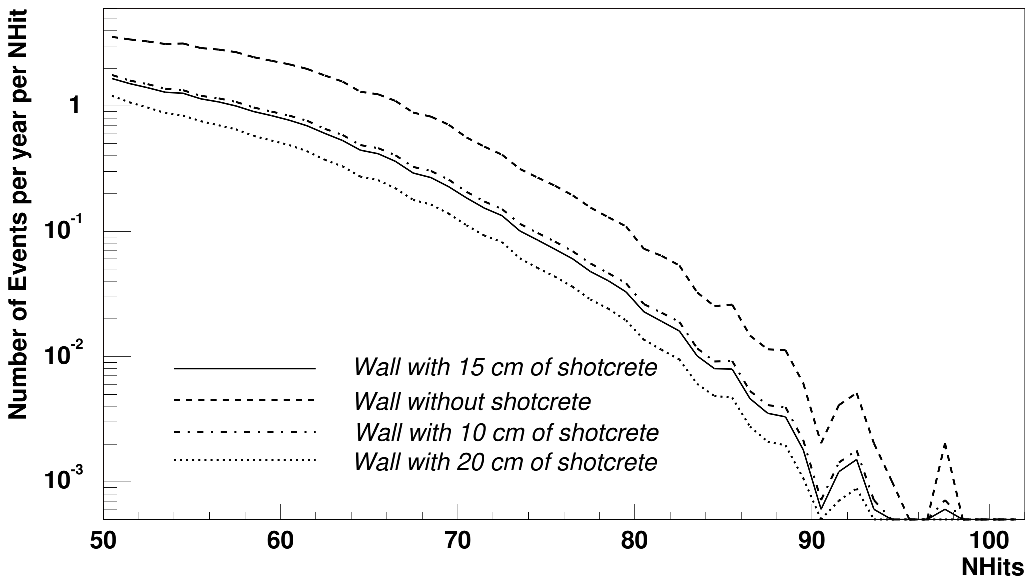

Figure 3.9: NHit spectrum from wall background events reconstructing inside AV for various wall configurations.

This figure should be compared with the similar graph of figure 2.2. Both plots are overlaid in figure 3.10. When using the SNOMAN "time fitter" algorithm, it was found that only some 5.5 events firing more than 50 PMTs would be fitted inside the D_2O region per year. According to Figure 3.10, the wall background is comparable to the PMT β/γ signal. This result is reassuring as it would indicate that this signal will not be a major background to the SNO detector.

3.4 Comparisons

The analysis presented in the previous section relied heavily on Monte Carlo simulations as well as on a thorough understanding of the nuclear processes taking place in the wall. Because the results obtained are unavoidably uncertain, a worth while exercise consists of comparing the results found to those from other independent investigations. Calculations of backgrounds in SNO have already been done in the past and various measurements have

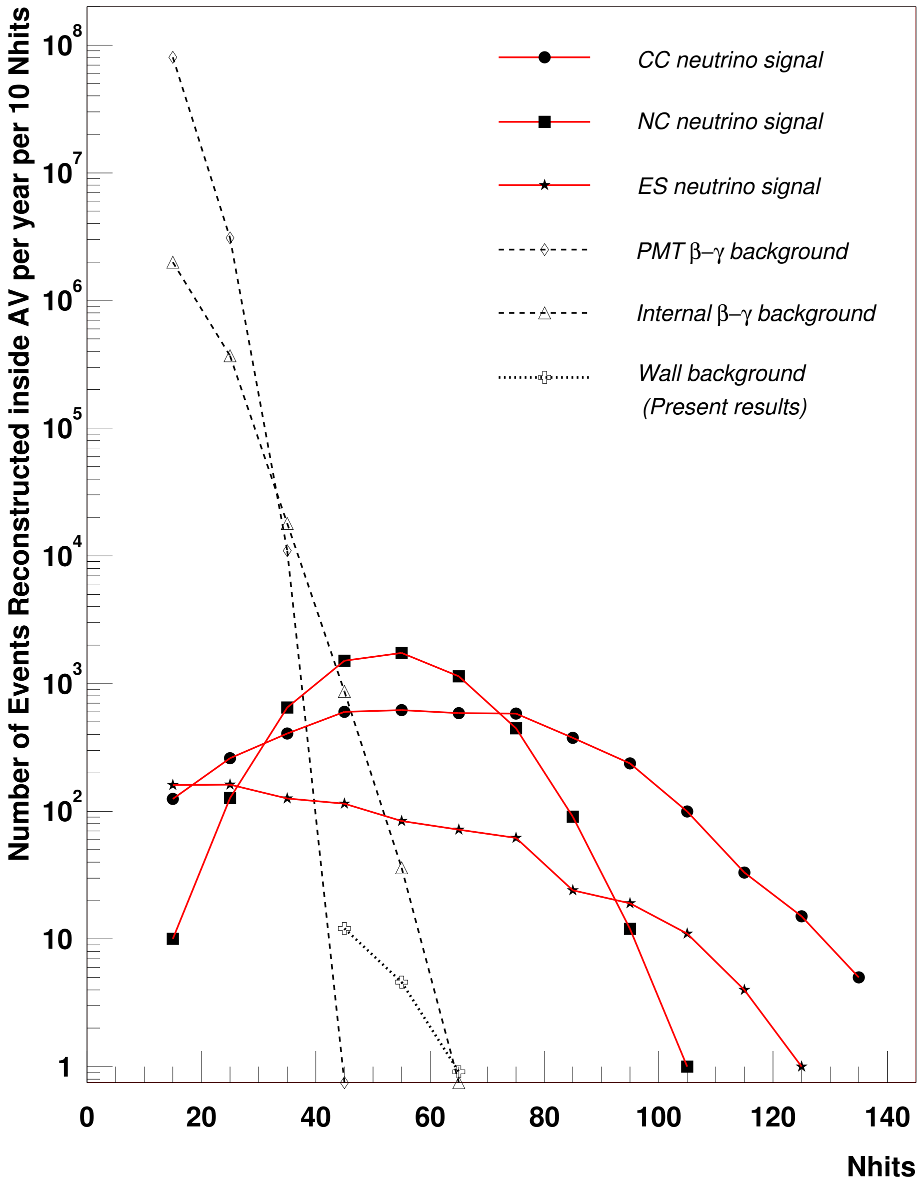

Figure 3.10: Expected signal and background NHit spectra in SNO for one year of counting in the case where salt has been added to the D_2O. Full SSM for NC and $1/3$ of SSM for CC was assumed. The three neutrino spectra have been taken from [24]. The two β/γ backgrounds are from the more recent analysis found in [25].

Location	Measured Rates (cm^{-2} s^{-1})	Deduced Rates (cm^{-2} s^{-1})
5400' level norite	1.7×10^{-6}	3.5×10^{-6}
5600' level granite	9.0×10^{-6}	1.9×10^{-5}
5600' level gabbro	1.2×10^{-5}	2.3×10^{-5}
5600' level red granite	1.6×10^{-5}	3.2×10^{-5}

Table 3.2: Neutron fluxes measured in the Creighton Mine. A variation is observed with rock type. It should be noted that these early measurements were not performed at the SNO location [56]. The deduced rates represent the experimentalists estimate of what the neutron fluxes really were at these locations.

been performed in the SNO cavity itself or in other similar locations and can be used for comparison.

3.4.1 Neutron Flux Comparison

The neutron capture density in the wall has been worked out as part of the analysis, helping in understanding where neutrons are preferably stopped. This quantity has been calculated in the past by Heaton [32], for a geometry somewhat different from the present one. However, whether or not steel meshes are laid against the rock, whether the cavity is filled with air or with water, the neutron capture density deep within norite should be unaffected. Heaton found that far from the surface, some 10 neutrons should get captured per year per cm^3. This result was found for uranium and thorium concentration levels lower than those used in the present study. Raising this rate by a factor of 30% should make comparisons possible. Figure 3.1 indicates that, according to the present model, some 12.5 neutrons get captured per cm^3 per year in the rock. This is very close to the corrected number prescribed by Heaton of 13 neutrons per cm^3 per year.

Back in 1986, measurements of the neutron flux were performed in the Creighton mine using BF3 neutron counters [56]. The results from this set of measurements are given in table 3.2 and could be loosely used for comparison. To do so, the wall simulation had to be changed to account for the fact that no concrete or polyurethane shielding were present at

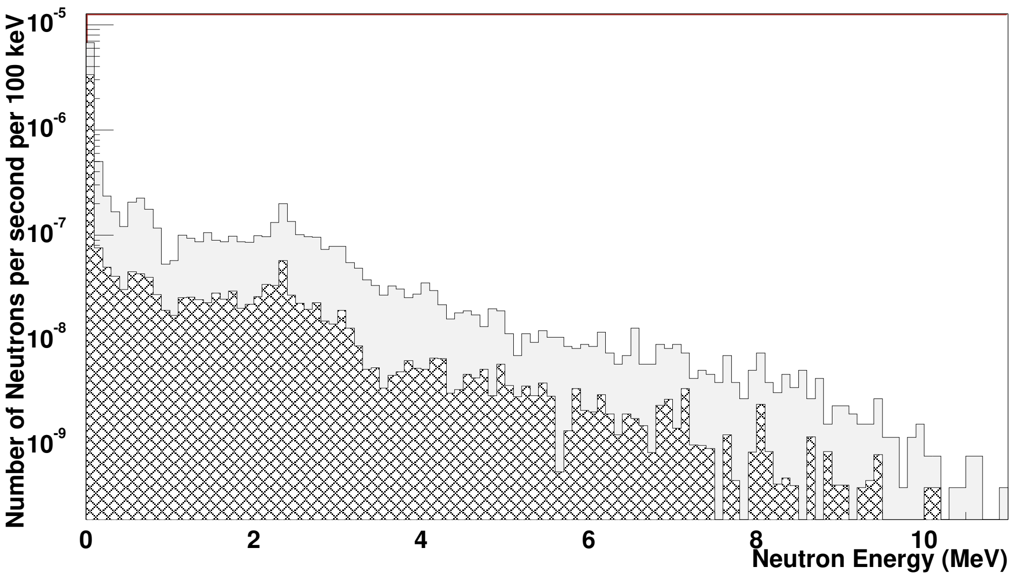

Figure 3.11: Energy spectrum of neutrons leaving the wall for both shielded (hatched histogram) and non-shielded (shaded histogram) configurations.

the time, and air was in direct contact with the rock. The neutron flux spectrum that was calculated for both shotcrete shielded and non-shielded surface are presented in figure 3.11. The fluxes from the various energy regions are given in table 3.3. These results show that more thermal neutrons will leave a shielded wall than a non-shielded one. This was to be expected as the shotcrete layer will moderate some of the more energetic neutrons.

		Neutron Flux (cm^{-2} s^{-1})	
Energy Region		with shielding	without shielding
Thermal	(0 — 0.5 eV)	2.36×10^{-6}	1.03×10^{-6}
Epithermial	(0.5 eV — 0.1 MeV)	1.00×10^{-6}	6.08×10^{-6}
Fast	(0.1 MeV — up)	1.10×10^{-6}	4.96×10^{-6}
	Total	4.46×10^{-6}	1.21×10^{-5}

Table 3.3: Calculated neutron fluxes for the air-filled SNO cavity for both shotcrete shielded and non-shielded configurations.

Calculated values from table 3.3 and the measured value of table 3.2 are found to have generally the same order of magnitude. However, very little more information can be extracted from this comparison, given the large variation in results found in table 3.2. This is due for the most part to the fact that the neutron production process depends highly on the composition and contamination of the host rock, two quantities which will widely change with location.

To measure the neutrons from the neutrino NC reactions in the detector, arrays of ^{3}He proportional counters will be lowered into the AV. Some of these NCDs are presently stored underground, in the control room, a few meters away from the SNO cavity. Rough neutron flux measurements tests have been performed with these instruments to verify that they were working properly. The preliminary number found indicate a thermal neutron flux of $(4.80 \pm 0.17) \times 10^{-6}$ neutrons per cm^2 per second [57]. This rate, measured in a location where walls were not as carefully shielded as in the cavity, have the same order of magnitude as the one found by the present calculations.

Neutron fluxes have also been measured in various other underground laboratories around the world and can be found in the literature. Some of these are listed in table 3.4. They provides an additional verification that the numbers found by Monte Carlo modeling have the right order of magnitude. Once again, variations from one laboratory to the next are in no way surprising. The rates for SNO are comparable to those found in other low radiation laboratories. This is true, even though norite is a much "dirtier" rock than for example the limestone found at the Gran Sasso location (see Appendix A for compositional information about both norite and limestone), thanks to the shotcrete shielding layer.

3.4.2 Water-Filled Gamma Ray Flux Comparison

A SNO scientific and technical report (SNO-STR) was written in 1994 by Skensved and Robertson which was entitled "Summary of Backgrounds in SNO" [24]. Using a Monte Carlo code developed by Skensved [62], and starting from the information available at the time,

Location	Thermal neutron flux (cm^{-2} s^{-1})	Epithermal neutron flux (cm^{-2} s^{-1})	Fast neutron flux (cm^{-2} s^{-1})	Reference
Gran Sasso Laboratory	$(2.05 \pm 0.06) \times 10^{-6}$	$(1.28 \pm 0.31) \times 10^{-6}$	$(2.56 \pm 0.27) \times 10^{-6}$	[58]
Gran Sasso Laboratory	$(1.08 \pm 0.02) \times 10^{-6}$	$(1.98 \pm 0.05) \times 10^{-6}$	$(0.23 \pm 0.07) \times 10^{-6}$	[59]
Broken Hill (Australia)	$(1.94 \pm 0.11) \times 10^{-5}$	$(1.55 \pm 0.30) \times 10^{-5}$	—	[60]
Laboratory of Modane	$(4.0 \pm 1.0) \times 10^{-6}$	—	$(1.6 \pm 0.1) \times 10^{-6}$	[61]
SNO Detector (Present Calculated Results)	2.36×10^{-6}	1.00×10^{-6}	1.10×10^{-6}	—

Table 3.4: Neutron fluxes measured in various underground laboratories across the world. It should be noted that different authors have slightly different definitions of Thermal, Epithermal and Fast energy regions. The two Gran Sasso results come from independent measurements made at two different locations in the Laboratory.

estimates of background signals for an operational detector were calculated and presented in this internal paper. This independent work included predictions for the cavity wall gamma contribution. This was done by following a series of steps akin to those taken in the present analysis. Neutrons generation and captures were modeled. The number of gamma ray produced was calculated based on the number of radiative captures for all elements and summed into 5, 7 and 9 MeV bins. Further Monte Carlo (EGS4 simulation [63]) followed these gamma rays through water. Those successfully getting through this shield were histogrammed according to their energy and direction, and fed into a Čerenkov Monte Carlo code.

An other background for SNO comes from gamma rays coming from the PSUP. This steel structure will release high-energy gamma rays upon radiative captures of neutrons produced nearby in the PMTs (from (α,n) in the glass). This signal is expected to look very similar to that of the wall since both cover a similar energy range and will be reconstructed as coming radially inward. For this reason, the authors of the report decided to add both contributions in a single histogram, without including any detail as to the relative contribution of each channel. However, a previous SNO-STR-report from the same authors [64] indicated that, according to their calculations, both of these backgrounds would have the same magnitude and shape. According to this statement, it was assumed that the rates presented in their summary paper could be halved to retrieve the wall contribution.

The radioactivity levels they used to get the number of neutron produced in the wall were lower than the present ones. A contamination of 1.2 ppm uranium and 3.3 ppm thorium was assumed for norite, while 1.08 ppm uranium and 0.70 ppm thorium were used for shotcrete. With these values, the number of neutrons generated is roughly half of what was generated in the present analysis. To account for this discrepancy, and in order to still allow a valid comparison to be made, the rates found by this study needed to be doubled.

These particular calculations had been done before the cavity was fully excavated. This work assumed 12.5 cm of shotcrete would cover the wall. Also, the wall itself is further back in reality than it was in the simulation. The implication of these two variations can only be assessed qualitatively. Both of these will induce a slight overestimation of the number of gamma rays reaching the heart of SNO. However, the most significant problem in the way of comparing results comes from the very low statistical accuracy of Skensved and Robertson's analysis for high NHits events. Indeed, at the time these calculations where done, the performance of available computers made impossible the modeling of very large numbers of Monte Carlo events.

The final answer given by the report was in terms of a NHit spectrum from events reconstructing inside the D_2O. This spectrum is shown in figure 3.12 accompanied by the results from the present analysis.

The results from Skensved and Robertson predict a higher flux than the present analysis. This could be simply due to the overestimation resulting from simulating a detector with thinner shotcrete and water shielding layers. It is also possible that the shape of their final spectrum was altered by having regrouped gamma rays in only 5, 7 and 9 MeV bins.

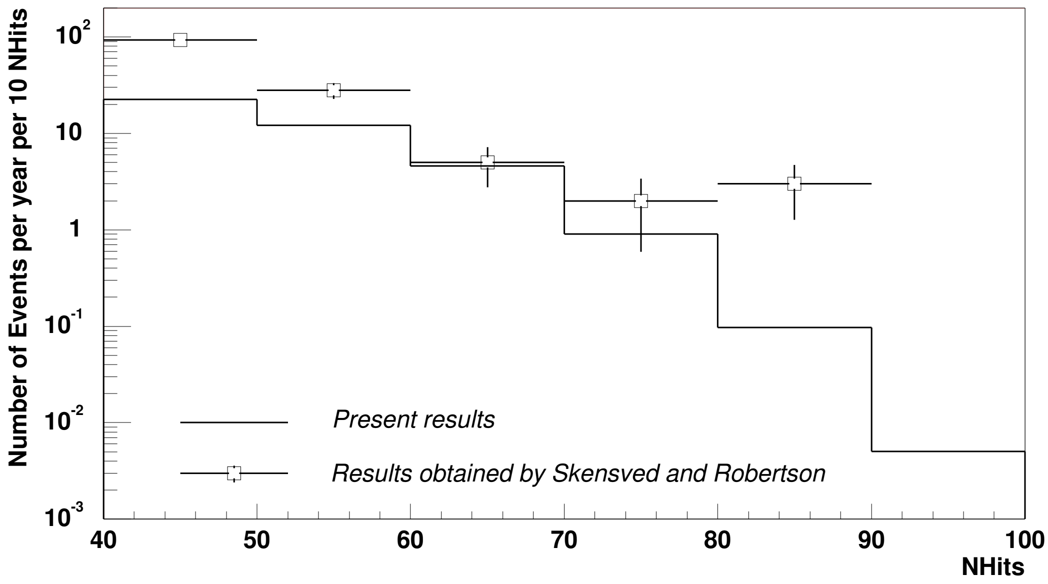

Figure 3.12: NHit spectrum from wall background events reconstructing inside the AV according to the calculations presented in this chapter and calculations done by Skensved and Robertson. The error bars placed on the numbers from Skensved and Robertson are purely statistical.

Above 70 NHits, the numbers presented by this early analysis should be taken with caution because of their very low statistical accuracy. The error bars shown in figure 3.12 are statistical only and therefore only represent lower estimates, systematic errors not having been included. Furthermore it should be noted that, because both analyses were done using different Monte Carlo programs and reconstruction "time fitters", an unavoidable and unquantifiable systematic difference should be expected. This could be the cause for another difference. One would expect the slope of the two spectra to be similar given that the gamma ray attenuation in water of both Monte Carlo used the same (EGS4) package. Different energy-to-NHit scales could explain this situation. So could the fact that the present analysis used, for part of the calculations, equation 2.5, which does not account for scattered down gamma rays. All this makes any profound comparisons impossible. However, one can say that both results agree relatively well given the many uncertainties.

3.4.3 Air-Filled Gamma Ray Flux Comparison

No measurement of the gamma ray flux at the AV in a water-filled detector has been made that could be used for a direct comparison of the present results. The only measured SNO cavity gamma ray flux available had been acquired during the construction phase, when the water shielding was not yet in place and the detector itself was only half-built. Obtained with a large-volume NaI(Tl) detector which was located at the bottom of the cavity, the data amounted to 1490 hours [65]. The spectrum measured is expected to be different from that effectively leaving the wall in a water-filled configuration. One reason for this will be the change in the neutron capture density distribution discussed earlier. Furthermore, in an air-filled situation, neutrons escaping the wall are in a position to get captured in the wall on the other side, or on the material present in the cavity at that time. Neutron capture on polymers such as the acrylic or the PMT plastic supports will generate low 2.2 MeV gamma-rays typical of hydrogen capture. But, high-energy gamma rays will also be produced when neutrons are absorbed by iron, nickel or chromium nuclei. Many such gamma rays have probably been recorded by the NaI detector, making any comparison with Monte Carlo simulations that much more difficult.

At the time this measurement was made, much steel was present in the cavity. The PSUP is an assembly of stainless steel trusses and bolts which, when complete, weighs about 16 tons. Only about half of this amount had then already been installed. However, at that phase in the construction of SNO, much equipment was present in the cavity. Industrial lifts, hoists, man-lifts, AV support and other scaffoldings, all mostly made of steel, filled the cavity and acted as targets for wandering neutrons.

The gamma ray spectra deduced from such a NaI detector based measurement cannot be used for a straight comparison of the results obtained before. To harmonize the model and the actual measurement, a new set of Monte Carlo simulations were performed. These were aimed at mimicking as closely as possible the specific particularities of the air-filled measurement.

The first step consisted of simulating the wall, as before, for the case of an air-filled cavity. The neutrons that were found to exit the shotcrete layer were then independently modeled, with the appropriate energy spectrum, to impinge on a complete air-filled SNO detector, at the heart of which 30 tons of stainless steel had been placed in the shape of a spherical shell. This gave an idea of where neutrons would be stopped. The result of that last stage was scale by a factor of a half to account for the unfinished state of the detector. As a result, half of the AV, half of the PSUP as well as an effective 15 tons of steel were assumed to be present in the cavity. Thirdly, the gamma ray flux from these neutrons capturing back in the wall was found independently. The spectra from each stage were added up to provide an estimate of the gamma ray flux in the cavity. This total calculated spectrum should provide a decent framework for comparing Monte Carlo and measurements. Figure 3.13 shows the uncorrected spectrum (as coming out of the wall when neutrons leaving the surface were not tracked any further), the spectrum for a full half detector scenario, as well as the results of the measurement made with the NaI detector.

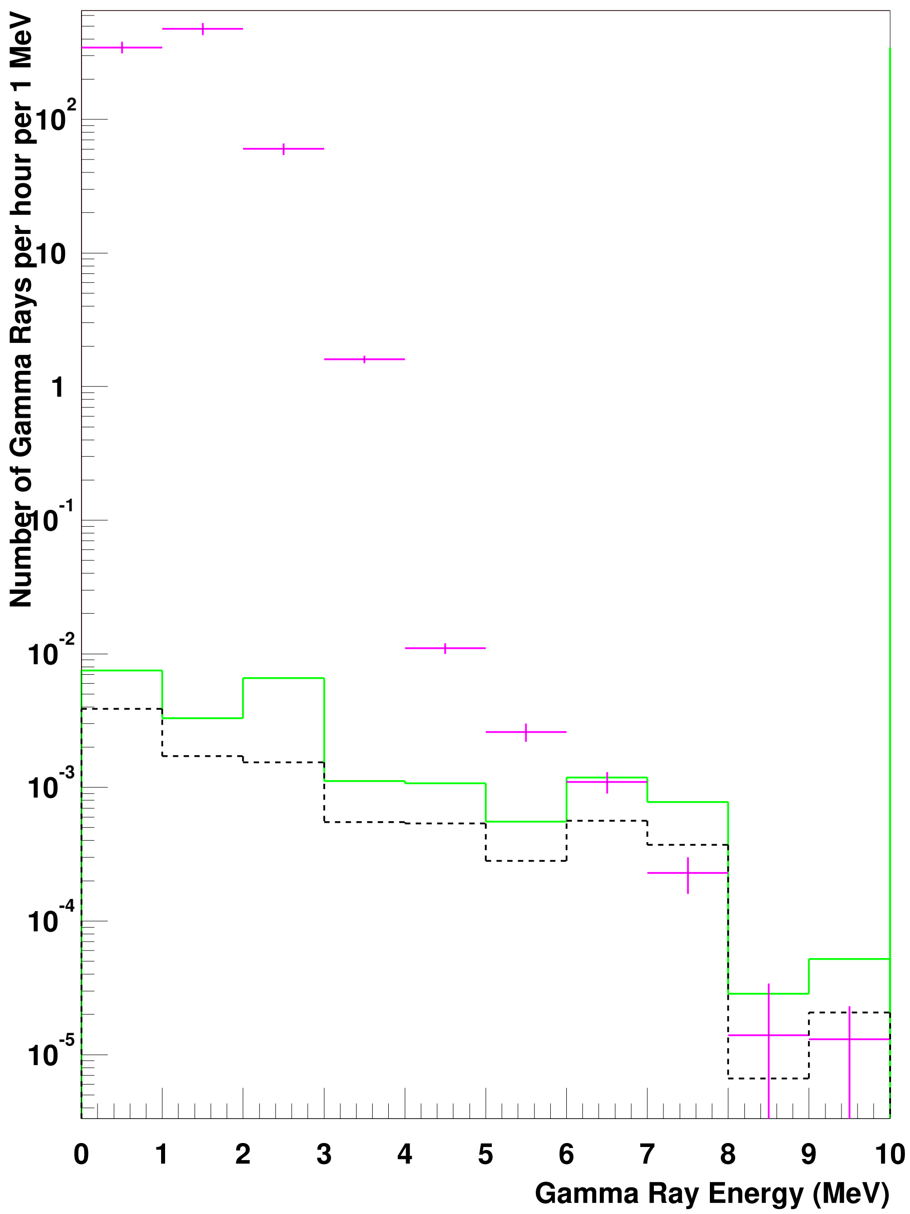

Figure 3.13: Gamma ray spectrum in the SNO cavity at the time of the detector construction as measured using a NaI detector (error-barred histogram) and as calculated by the present SNOMAN Monte Carlo analysis (solid line). The analysis intermediate result (the spectrum calculated when neutrons leaving the wall were not tracked any further) is also shown (dotted line).

Once again, a lack of agreement at low energies was expected. For energies above 6 MeV, measurements and calculations only slightly disagree as the simulation predicts somewhat too many high energy gammas. This could be explained if, in the simulation, too much steel had been assumed to be present in the cavity. This deviation at the high end of the spectrum is not as strong as the one observed between 4 and 6 MeV where more gamma rays are observed than what the calculation predicts. At these energies, (n,γ) processes are still expected to be the dominant source of gamma rays. It is possible that part of the measured excess could be due to the spectral tail from gamma rays of nuclear decay (from ^{208}Tl, ^{214}Bi, ^{40}K or ^{222}Ra isotopes), fission origin, or (n,γ) capture on other elements than steel (like for example aluminum) not accounted for in the analysis.

The relatively good agreement between calculated results and measured rates in the high energy region gives further reassurance that the present calculations are generally correct above 6 MeV. Fully understanding the measured results of the low energy region would require a lengthy, much more detailed, analysis beyond the scope of this thesis.

Chapter 4

A Calibration Source to Study the Cavity Wall Background

By surrounding the D_2O core of the detector with a light water shield, the number of background interactions taking place within this volume has been greatly reduced. However, many low energy internal signals will still occur in that region. Internal β/γ signals as well as the numerous PMT β/γ events, taking place in the water shield but mis-reconstructed as though coming from within the heavy water volume, will swamp the low energy end of the neutrino signal and set the working threshold of the detector. The calculations presented in the previous chapter have shown that very few gamma rays originating from the cavity wall are expected to cross the AV. But, once again because of the inability to accurately reconstruct the interaction vertices position, some of these gamma rays Compton scattering in the light water will present a background to the neutrino signal. According to calculations, the rate for such background events is lower than the neutrino rate. For this reason, as opposed to the two β/γ signals mentioned above, the cavity wall background will not set the detector threshold. Instead, by applying a correction factor to the total neutrino flux measured, the wall background will be subtracted to leave only those events which are neutrino interactions. In order to do that, both the shape and magnitude of this background need to be known accurately. The calculations presented in chapter 3 were aimed at getting such an information. However, many assumptions, simplifications and uncertainties went into them and the results they provided could only be used as first order estimates and these calculations are only a first step towards understanding this signal. An actual measurement should be made. This chapter investigates the feasibility of making a calibration source that would make possible a measurement of the wall background signal.

4.1 Wall Background Calibration Source Options

4.1.1 General Idea

All calculations and models agree that the wall background signal is weaker than the neutrino signal in the energy region above the threshold. It is therefore impossible to measure this background directly with SNO: recording a single event a day hidden among more than 20 neutrino events would not yield the information needed. A way should be devised of temporarily getting more events from the wall to be registered by SNO. By doing so, one could directly answer what is the response of the detector to such a type of event. Virtually all background interactions of wall origin recorded by SNO come from gamma rays. They are produced in copious quantities in the wall, as seen in the previous chapters, but the greatest majority are attenuated before reaching the heart of the detector. The only way to get more gamma rays inside the detector to allow a measurement would be to reduce the amount of shielding these particles have to go through. However, the water shield cannot be removed, but the same effect could be achieved by bringing the wall closer to the detector. Gamma rays produced in a "piece of wall" enclosed in a container and placed in the light water, inside the PSUP volume, would only be attenuated by a relatively small factor and a fair fraction could trigger a response from SNO. A series of measurements of that nature would provide information about the exact shape of the energy spectrum from wall events. By displacing such a source of wall gamma rays, the amount of water shielding could be changed, allowing the study of their attenuation and the systematics of their mis-reconstruction. By knowing how the shape and rate of this gamma ray signal varies as a function of water thickness, the exact wall background could be found by extrapolation.

In reality, there are many factors that need to be considered which complicate the design of such a source. The first is a simple problem of rates. A typical wall background calibration run should be done relatively quickly, in a matter of hours, and in that amount of time a sufficient number of gamma rays should have been measured by SNO to permit statistically meaningful analysis. In norite, some 2.5 gamma rays are expected to come out of every (n,γ) reaction. Given a production rate of 12.8 neutrons per year per cm^3 of norite, if all capture radiatively in the rock, fewer than 20 gamma rays would be created every second within a 5 liter norite block. Only about 2 of these would penetrate through 50 cm of water shielding. Such a signal is far too faint to extract useful information, and that even though this quick calculation considered a most optimistic (and unrealistic) scenario. Indeed, neutrons produced in such a block are far from guaranteed to capture in the rock. They will be much more likely to be absorbed in the surrounding water.

Gamma rays reaching the detector from the cavity wall come from interactions which took place in norite, in shotcrete or in the steel mesh. Therefore, if the cavity wall signal is to be accurately reproduced by a calibration source, norite as well as shotcrete would need to be included. This is confirmed by figure 3.8 presented in the previous chapter which showed the relative intensity of gamma rays entering the water and coming from norite, shotcrete and steel. At the high end of the spectrum, about half of the gamma rays come from the rock while half comes from the shotcrete shielding. Table 4.1 gives the detailed fractions extracted from this figure. In principle, an appropriate design for the wall calibration source should include an adequate mixture of norite and shotcrete that would provide the right ratio of gamma rays from each. However, finding the proper combination of these materials is not strait-forward nor is making sure that neutrons will capture in the two in the right ratio. A more practical approach would consist of making two different calibration sources: a norite source and a shotcrete source. By combining data from both calibration runs, the ratio can be tuned when the analysis is done.

	Gamma Rays produced		
with Energies above	in Shotcrete (%)	in Norite (%)	in Steel (Mesh) (%)
9 MeV	27.6	63.6	8.9
8 MeV	38.0	55.1	6.8
7 MeV	22.2	74.5	3.3
6 MeV	58.1	40.5	1.5
5 MeV	57.1	41.5	1.3
4 MeV	55.9	43.0	1.1
3 MeV	55.4	43.7	0.9

Table 4.1: Percentage contribution of shotcrete, norite and steel to the cavity wall gamma ray flux. Both norite and shotcrete are to be accounted for the high-energy gamma ray flux leaving the cavity wall.

To these issues, other considerations, including safeguarding detector purity, source shape and encapsulation, also should be addressed and will influence the gamma ray generation process.

4.1.2 Calibration Source Deployment Mechanism

Should the wall background calibration source be a simple block of rock or a more complex construct, its shape and size will be limited by the geometry of SNO itself. To insure that no light leaks into the detector, and to insure that no radioactively-loaded dust or air enters it, all openings connecting the deck above SNO and the actual detector have been sealed and a pure nitrogen cover gas extends over the water. Only a few hatches still allow access to both light and heavy water regions. These are kept shut except when a calibration source needs to be lowered inside the detector. In order to maintain confinement, any object going inside the detector is first fed into a cylinder — a so-called source box — which can then be evacuated and connected to one of the hatch gate valves. It is 4 feet long and its inner diameter is $5\frac{1}{8}$ inches. Any calibration source must be able to fit inside this pipe and through these valves (which are $5\frac{1}{4}$ inches in diameter). However, the totality of this volume cannot be taken by the source. Apart from proper clearance on the sides to insure proper deployment of the device, room should be left for a manipulator carriage. This instrument serves as a connection between the source and the rope system that drives it. It also serves as an added weight for the sources which are buoyant. This carriage is 14 inches long. When it is lowered in the D_2O, it is tight to a set of three Vectran ropes driven by motors. These will allow the source to be displaced on one of two planes inside the AV. However, no such off-axis motion is made available to devices brought down to positions inside the light water. For these, only the center rope is attached, providing simple up-down motion.

Many sources need to be provided with electrical power, gas, or light from a laser. This is achieved by having an umbilical containing wires, gas lines or fiber optics extend to the source. This umbilical is rolled on a array of pulleys up on the deck, a so-called umbilical retrieval mechanism (URM), and unrolls as the source is lowered in the detector. Any calibration instrument brought down into the detector is connected to such an umbilical, even when it does not need to receive any signal from the deck. It acts as a safety line in the unlikely event of the Vectran rope breaking. These ropes, which have been chosen for their strength and durability, are changed periodically. The center rope which would hold a wall calibration source could support weights of as much as a hundred kilograms without risks of breaking. For this reason, and because its immersion in water will reduce its effective mass, the weight of the source will not be a design factor.

There are a total of 6 outer calibration access ports, located at various distances from the central axis of the detector. Each opens up on a guide tube, a stainless steel pipe which leads to the inner light water region (inside the PSUP). The position of these openings are listed in table 4.2. Given than the AV has an inner radius of 600 cm, it is clear from this table that only two ports, number 4 and number 5, will provide the full range of water shielding thicknesses required to do a comprehensive measurement. By utilizing the fourth port, a calibration source could be brought as close as 31 cm, or as far as 504 cm, from the D_2O (while staying inside the PSUP volume).

Port Number	Deck Coordinate X (cm)	Deck Coordinate Y (cm)	Distance from Detector Central Axis (cm)
1	361.0	193.0	409.4
2	-112.1	104.1	153.0
3	-361.0	193.0	409.4
4	-596.0	208.0	631.2
5	-586.1	-252.4	638.1
6	118.1	-119.4	167.9

Table 4.2: Cartesian and radial positions of the outer calibration access ports. The deck coordinate system has the X-axis pointing towards the control room. Only port number 4 and 5 provide full source deployment latitude.

4.1.3 Loaded Uranium and Thorium Source Option

The issue of source strength is a very important one. A way has to be found to increase the number of gamma rays produced by the source above that of a simple block of rock. By making the source bigger, so that it may contain more norite or shotcrete, the gamma ray yield would be increased. However, as explained previously, the volume is limited by the size of the source box.

The gamma ray spectrum from the source should be as similar as possible to that coming from the wall. This excludes the simplistic approach of using gamma rays from the radioactive decay of some arbitrary isotope. Getting the right distribution of gamma ray energies can only be done by reproducing the basic generation processes as they take place in the wall. All the high-energy wall gamma rays trace their origin to the presence of uranium and thorium isotope impurities, and their decay products, in the material. Apart from a fraction coming from spontaneous fission of ^{238}U, α-particles released by these isotopes are responsible for the creation of all the neutrons which will capture on nuclei to produce gamma rays. The (α,nγ) and (α,pγ) reactions are also due to these α-particles. The production of gamma rays could therefore be increased by loading a wall-like source with additional α-emitters. Processes taking place in the wall could be faithfully reproduced by increasing the concentration of uranium and thorium in the material making up the source. It is expected that the neutrons would thereby be created with the same energy spectrum as those in the wall. Some of these neutrons could then be captured by the host material and generate the proper gamma ray spectrum.

In the wall, norite produces some 13 neutrons a year per cm^3. A simple scaling of this rate indicates that a norite calibration source of 5 liters, with one eighth of the weight being due to added uranium and thorium decay chain isotopes, would yield some 40 neutrons a second. For shotcrete, which normally produces about 3 neutrons a year per cm^3, a similar source would give a dozen neutrons a second. Such rates are somewhat low and these simple estimates represent higher limits.

In natural rock, the radioisotopes impurities are disseminated in the material and are in intimate contact with the host elements. This makes the α-captures possible. Indeed, α-particles lose their energy very rapidly through scattering, and for neutrons or direct gamma rays to be produced, light nuclear targets must be in close proximity, within a few tens of microns, of the α-emitters. For a uranium-thorium loaded source, added isotopes will need to be evenly distributed in the material. This can be done fairly easily for shotcrete. Concretes are made by mixing cement with water, alone or in combination with sand, stone or similar materials. Cement is a very fine powder. At the mixing stage, isotopes can be combined with the cement and water. The resulting paste will harden into a shotcrete with uranium and thorium impurities buried in it, in direct contact with the material.

In the case of a norite source, this intimate contact is much more difficult to ensure. The rock needs to be finely pulverized into a powder to which uranium and thorium can be added. The resulting radioactive dust could then be placed in a calibration source. However, security issues would arise at this point. If such a source was to break open, the result would be catastrophic as this very volatile, highly radioactive, powder would immediately dispersed. If this was to happen inside the detector, or even on the detector deck, the consequences could be terrible. This worry does not occur for the shotcrete source which would have cured into a solid block. By encapsulating the radioactive norite dust inside a polymer potting, a much safer, solid, block could be obtained. The inconvenience of this technique is that this encapsulation could reduce the direct contact between isotopes and rock sought for in the first place. Furthermore, it is expected that this polymer would absorb neutrons which would otherwise have been captured in the rock to produce the desired gamma ray signal. Finally, by adding such a potting compound reduces, probably by a factor of 25 to 40 %, the effective volume of rock in the calibration source. Another way of encapsulating the norite powder would be to make norite "sinter blocks" by compressing and heating up the dust in a special press. This technique as well as those presented before are complicated by the fact that large amounts of open radioactive sources are to be handled.

The main advantage of using such a source would be that, by starting gamma ray production from the creation of α-particles, it would be possible to generate direct α-induced gamma rays. However, in order to get these gamma rays with the same energy distribution as those in the cavity wall, the very same set of α-particles which are created in this wall have to be produced in the source as well. This means that the calibration source would need to contain all the uranium and thorium decay-chain elements in secular equilibrium. Uranium and thorium ore would contain all the α-generating isotopes of the decay chain in the right equilibrium proportion. However, this kind of material can be difficult to obtain, making the manufacture of the sources more complicated. Because α-induced gamma rays only constitute a second order contribution to the overall spectrum leaving the wall, the idea of properly reproducing direct gamma rays could be dropped and uranium and thorium oxides, more readily available but not in secular equilibrium with their daughter products, could be used in making these sources.

4.1.4 Neutron Source Option

This fact that only a few of the gamma rays making up the spectrum are expected to come from direct α-captures leads to the idea that the gamma ray rate in a calibration source could be increased by simply generating neutrons in the material. Compact neutron sources based on the use of radioactive material can be produced. Used in medical, industrial and basic research fields, these have been the subject of development research and some models are available from manufacturers.

The only radioactive decay process by which neutrons are directly produced is the spontaneous fissioning of heavy nuclei. The ^{252}Cf isotope is by far the most common material used to produces such neutron sources. With an impressive yield of 2.3×10^{12} neutrons per second per gram, little of this element would be needed to increase a calibration source rate. Like in the case of ^{238}U presented in chapter 2, the energy spectrum shape is well represented by a Maxwellian distribution (equation 2.6). With a "temperature" τ measured to be 1.42 MeV, this spectrum peaks around 3 MeV. The effective half-life of ^{252}Cf is 2.65 years: long enough to cover the expected usage life time of a wall calibration source.

In addition to not producing direct α-capture gamma rays, such a neutron source exhibits one major problem in that it produces gamma radiations of its own which will significantly distort the final gamma ray spectrum. On average, each fission yields 10.3 such photons with a total energy of 8.2 MeV. The energy distribution peaks below 1 MeV and monotonically exponentially decreases. Measurements have shown that gamma rays with more than 4 MeV of energy are created in more than 10% of the decays [66]. This rate is unacceptably large and this particular option had to be abandoned.

Another way by which compact sources are making neutron is by the (α,n) process. Within the overall dimension of a few centimeters, sources of that type can produce, depending on the target and the α-source used, on the order of 10^6 neutrons per second. Beryllium is the most common target used. Stable alloys of the form MBe_{13}, where M represents an actinide element (^{239}Pu, ^{210}Po, ^{241}Am or ^{242}Cm to name the most common ones used), can be made. However, here again, such a source is ineluctably accompanied by the frequent generation of gamma rays. By choosing the right actinide, direct decay gamma rays can be avoided, but some will still be produced by beryllium. In some cases, upon

α-collision, the resulting daughter nucleus will be left in an excited state from which it will decay to the ground state by emitting a 4.43 MeV gamma ray. For typical α-Be sources, this yield is in the range between 0.5 and 0.75 gamma rays per neutron [67].

In the place of beryllium, alternate targets are sometime used in making compact neutron sources. However, most of these other elements will too, some fraction of the time, generate gamma rays following α-capture. The only way to avoid these gamma rays from being produced would be to ensure that the nucleus resulting from the collision be produced directly in its ground state. This could be done by producing neutrons from lower energy α-particles. Unfortunately, less energetic α-particles also have a much lower probability of undergoing (α,n) reactions before being stopped. The use of light elements with negative Q-value as targets could also reduce the chances of producing excited nuclei as most of the energy of incoming α-particles would be used to compensate for the mass-energy difference in creating the new element. This technique would similarly reduce the production rate of neutrons as many α-particles that would otherwise have produced a neutrons would now lack energy to do so. With a Q-value of -2.79 MeV, lithium could be used to make such a source. Though rarely used, lithium has on occasion been employed in the design of neutron sources. Figure 4.1 shows the energy levels to which the lithium nucleus can be brought upon α-capture [68]. It shows that, in order to produce a neutron, an α-particle needs an energy of at leased 4.38 MeV. The daughter nucleus produced by the capture is ^{10}B. The first and only excited state it can be placed into is 0.717 MeV above the ground state. This bound state is populated in a resonance. An α-particle with 5.51 MeV or more of energy will most likely produce such an excited boron nucleus. However, with 0.717 MeV of energy, the resultant gamma ray would be very weak. Such a low energy gamma ray will likely be attenuated before leaving the source. Furthermore, a single of these gamma ray will, by Compton scattering in the light water, trigger fewer than ten of the SNO PMTs. This is below the threshold set for the detector. The worry that two or more of these gamma rays could be coincident does not arise as the time resolution of SNO is excellent (for two

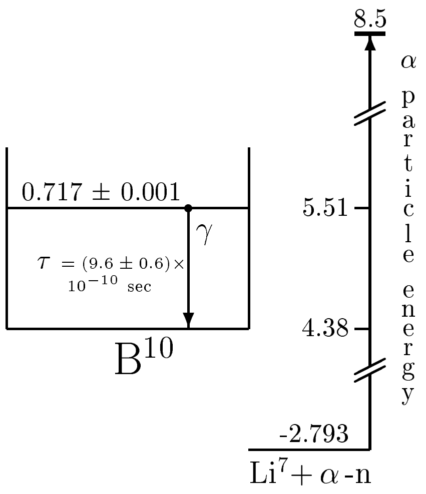

Figure 4.1: Energy levels and required α-particle energy for (Li^7 + α) reaction. Energies are in MeV. Li^7 has a Q-value of -2.793 MeV.

successive events to be registered by the detector as coming from a single event these would have to be less than 400 nanoseconds apart). Also, this "background" should not affect significantly the location at which the gamma ray events of interest would reconstruct.

When an α-particle captures on lithium, because of its high threshold of 4.38 MeV, little energy is available to the exiting neutron. While a beryllium-based source will produce neutrons with energies of up to 11 MeV, a lithium target struck by a typical actinide decay α-particle (of 5 to 6 MeV) will never produce neutrons of more than 2 MeV. The majority of the neutrons generated by a lithium-actinide source will in fact have less than 1 MeV. As virtually all neutron captures occur at thermal energies, the actual spectrum with which neutrons are created in the wall calibration source do not have to be equivalent to that of neutrons in the wall. As a matter of fact, producing lower energy neutrons is advantageous. Such neutrons will reach thermal energies and capture much sooner than they would have had they been more energetic. This means that neutrons will generally capture "closer" to the calibration source and as a result more of these captures will actually occur within the source. For this reason, such a lithium based neutron source gets more thermal neutron captures in norite or shotcrete than an equivalent uranium-thorium source. This is further heightened by the fact that, in a uranium-thorium source, neutrons are produced uniformly within the volume. While neutrons in the compact lithium-actinide source design are created in the core of the calibration device, a homogeneous distribution of uranium and thorium will generate neutrons significantly closer to the water, making their escape from the source much more likely.

The use of a compact neutron source at the heart of a wall calibration device filled with norite or shotcrete would prove to be much safer than the radioactive concrete or potted norite dust of the loaded uranium-thorium source. Neutron sources are typically encapsulated in a double-walled stainless steel housing. Also, in this case, norite would not have to be ground to powder; a block would simply have to be cut to fit inside the main container, with a proper void to place the neutron source in. This would make the manufacturing of the calibration source much easier.

Even though lithium-based sources are not as active as other similar neutron sources, a yield of 1,000 neutrons per second, more than sufficient for the wall calibration device, could easily be obtained. This option would therefore seem to offer many advantages over the loaded uranium-thorium alternative. This source will only reproduce gamma rays from the cavity wall coming from neutron captures. None of the direct α-induced gamma rays will be generated by the calibration source. This should be acceptable given that, as described in previous chapters, this channel is only a secondary one which could be ignored.

A more problematic issue could be that of neutrons capturing on the actinide making up the neutron source. These elements generally have high thermal capture cross-sections. For typical applications, this is generally not a problem since these neutron sources are used to produce fast neutrons which will then be utilized some distance away from the active core where they were produced. Also, in many neutron experiments and applications, low gamma ray pollution is not a criterion. Making a wall calibration source for SNO is another matter. By embedding the source in a device surrounded by a neutron reflector and moderator, namely water, thermal neutrons are bound to get captured in the active region of the neutron source. The preferred actinide selected at the moment to make such a lithium-based source is ^{244}Cm (with a half-life of 17.6 years). It produces 5.81 MeV α-particles with a 77% branch and 5.76 MeV α-particles with a 23 % branch. This is a typical α-emitters used in making such (α,n) sources. With a thermal capture cross-section on the order of 15 barns [69], which although high is less than most other actinide α-emitters (^{238}Pu often used in making compact neutron sources has a $\sigma_a \simeq 1000$ barns); many neutrons could be radiatively captured by this curium. The question to be asked is whether high energy gamma rays will be produced as a result of these captures. Literature does not provide any information on this matter. Some actinides, like ^{238}Pu and ^{243}Am, are known to liberate multi-MeV gamma rays upon neutron capture while others, as ^{241}Am or ^{238}U, are relatively quiet [70]. However, even if the thermal captures on ^{244}Cm were to produce very high-energy gamma rays, because a total of only about 1 milligram of curium is expected to be used in making the neutron source, this should not substantially distort the calibration source overall gamma ray spectrum. Monte Carlo tests will be presented latter that support this claim. But this problem of thermal neutrons getting captured in an actinide isotope will very likely play a major role in the case of a loaded uranium-thorium design. Indeed, a least a kilogram of heavy isotopes is to be used in making such a source. This extra material will most likely capture a fraction of the neutrons and generate spurious gamma rays.

This last point, as well as others made before indicates that the neutron source option appears much more promising than the loaded uranium-thorium alternative and was therefore investigated further.

4.2 Monte Carlo Study of Source

As presented in chapter 3, because of the complex nature of neutron transport and interactions, the investigation of gamma rays from neutron captures in the wall relied on the use of Monte Carlo simulations. This powerful tool can again be used in understanding how a wall calibration source will behave *in situ*. Indeed, as in the study of the cavity wall radiation, getting a clear picture of the gamma ray spectrum to be produced in such a source requires an understanding of where neutrons capture. Such an analysis was performed using the SNOMAN Monte Carlo code. This section presents the Monte Carlo analysis of this design and the results obtained from such an analysis.

4.2.1 Source Geometry

The geometry of a wall calibration source based on a lithium-actinide neutron emitter is somewhat complex as it is constituted of a number of different regions. The dimensions and shapes of these elements are to be optimized. For example, the calibration source should be made as big as possible so that it can contain the largest possible volume of rock or concrete and thereby insure that a large fraction of the neutrons produced will get radiatively captured in this material (as opposed to being simply captured by the surrounding water). The dimensions of the source are dictated by the interlock box in which it must be placed, along with the manipulator carriage, before being lowered inside the detector. The largest acceptable source would be a cylinder, 2 foot long and 4 inches in diameter.

For cleanliness reasons, only a few materials can be allowed to come into contact with the water of the detector. The outer canister making the source will have to be made of one of these materials. Because the substances placed inside the source would immediately contaminate the water if it was to be put in contact with it, to the extend that the SNO experiment could possibly have to be abandoned, it is paramount that the outer volume be as strong as possible to prevent it from breaking. The only acceptable material for the canister is stainless steel. This can prove problematic as this medium will certainly capture some of the neutrons created in the source and generate high-energy gamma rays which will distort the overall spectrum produced by the source. To minimize this effect, the wall thickness of the stainless steel canister will be made as thin as possible. The thinest, adequate, stainless steel pipes readily available from manufacturers have 2.1 mm thick walls. In order to get thinner walls, the cylinder would have to be custom made by rolling a thin steel sheet. It was estimated that the thinnest wall that could safely be made in this manner would be 0.5 mm. Such pipes could then be welded shut by 2 plates. These need to be wide enough to safely hold the weld. Furthermore, the top plate will need to be connected to a connecting shaft of some sort that will attach to the manipulator carriage, and therefore thicker. A 1/4 inch thick stainless steel plate will be used to construct the top cap while a 1/8 inch thick sheet will be used to make the bottom end cap. A number of technical limitations makes it impossible to make thinner end plates.

The design of the compact lithium-actinide neutron source has not been finalized, and its detailed dimensions have not yet been decided. However, the overall size and shape are known. Like other typical (α,n) sources, it will be made of a cylindrical stainless steel capsule, some 2 inches high and 1.5 inches in diameter, housing the active component, also in the shape of a cylinder, about 1.5 inches high and 1 inch in diameter (figure 4.2).

All this information should be conveyed to SNOMAN in order for the Monte Carlo program to simulate where neutrons will capture and how gamma rays will be released. The functionality of SNOMAN which allows the design of calibration source in the D_2O region was used in the work presented in chapter 3 when simulating the wall. It was utilized in the analysis of the wall calibration source as well. Its flexibility permits the simulation of the various components of the source described above. There is however one aspect that SNOMAN cannot account for: the active region of the neutron source. Indeed, Curium is not a medium which the program can simulate. Neutron interactions in this central region were therefore simply ignored at first by setting this volume as being filled with vacuum. Because in reality, some thermal neutrons will get captured by ^{244}Cm which has a large

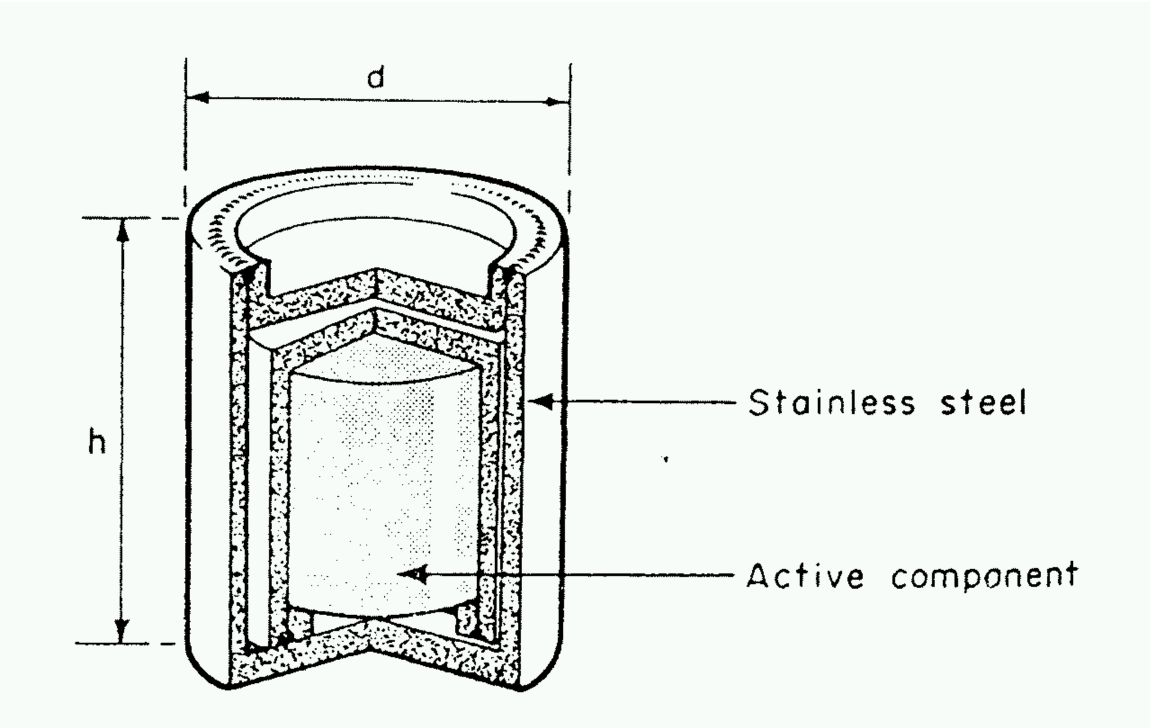

Figure 4.2: Typical capsule used for (α,n) neutron sources. The source which will be used for the present design will have approximate dimensions of d = 1.5 inches and h = 2 inches, and the stainless steel walls will be a 1/4 inch thick. (picture taken from [71]).

neutron absorption cross-section, this omission could have important repercussions on the way neutrons capture over the whole of the source. It is possible that curium would absorb neutrons which would have otherwise captured in the norite or shotcrete while leaving unaffected the capture landscape in the stainless steel walls and water regions. SNOMAN can test this hypothesis by using one of the media which are available in the code.

Curium has a thermal neutron capture cross-section of the order of 15 barns and a scattering cross-section of about 12 barns [72]. With a capture cross-section of 4.4 barns and a scattering cross-section of 17.3 barns, nickel is the closest match to curium available in SNOMAN, as far as neutron diffusion and capture properties are concern. One test will be to see if neutrons capture differently in norite or shotcrete when the medium of the neutron source active region is switched from being vacuum to being nickel.

In the Monte Carlo simulation, it is also possible to include the manipulator carriage above the calibration source. A cross-section of the final source geometry as defined within SNOMAN is shown in figure 4.3.

4.2.2 Neutron Captures and Gamma Rays from the Source

The first goal in simulating the source was to get a comprehensive understanding of where neutrons would capture when the source is surrounded by light water. This was done by placing the calibration source described above and its manipulator carriage at the center of a light water filled SNO detector. Neutrons were then isotropically generated inside the active region of the neutron source. The lithium-curium source is indeed expected to produce neutrons in a spherically symmetric manner as, despite its cylindrical shape, because of its small size, neutrons leaving the source from the sides will have passed through roughly the same amount of material as neutrons leaving from the ends and should therefore have a similar energy spectrum and relative intensity [67]. The exact neutron spectrum of the neutron source is not known at this time, but the scientists in charge of building this lithium-curium neutron source are currently working on this question and will soon get the details

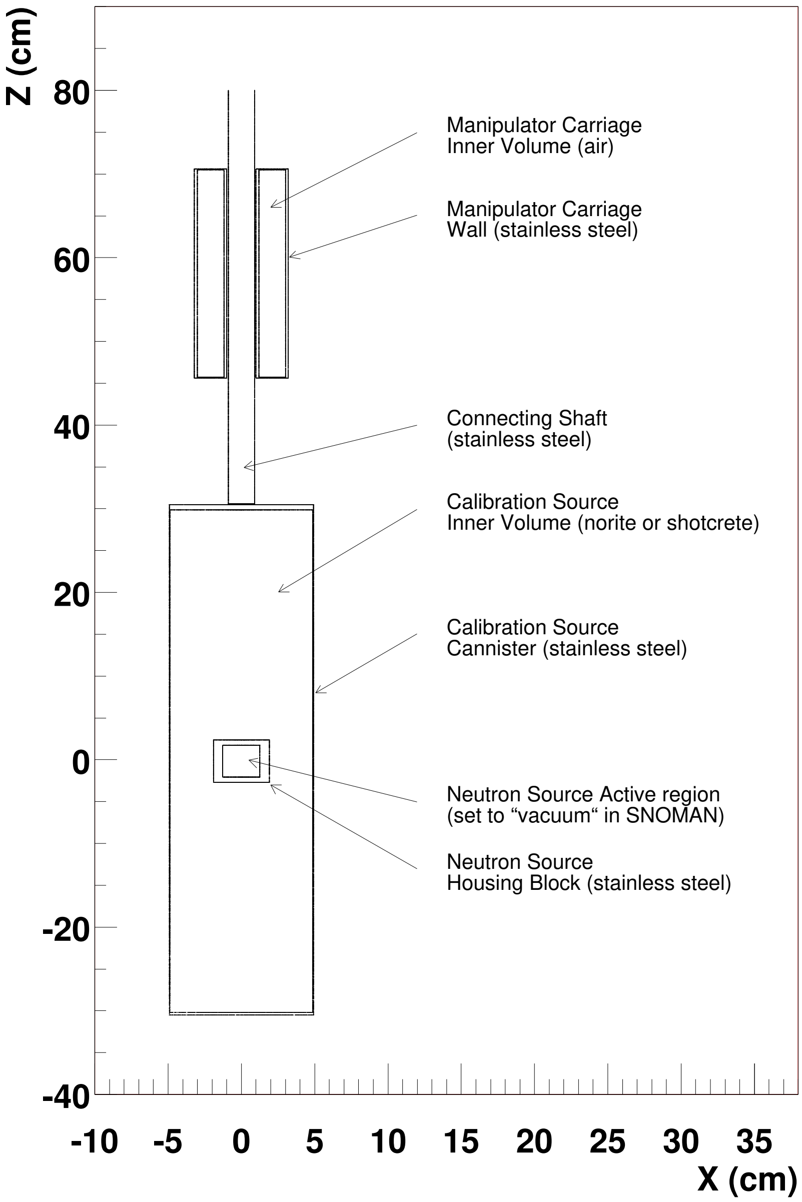

Figure 4.3: Cross-section of the wall calibration source as modeled in SNOMAN. Attached to the calibration source is a connecting shaft and the manipulator carriage. The inner volume of the manipulator carriage can be filled with lead if the source needs to be made negatively buoyant. In the case of a wall calibration source, this volume will simply be filled with air.

sorted out. However, from results obtained in the past [67] and from energy-kinematic calculations, it is understood that neutrons leaving the central region of the (α,n) source should have energies between 0 and 1 MeV. The simulation simply produced neutrons with a flat energy distribution in that 1 MeV bin.

It is foreseen that some of these neutrons will moderate within the rock and be captured. But a large number will have enough energy to get through it and enter the surrounding water. Light water will act as both a moderator and a reflector and a fraction of the neutrons will head back inside the source with thermal energies. However, in doing so, they will have to go through the stainless steel wall of the canister that contains the rock or the shotcrete, and may get captured in it. For this reason, various wall thicknesses were simulated in order to understand the importance of this effect. Sources with 0.5, 1, 2.1 and 4 mm thick walls were simulated for both norite and shotcrete calibration sources. Each SNOMAN simulation involved the generation of 100,000 neutrons, thereby assuring statistically meaningful results.

Figures 4.4 and 4.5 present the results obtained from these simulations. They show in which media neutrons were captured. As expected, an overwhelming majority of the neutrons were absorbed by the water. For those which were not, the ratios of neutrons stopped in norite or shotcrete to neutrons stopped in steel depend directly on the amount of steel present. This is shown more clearly in figures 4.6 and 4.7. Even in the case where the canister wall was made as thin as possible, about as many neutrons captured in the steel as it did in the norite or shotcrete. The details of neutrons captured in the manipulator carriage or the connecting shaft were not shown in these figures. Indeed, it was found that less than 0.01% of the neutrons would get captured in these materials.

The number of neutrons captured in the neutron source steel housing could be reduced if less of the material were used or if that source were made smaller. The simulation assumed 1/4 inch thick wall for this source. However, it is clear from these figures that the parameter that plays the greatest role is the canister wall thickness and that reducing the number of

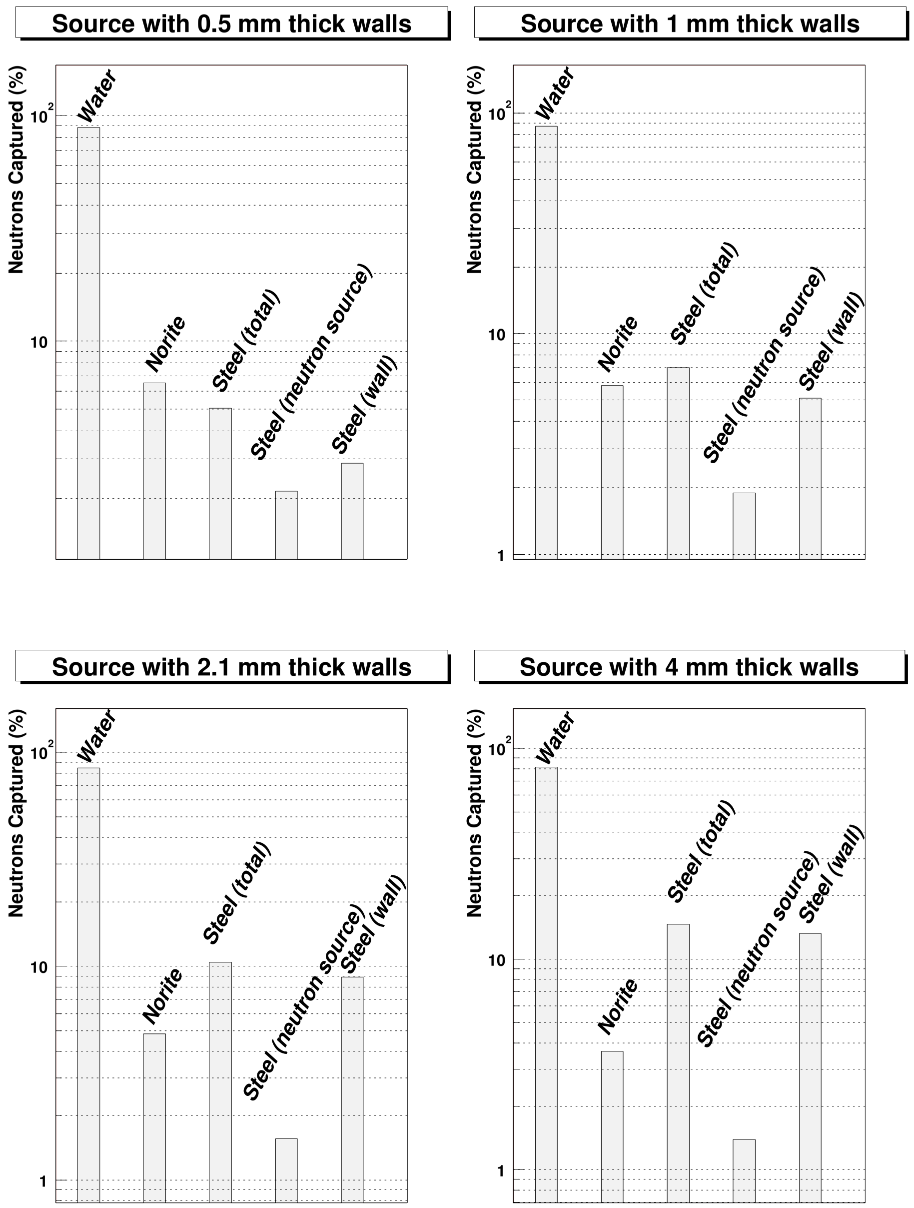

Figure 4.4: Neutron capture location in norite wall calibration source for various canister wall thicknesses.

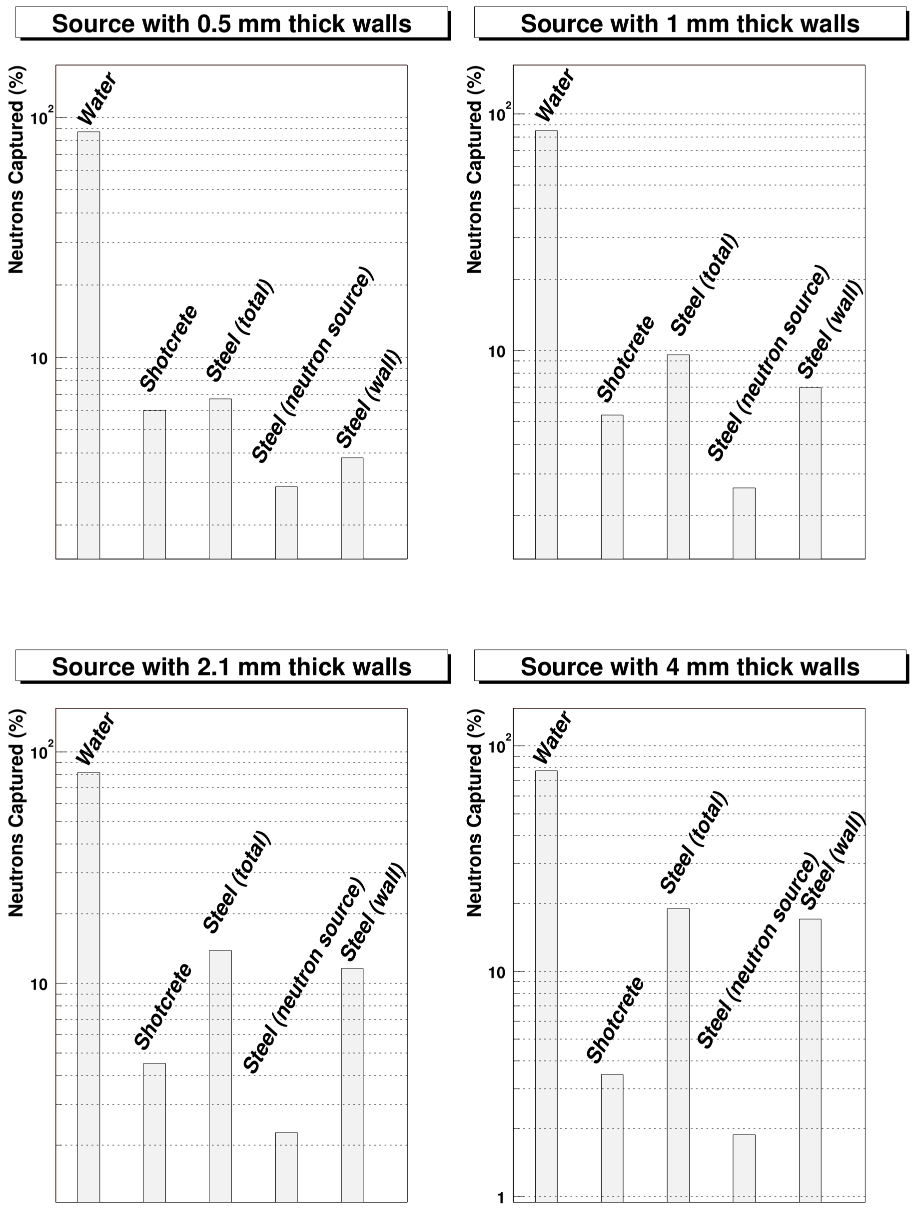

Figure 4.5: Neutron capture location in shotcrete wall calibration source for various canister wall thicknesses.

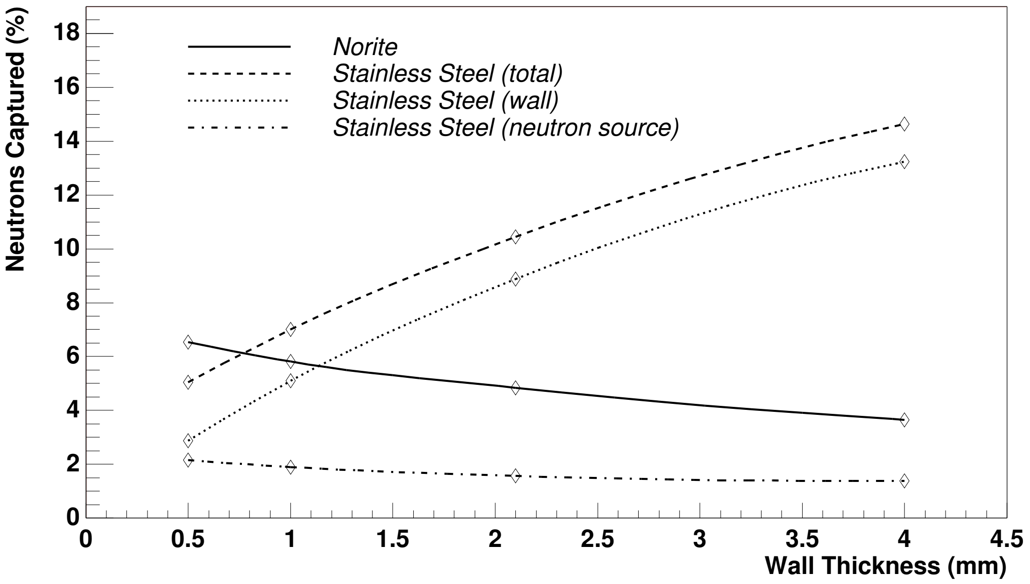

Figure 4.6: Variation in the relative neutron capture density for norite wall calibration sources of increasing wall thickness.

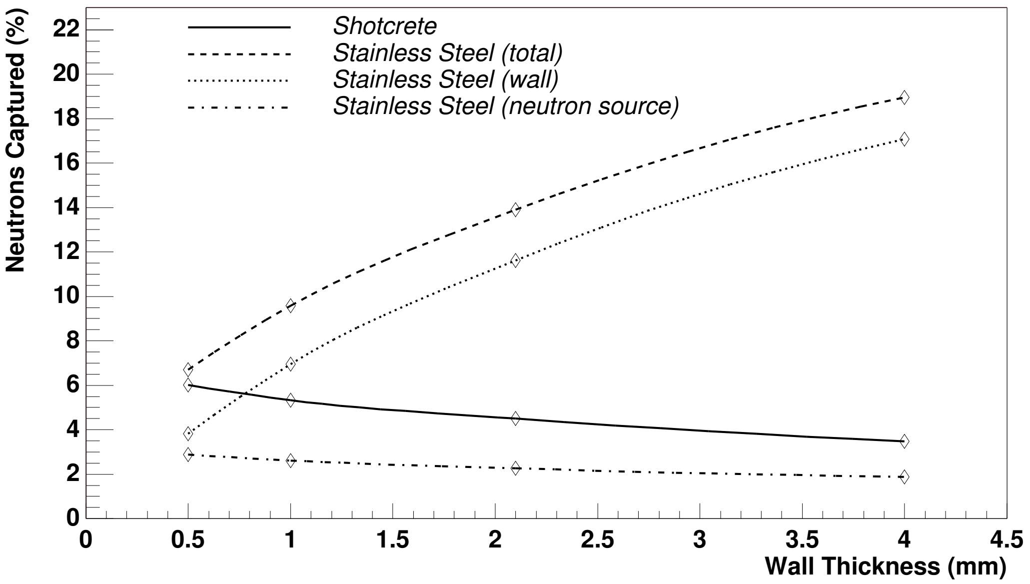

Figure 4.7: Variation in the relative neutron capture density for shotcrete wall calibration sources of increasing wall thickness.

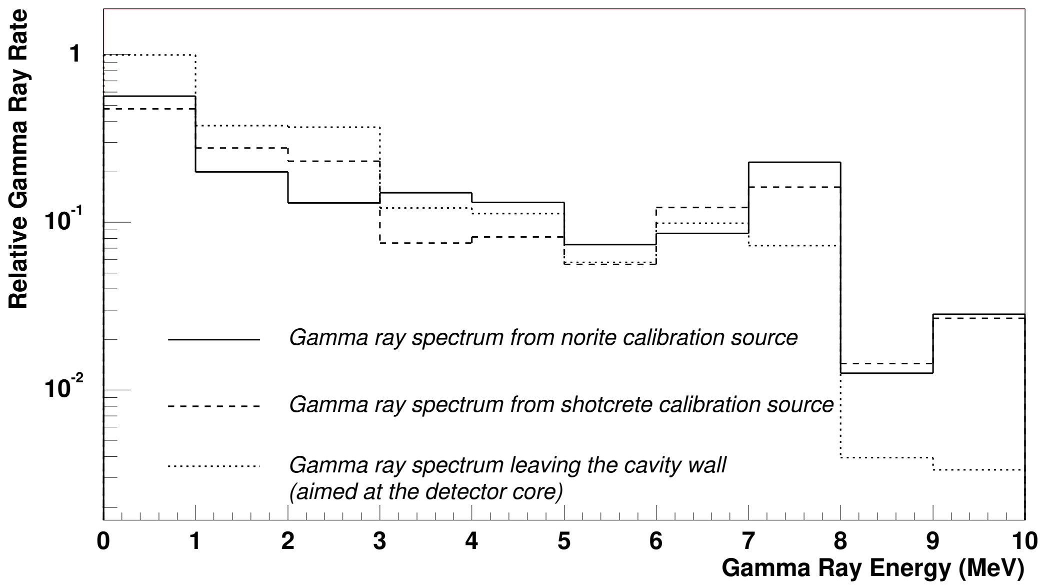

Figure 4.8: Relative gamma ray spectra leaving the wall calibration sources (0.5 mm thick canister wall design) along with gamma ray spectrum leaving the wall and directed at the heart of the SNO detector.

gamma rays of steel origin implies that the 0.5 mm thick wall design be adopted.

Buckling calculations were performed to insure that such a thin wall could withstand the water pressure imposed by an immersion in the detector. The pressure at the bottom of SNO, where it is highest, was found to be 365 kPa. It was found that this would induce a buckling force of about 22 kN in the 0.5 mm thick wall canister, but that it would take at least 75 kN force for the container to buckle in the most pessimistic scenario (where the canister is filled with vacuum).

Figure 4.8 shows what the gamma ray spectra leaving the 0.5 mm wall norite and shotcrete calibration sources are. Because the exact rate at which neutrons will be created in the neutron source is not defined yet, the numbers are only relative. Also presented in this figure is the relative gamma ray spectrum leaving the cavity wall and directed at the detector as found from the analysis of chapter 3. Apart from the distortion of the spectrum due to gamma rays having to cross the water shielding and overlooking direct α-induced

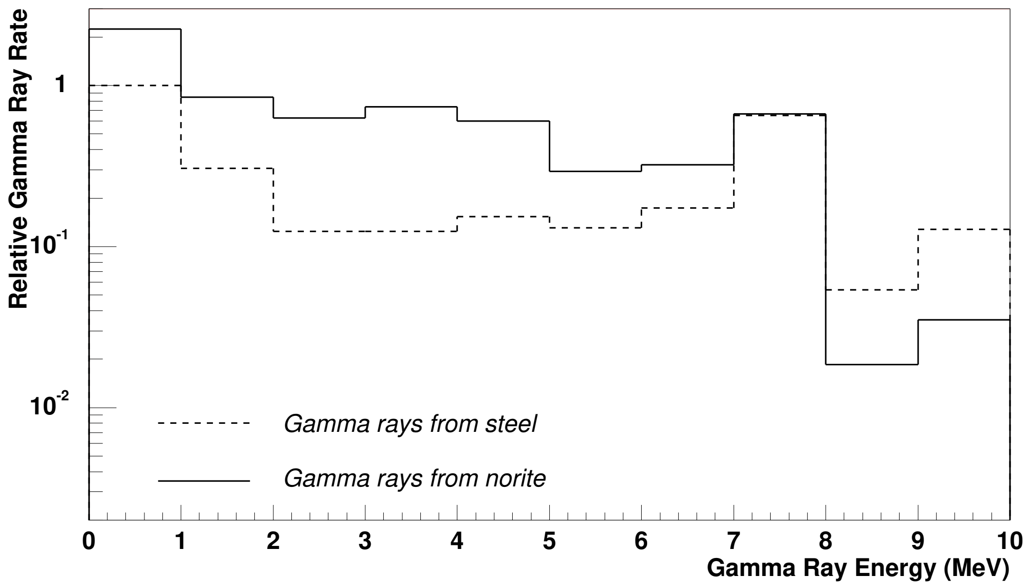

Figure 4.9: Gamma ray spectra of steel and norite origin leaving the norite wall calibration source.

gamma rays, this spectrum should be a linear combination of a norite spectrum and a shotcrete spectrum. In other words, it was hoped that, by using two calibration sources, the wall gamma ray spectrum could be reproduced. It is clear from this figure that a major deviation is present at high-energies. The calibration sources produce too many gamma rays with energies above 7 MeV. This is due to gamma rays coming from neutrons capturing in the source steel walls. This is confirmed by figures 4.9 and 4.10 which present the detailed gamma ray flux from both sources. It is seen that a large fraction of the gamma rays, especially at high-energies, are coming from the steel. This is particularly flagrant for the shotcrete source given that the low iron, chromium and manganese content of this concrete calls for very few radiative neutron captures yielding gamma rays with more than 7 MeV of energy.

This situation is unfortunate, yet nothing simple can be done to reduce the production of undesired high-energy gamma rays. As mentioned before, stainless steel is the only acceptable material for constructing the housing canister containing the highly "dirty" norite

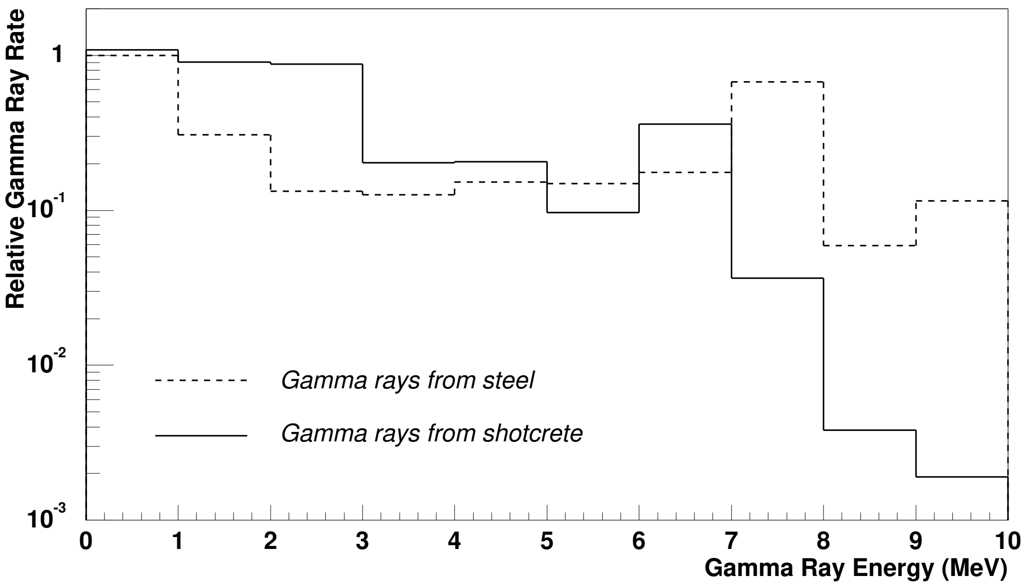

Figure 4.10: Gamma ray spectra of steel and shotcrete origin leaving the shotcrete wall calibration source.

and shotcrete blocks. The use of reflectors was also investigated. By surrounding the rock core by a layer of material that would redirect neutrons towards the norite or the shotcrete, it was thought that the number of neutrons capturing in the walls could be lowered. Typical reflectors used in nuclear reactors are beryllium, graphite and water. A 3 cm thick cover of one of these materials would typically reflect up to 80% of incoming thermal neutrons [73]. However, faster neutrons will pass through such a shield virtually unaffected. Because the central neutron source produces fast neutrons, using such a reflecting material would only make matters worse. Fast neutrons produced inside the source would traverse the rock, the reflector and the wall, be moderated in the light water, be reflected in the source with thermal energies, pass across the wall and reach the reflector again. Only this time this reflector would effectively scatter neutrons backwards away from the norite or shotcrete core, towards the steel and water.

Since gamma rays from thermal neutron capture in steel cannot be eliminated, it it important to understand it. This can be achieved by measuring the response of SNO to wall calibration sources of increasing wall thicknesses. Using two or more thicknesses of steel, and carefully comparing the results obtained and the Monte Carlo predictions, it should be possible to isolate the stainless steel component of the gamma ray spectrum. This should then make it possible to subtract off the undesired steel contribution and extract a "clean" wall background signal from the calibration source.

Also, the steel spectrum which the source creates can be used to get a handle on an other background: that of gamma rays from the PSUP. It is known that the stainless steel present in the PSUP will capture some of the neutrons produced in the PMT glasses. Though this particular background has not been studied in the present work, previous calculations indicate that this background should have the same order of magnitude as the cavity wall background. The gamma ray spectrum from this signal will be faithfully reproduced by the wall calibration source. For this reason, the wall calibration source could be effectively used as a "wall and PSUP calibration source".

As explained before, the impact of having a curium core in the calibration source can be probed using nickel as a substitute medium. This test was performed for the 0.5 mm thick wall design. By having the whole active region of the neutron source made of nickel, when in fact only about 1 milligram of curium will be present, this check took a most pessimistic approach. Some 10^5 times more thermal neutrons should be stopped by a full nickel core than by 1 milligram of curium. The results, presented in figure 4.11, show that the presence of some 20 cm^3 of a material with a high thermal neutron capture cross section does not affect very much the way in which neutrons capture in the calibration source as a whole. Only on the order of 1% of the neutrons generated were found to be captured by the nickel. Though it is not known how energetic the gamma rays produced by thermal neutron captures on ^{244}Cm, it is safe to say that the worst possible situation would be for each capture to produce 3 gamma rays with energy higher than 7 MeV (a spectrum worst than that of steel). Taking this most pessimistic estimate, and scaling the number

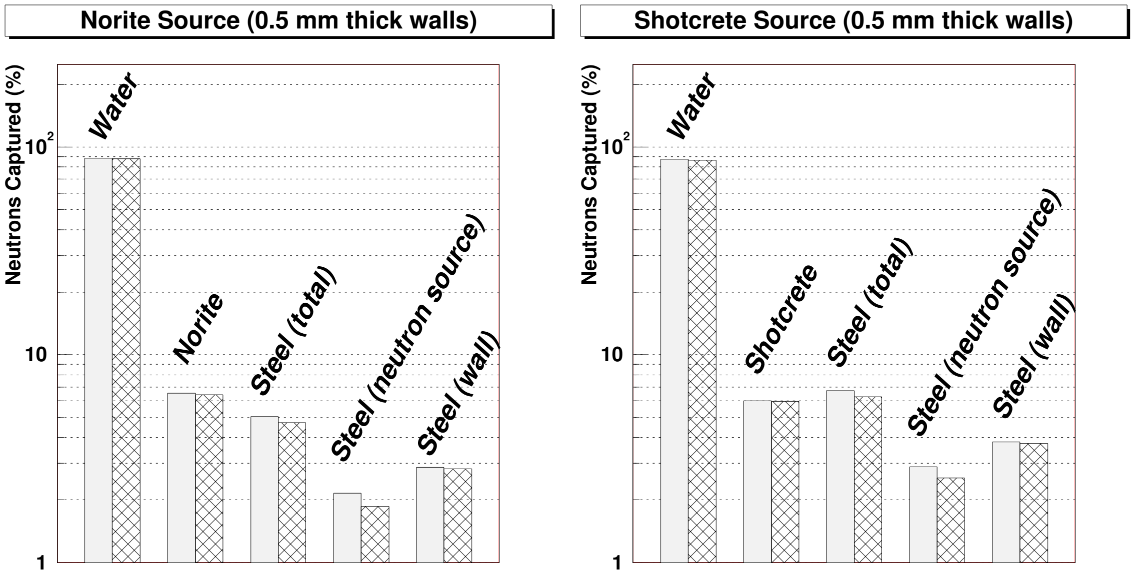

Figure 4.11: Comparison of simulations done of the wall calibration sources in the case where the effect of the active region of the neutron source was not accounted for (shaded histogram) and when its effect was approximated by loading this region with nickel (hatched area).

of captures in nickel to what it would be for 1 milligram of curium, it was found that the gamma ray flux from curium was about five orders of magnitude smaller than the overall expected flux coming out of the source. This result is a strong indication that the presence of ^{244}Cm will not affect the performance of a Cm/Li wall calibration source.

4.2.3 Response of SNO to the Wall Calibration Source

Knowing the gamma ray spectrum from the source is not sufficient to deduce from the data what the cavity wall gamma ray background is. Some of the characteristics and systematics of the SNO detector will also need to be understood. The next step in studying the Cm/Li wall calibration source design was therefore to investigate how SNO would respond to it. SNOMAN makes it possible for a generic calibration source to be designed and positioned in the light-water region of the detector. However, the range of possibilities in modeling such a device is much more limited than what was achievable for a source in the central region. Indeed, while the calibration source modeled in the D_2O region of the detector was composed of a neutron source steel housing and active region, a norite or shotcrete region as well as a stainless steel canister wall, the H_2O region replica could only be composed of two regions: the steel canister and the rock or concrete interior. Also, the manipulator carriage could not be simulated in this area of the detector. Such limitations demanded that the source be simulated differently. To account for the steel making up the neutron source, as well as some of the steel from the manipulator carriage and connecting shaft that could not be simulated, the canister walls were made thicker. The amount of steel added was chosen such that the relative number of neutrons capture in the steel and norite found for the proper source would be conserved. Also, because no active region existed as such in this alternate source, neutrons had to simply be generated along a line located where the major axis of the neutron source would have been.

By using one of six access port, a calibration source could be lowered in specific areas of the light water region of SNO. The source was simulated as though it had been lowered through the fourth calibration port, located 631 cm from the central axis of the detector. Four different vertical positions, along this 631 cm radial line, were modeled in SNOMAN for both norite and shotcrete sources. These sites are presented in figure 4.12. At Z=0 cm, the center of the source was located on the equatorial plane of the AV, 31 cm from the D_2O. With the center of the calibration source at Z=504 cm, the top of the device was at the level of the PSUP, a position passed which the source would start entering the guide tube. At that uppermost position, the center of the source was located 208 cm from the D_2O. The other two locations chosen were Z=279 cm and Z=403 cm where the center of the source were, respectively, 90 cm and 149 cm from the interior of the AV. Making such a series of measurements is the only way to get a handle on the intrinsic systematic uncertainties of SNO.

The 0.717 MeV gamma rays which a Cm/Li neutron source would produce should be of

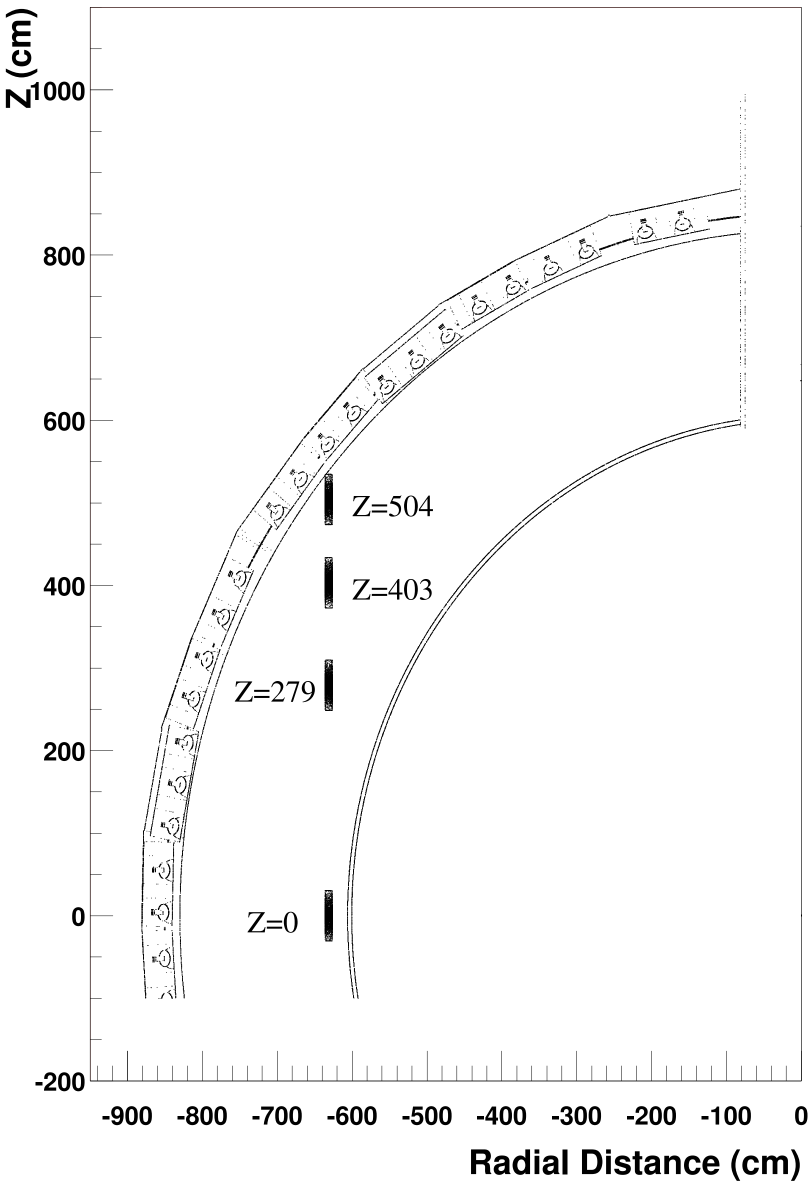

Figure 4.12: Locations at which the calibration sources were simulated in the light water region of SNO. At Z=0, the center of the calibration source is 32 cm from the D_2O. At Z=279, the center of the calibration source is 90 cm (32 cm + 59 cm) from the D_2O. At Z=403, the center of the calibration source is 149 cm (90 cm + 58 cm) from the D_2O. At Z=504, the center of the calibration source is 208 cm (149 cm + 59 cm) from the D_2O.

no concern as these would trigger fewer than ten PMTs. These were not simulated either. Also, no gamma rays from thermal neutron capture on curium were modeled.

The majority of the neutrons produced by the Cm/Li source will get captured by the light water in which the source is immersed. This will prove to be a background to the measurement. It is the hydrogen nuclei which will radiatively capture these neutrons. Each one of these captures will liberate a 2.223 MeV gamma ray which will be energetic enough to trigger a response from SNO. The bulk of the recorded events will actually come from these 2.223 MeV gamma rays. Due to their relatively low energy, this signal will only dominate the low end of the NHit spectrum measured by SNO and leave the region of interest, above 5 MeV, unaffected.

Especially in the case where the calibration source is located close to the AV, an other possible background could come from neutrons entering the D_2O region of the detector and capturing on deuterons. This would result in a 6.25 MeV gamma ray that would be mistaken for one of the high-energy gamma rays of interest from the source. It was found however, that out of 250,000 neutrons simulated in a source placed at the Z=0 cm position, none had entered the D_2O. By assuming that some 1,000 neutrons will be generated every second by the Cm/Li source, this simulation would represent about 250 seconds or running time (4 minutes and 10 seconds). As will be shown in more detail later, this short time will be sufficient to get all the information needed for this equatorial position. This says that virtually no deuteron neutron captured gamma rays should be recorded while making a wall calibration measurement.

As the source is brought closer to the PSUP, some of the neutrons produced by the calibration device should be expected to reach the steel truss making up this structure, or reach the edge of the stainless steel guide tube, and produce high-energy gamma rays characteristic of thermal capture in steel. As the version of SNOMAN used did not simulate the steel in the PSUP, this signal was not modeled. However, this background is not expected to be significant. It was found that, in light water, neutrons generally do not wander farther than 20 cm from the edge of the calibration source. This, plus the previous result that showed that less than 0.01% of the neutrons produced in the source would capture in the stainless steel manipulator carriage, suggests that this background, for particularly high vertical positions of the calibration source, could be safely ignored.

In an actual measurement, facts about the events have to come strictly from the number of PMTs hit in a certain time window, and the position of these triggered tubes. The position of an event is reconstructed using an algorithms called fitter. The standard fitter is the time fitter which calculates photon time of flight (after discarding eventual, obvious, out of time PMTs which could be due to Rayleigh scattering or, in the case of read data, to PMT noise) to find the most likely origin of the photons which caused the set of PMT trigger. The time fitter however is not perfect and will reconstruct some events which occurred outside the AV, inside, and some from inside, outside. Of these two, the first is the most likely. This is due to a characteristic of the fitter called the fitter pull. As light is delayed on its way towards a PMT, it will seem to that one PMT that the vertex from which the photon was produced is further away than it really is. However, because the light generated by events in SNO are anisotropic (most events will create Čerenkov radiations), one hemisphere will unavoidably get more photon (and therefore PMT hits) than the other. The PMTs firing in the backward region are very important in reconstructing the vertex. Because they are less numerous, delayed backward photons have a much larger effect than forward delayed ones. This translates into an overall systematic shift in the forward direction. Here gamma rays will be coming radially inward towards the AV; the reaction they will cause will be reconstructed further in, and some of these will be "pulled" inside the AV. This effect is likely to affect actual wall background events as well.

In studying the response of SNO to a wall calibration source, the quantity of interest is the NHit spectrum (which relates to the energy) of events which reconstruct inside the AV. In the present case, varying the radial cut can provide information on how the water shielding affects the propagation of gamma rays. Figures 4.13 and 4.14 show the NHit spectra measured by SNO for wall calibration sources located at the four positions described previously according to simulations. One of the curves plotted represent the NHit spectrum of all events which do reconstruct somewhere (some ill-defined PMT patterns can fail the tests imposed by the time fitter and not reconstruct at all). The second curve presented is the NHit spectrum of only these events that are inside a sphere, centered around the AV, of radius r=650 cm. For the Z=0 cm position, such a spectrum was not included as it would have inclosed the calibration source itself. The last spectrum is that of events reconstructing within the AV (radius r=600 cm). Every one of these exhibit a peak at low NHits. This is due to the 2.223 MeV gamma rays produced by neutrons capturing on hydrogen in the water. Though these obviously occur outside the AV, a fraction of these events reconstruct in the D_2O region.

As expected, by raising the source, the gamma rays have to pass through a thicker water shielding and fewer of them reach the AV and cause an event in the D_2O. From this will come the possibility of extracting what the response of SNO to the cavity wall signal will be. However, it also points at an obvious limitation. A calibration source positioned at high Z locations should be run for long times before enough interesting events are to be recorded to make a statistically sound interpretation. The results in figures 4.13 and 4.14 for Z=0 cm and Z=279 cm were obtained by simulating 250,000 neutrons, which could translate into about 4 minutes of actual run time (given a Cm/Li source producing 1,000 neutrons/second). For the higher two locations, 2,500,000 neutrons were simulated so as to get better statistics. This would correspond to a little more than 40 minutes of actual running. The spectra seem to indicate that though 5 minutes would be long enough to get all the desired information from position Z=0 cm, a few hours could be needed to get a statistically sound data set for the Z=504 cm location. But even then, these figures seem to indicate that an experimentalist would have enough time to set the calibration source into this high position, collect data, and retract the source within the allocated underground time of one shift (normally less than 8 hours).

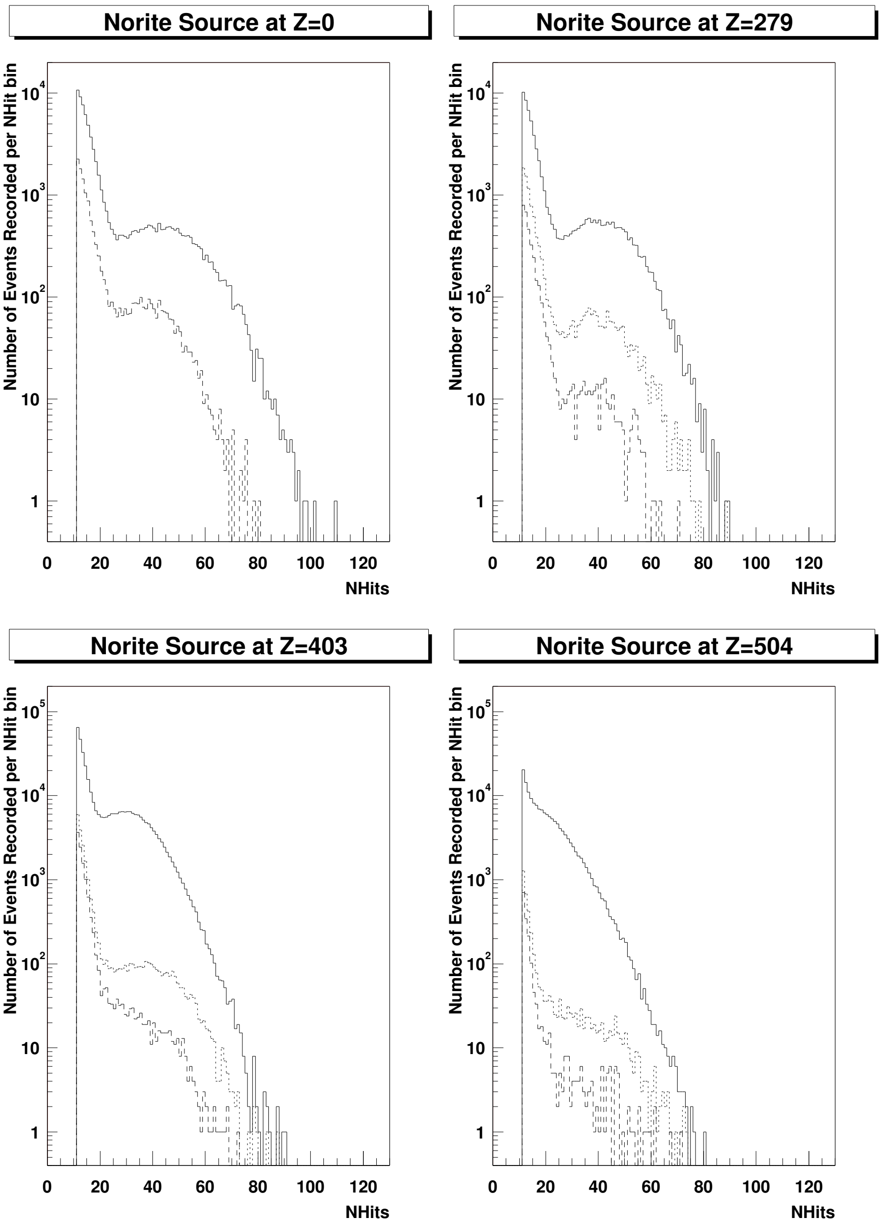

Figure 4.13: NHit spectra from norite source at various locations. For each location, three spectra are shown: the full NHit spectrum, of all the events reconstruction (solid histogram), the NHit spectrum of events reconstructing inside the r=650 cm sphere (dotted histogram), and the NHit spectrum of events reconstructing inside the AV (dashed histogram). Z=0 and Z=279 cm histograms are the result of generating 250,000 neutrons in the calibration source, while histograms for Z=403 and Z=504 cm were found when 2,500,000 neutrons were simulated.

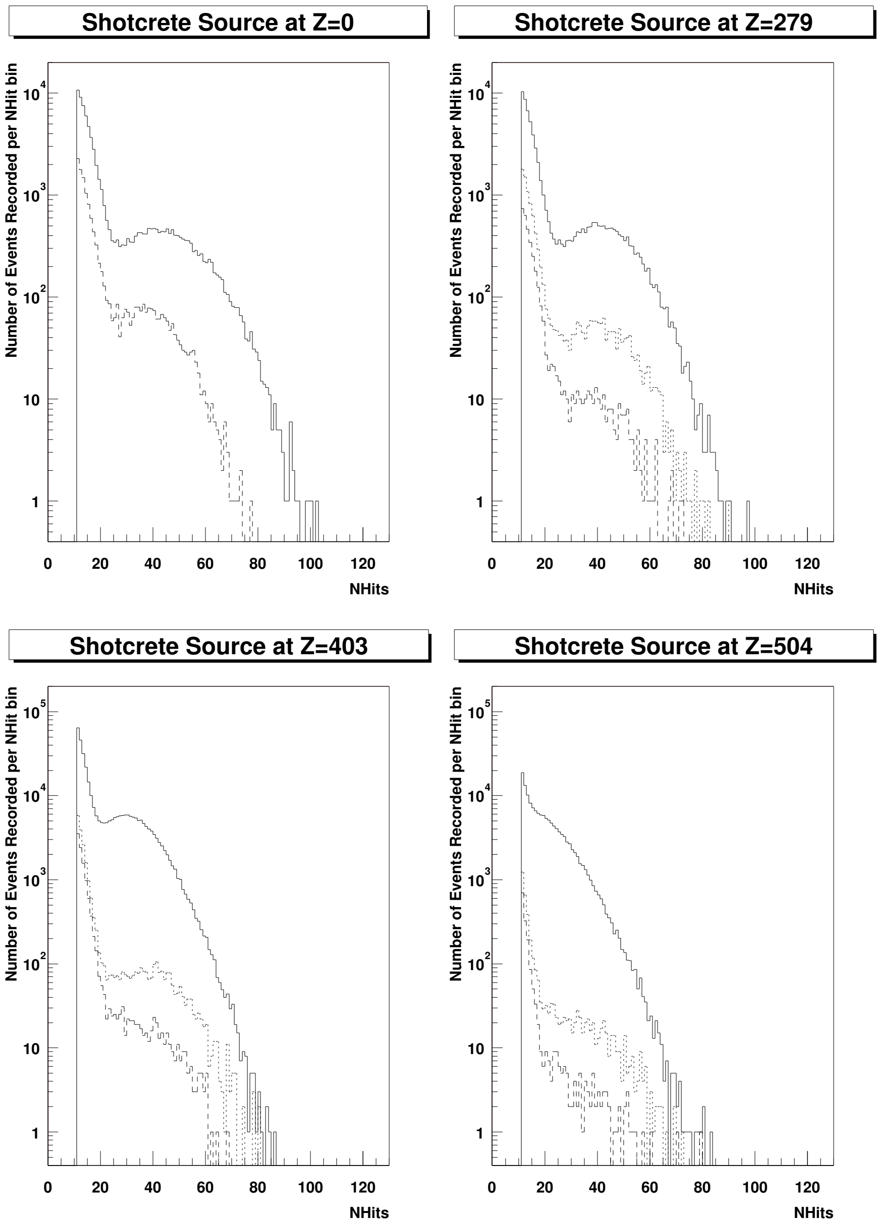

Figure 4.14: NHit spectra from shotcrete source at various locations. For each location, three spectra are shown: the full NHit spectrum, of all the events reconstruction (solid histogram), the NHit spectrum of events reconstructing inside r=650 cm sphere (dotted histogram), and the NHit spectrum of events reconstructing inside the AV (dashed histogram). Z=0 and Z=279 cm histograms are the result of generating 250,000 neutrons in the calibration source, while histograms for Z=403 and Z=504 cm were found when 2,500,000 neutrons were simulated.

The spectra presented in figure 4.13 and 4.14 exhibit other expected characteristics that should be mentioned here. As the calibration source is raised upward, the end-point of the NHit spectra are seen to come to lower and lower values. This is due to the fact that as the source is brought closer to the PSUP, a smaller number of PMTs cover an increasingly large solid angle around the source. This can be seen from looking at figure 4.12. Equipped with light concentrators, the PMTs can detect light coming with angles up to 56^o from the normal axis of the PMT [74]. This indicates that events taking place further than 705 cm from the center of the detector will not be seen by all the PMTs. This effect becomes more and more pronounced as the radial location of the event is increased. For this reason, many photons produced by source-induced interactions will end-up hitting the same PMT, thereby reducing the total number of PMTs firing for a given event. This fact, that some PMTs will record many photons, will be evident when looking at the charge deposited on the PMT anodes for each event (which is a function of the number of photons which have stuck the tube). This situation implies that for such high vertical positions, the energy scale (number of NHits per MeV) will change. This will need to be born in mind when analyzing real data. The Monte Carlo, here again will be useful in making sense of the measurements.

For the Z=504 cm position, the gamma rays produced have to cross such a thick water shield that the rate of events reconstructing inside the AV becomes very low. So low in fact that it is important to make sure that this rate will still be larger than that of neutrino interaction in the D_2O (which have now become a background of its own to this measurement). In figure 4.15, the signal from the shotcrete source located at Z=504 cm is compared to the sum of all the other signals recorded by SNO (and shown in figure 2.2). This assumes that 1,000 neutrons would be produced per second in the calibration source. One sees clearly that even for such a high vertical position, the shotcrete source signal will still be stronger than the neutrino signal in the region of interest (above 30 NHits). Results above 50 NHits exhibit irregularities which can be attributed to Monte Carlo statistical uncertainties. Though no quantitative measure of these fluctuations could be made, it is

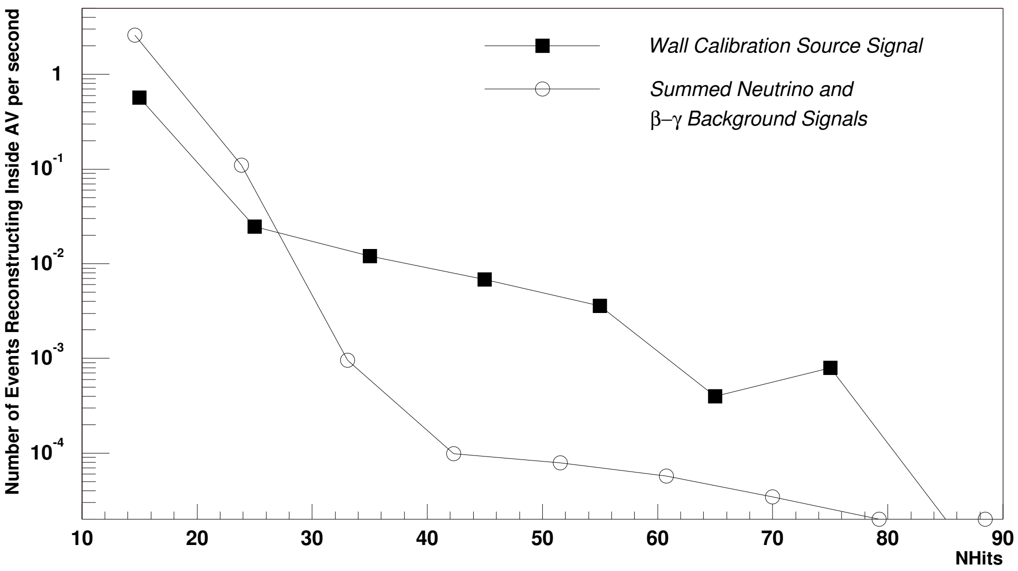

Figure 4.15: Comparison of the signals from a shotcrete source at Z=504 cm and from all other backgrounds (including neutrino events) reconstructing inside the AV. This assumes that 1,000 neutrons are produced in the calibration source per second.

believed that they will not affect the conclusion that a shotcrete wall calibration source measurement can be made and useful data could be extracted from it for any position inside the PSUP volume. A similar result is expected for the norite source.

Chapter 5

Conclusion

5.1 Summary

Gamma rays of up to 10 MeV are generated in the cavity wall of the SNO detector. A thick layer of light water surrounds the heart of the detector and serves as a shield against these energetic particles which could mimic a neutrino interaction. Some of these gamma rays however will penetrate this protective cover and interact inside the D_2O region of the detector, or close to it. Mostly because of the inability to accurately reconstruct where events take place, a number of wall gamma rays interacting in the light water will be mistaken for neutrino signals in the heavy water. In order to extract from the SNO experiment the solar neutrino rate, the spectral shape and magnitude of this high-energy background has to be thoroughly understood.

The first step toward such an understanding consisted in comprehending how gamma rays are produced in the cavity wall and calculate, from the information available about these processes, the characteristics of this flux. In the cavity wall, the majority of the gamma rays are produced following neutron captures. Neutrons find their origin in (α,n) reactions on light elements. Naturally present uranium and thorium chain isotopes are responsible for the liberation of α-particles.

Based on this fact, a Monte Carlo analysis was performed to estimate the overall gamma ray flux leaving the wall, the gamma ray rate at the AV, and the response of SNO to this background signal. The results obtained by such an analysis were found, in the region above

6 MeV (or 50 NHits), to agree relatively well, given the many assumptions and uncertainties surrounding these comparisons, with the previous calculations and measurements made. The NHit spectrum from the cavity wall background was found to have a magnitude similar to that of the internal β/γ signal, and therefore should not be a major interference to the neutrino signal SNO was built to detect. However, because the present calculations relied on various simplifications and assumptions, these results only represent first order estimates. To obtain a more precise understanding of how gamma rays from the cavity wall will be affecting the SNO detector, a concrete measurement of this elusive background needs to be made. The design of a wall calibration source that could be used to this end was investigated.

The feasibility study of a calibration source that would reproduce the gamma ray signal from the cavity wall pointed to the use of two separate devices: one filled with norite and the other made of shotcrete. In both cases, a compact neutron source would be embedded at the center of the source and produce neutrons which could then get captured on the respective materials. The preferred design for this compact source would rely on using an active component composed of an alloy made of lithium and curium. The ^{244}Cm would produce α-particles which would collide with ^{7}Li nuclei to produce neutrons with low kinetic energies (averaging around 0.5 MeV).

The rock or shotcrete block making the source would have to be encased in a stainless steel container. In order for the device to produce the largest number of cavity wall-like gamma rays, the calibration source would be made as big as it could given the size limitation imposed by the practicality of its deployment in the SNO detector. In the shape of a cylinder, the optimal device would be 2 feet long and 2 inches in radius. At the same time, the walls of the canister would need to be made as thin as possible so that a reduced number of neutrons would capture in the steel. The thinnest functional thickness that could be attained would be 0.5 mm. This design was carefully investigated. It was found that almost 90 % of the neutrons produced in such a calibration source would capture in the surrounding waters, causing the generation of 2.223 MeV gamma rays. Of those capturing inside the source, roughly 50% would capture in the norite or shotcrete while an other 50% would be captured in the stainless steel. However, tests have shown that only a negligible number of the neutrons would get captured by the curium present at the heart of the neutron source.

This calibration source would be attached, via a stainless steel connecting shaft to a manipulator carriage. This assembly could then be lowered, through a calibration guide tube, in the light water region of the SNO detector, in the volume between the PSUP and the AV. Provided with up and down motion, the device could be placed anywhere between 31 and 208 cm from the D_2O. This will make possible the investigation of the attenuation of the gamma rays in water with relation to the ability of fitters to properly reconstruct events.

Monte Carlo analysis of the response of the detector to such a calibration source indicate that even when using the thinnest, 0.5 mm, stainless steel thickness for the canister walls, a large quantity of high-energy gamma rays characteristic of thermal neutron capture on steel are still produced. This extra signal could be used to study an additional background, that of the steel in the PSUP structure enveloping the core of SNO. However, obtaining a clean wall-like signal should be possible by making a series of measurements with calibration sources of increasing canister wall thicknesses. This approach would permit the steel component of the signal to be extracted and then subtracted. With a final, clean, response of SNO to both a norite and a shotcrete source, it would be possible to deduce what the (n,γ) component of the cavity wall background is. This source will not, however, provide any information about that part of the background coming from direct α-induced gamma rays. This limitation should be inconsequential as it was found that only less than 3% of all gamma rays with more than 5 MeV created in the wall are coming from such (α,nγ) or (α,pγ) reactions. Similarly, any eventual gamma rays coming from the interaction of cosmic rays with the rock inside the cavity wall will not be considered by such a calibration source.

The duration of each calibration run needed to extract all the required information with adequate statistical accuracy will depend on the amount of water shielding present. Monte Carlo simulations indicate that equatorial positioning of the source only requires a few minutes of data taking while for positions close to the PSUP, as much as 5 or 6 hours of run time could be called for. In all cases however, it will be possible to prepare the source, deploy it, make the measurement, and retract it, within the underground time usually allocated to scientist.

5.2 Future Plans

The results presented in this thesis indicates that a wall calibration source based on the use of a compact neutron source could be used to extract the response of SNO to the cavity wall background. A set of guide lines concerning how to make the canister and which neutron source would be acceptable came out of this analysis. The next logical step would now be one of manufacturing these various components.

The Cm/Li compact neutron source described in chapter 4 needs to be constructed. This custom source is currently being developed and made by a group of SNO scientists from the Los-Alamos National Laboratory in the United States. Once it is built, a series of measurements could be done to assess its exact neutron production rate and determine the strength of the eventual gamma ray production background it produces.

While this is done, work should be done on assembling the canister that will hold the core of the calibration device. A detailed drawing of this piece of equipment is given in figure 5.1. The thin walled cylinder will be made by rolling a stainless steel sheet. A 1/8 inch steel plate will be welded to the end of this pipe. The top cap, made of a 1/4 inch plate fused to a connecting shaft will only be welded to the cylinder after the neutron source and the norite or shotcrete interior will have been placed in it. In welding the container shut, heat will be generated that could cause a pressure build-up in the source. To avoid such a situation, the top plate will need to be pierced with a hole for the air to get out. This opening will then have to be safely sealed off. This will be achieved by threading the hole and sealing it with a custom screw which will be spot welded to the top plate. In addition, a small O-ring will be placed in the head of the screw, pressed against the plate.

The set of required measurement calls for calibration sources with various canister wall thicknesses to be made. Instead of making a number of different sources, some special stainless steel covers can be built that could be slid on top of the existing thin walled sources. These will also need to be designed and manufactured.

Such a wall calibration source would be one of the most active source to be lowered inside of SNO. By no means should it ever be possible for it to get stuck in the detector. Given that the guide tubes could be found to have rough internal surfaces (given they were made by welding together several pipes), the point has been made that a conical hat could be placed above the manipulator carriage to facilitate the raising of the source up through these guide tubes. Similar gear, made of polypropylene, have already been made for the laserball calibration device.

Once the full norite and shotcrete calibration sources will have been assembled, before placing them inside of SNO, laboratory measurements will have to be made of their gamma ray spectrum. The information collected through these tests will make possible the fine tuning of the Monte Carlo and provide a first basis of comparison between the work presented in the present thesis and real measurements of rock and concrete gamma ray spectra.

The final analysis which will be done using the data obtained by the various wall calibration runs will rely heavily on comparisons with predictions made by SNOMAN. For this reason, in order to get a most correct basis for comparison, this program will have to be equipped with an adequate model of the cavity wall calibration source.

In the end, the response of the SNO detector to this calibration source, and through this analysis, an understanding of the cavity wall background, will be intimately correlated with the study of fitter reconstruction accuracy. Only with a complete comprehension of the systematics surrounding the use of the different fitter algorithms can a proper investigation

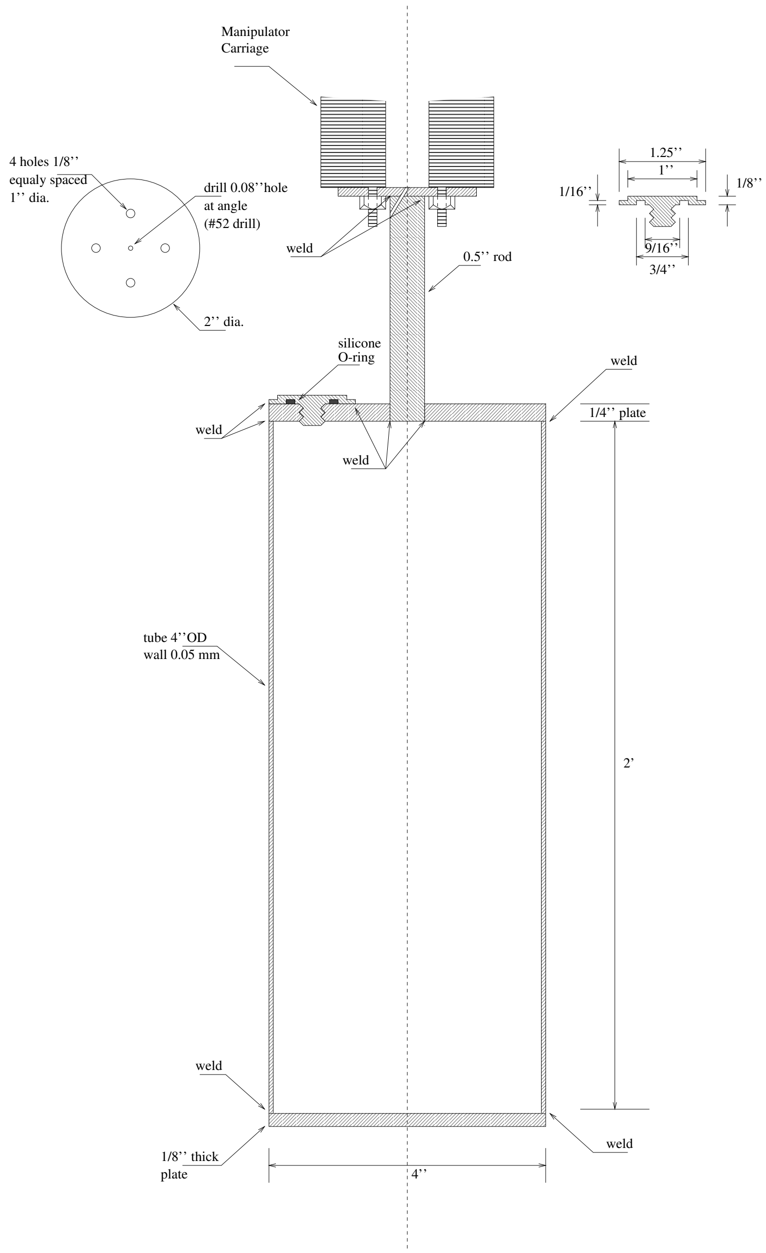

Figure 5.1: Preliminary blueprint of the final thin wall canister design (not to scale).

of the cavity wall signal be made.

References

[1] C. L. Cowan and F. Reines, Nature **178**, 446 (1956).

[2] W. Pauli, *On the earlier and more recent history of the neutrino (1957)*, edited by K. Winter, in: Neutrino physics (Cambridge University Press, 1991).

[3] D. Abbaneo *et al.*, CERN-PPE 97-154 .

[4] K. Abe *et al.*, Phys. Rev. Lett. **58**, 636 (1987).

[5] C. S. Kim and W. Marciano, Phys. Rev. D **37**, 1368 (1988).

[6] V. Castellani, S. Degl'Innocenti, W. A. Dziembowski, G. Fiorentini, and B. Ricci, Nucl. Phys. B (Proc. Suppl.) **70**, 301 (1999).

[7] J. N. Bahcall, *Neutrino Astrophysics* (Cambridge University Press, Cambridge, 1989).

[8] R. Davis, Jr., D. S. Harmer, and K. C. Hoffman, Phys. Rev. Lett. **20**, 1205 (1968).

[9] B. T. Cleveland, T. Daily, R. Davis, Jr., J. R. Distel, K. Lande, C. K. Lee, P. S. Wildenhain, and J. Ullman, Astrophys. J. **496**, 505 (1998).

[10] B. Cleveland *et al.*, Nucl. Phys. (Proc. Suppl.) **38**, 47 (1995).

[11] J. N. Bahcall, S. Basu, and M. H. Pinsonneault, Phys. Lett. B **433**, 1 (1998).

[12] J. Abdurashitov *et al.*, In edited by W. Hampel, *Proc. 4th Int. Solar Neutrino Conference.* MPIK Heidelberg (1997).

[13] T. Kirsten, Talk presented at TAUP97, (Gran Sasso).

[14] Y. Totsuka, Talk presented at 35th Int. School on Subnuclear Physics (Erice, 1997); Y. Suzuki, Talk presented at Neutrino'98.

[15] J. N. Bahcall, http://www.sns.ias.edu/˜ jnb/.

[16] L. Wolfenstein, Phys. Rev. D **17**, 2369 (1978).

[17] S. P. Mikheyev and A. Yu. Smirnov, Sov. J. Nucl. Phys. **42**, 913 (1985).

[18] C. Arpesella *et al.*, *Borexino proposal, Vols. 1 and 2* (U. of Milan, 1992).

[19] ICARUS Collaboration, *Proposal, LNGS-94/99 Vols. 1 and 2* (1994).

[20] ICARUS Collaboration, *Addentum to Proposal, LNGS-95/10* (1995).

[21] A. de Bellefon, Talk presented at TAUP97, (Gran Sasso).

[22] G. T. Ewan *et al.*, *Sudbury Neutrino Observatory Proposal*, SNO-87-12 (1987).

[23] *Scientific and Technical Description of the Mark II SNO Detector*, edited by E. W. Beier and D. Sinclair, SNO-89-15 (1989).

[24] P. Skensved and B. C. Robertson, "Summary of Backgrounds in SNO", SNO-STR-94-013 (1994).

[25] X. Chen, Ph.D. thesis, Balliol College, Oxford (1997).

[26] The SNO Water Group, *Scientific Review of SNO Water System*, edited by A. J. Noble, SNO internal report (1996).

[27] J. R. Lamarsh, *Introduction to Nuclear Engineering* (Addison-Wesley, 1983), second edition.

[28] R. D. Evans, *Atomic Nucleus* (McGraw-Hill, 1955).

[29] D. J. Littler, Proc. Phys. Soc. London A **64**, 638 (1951).

[30] D. J. Littler, Proc. Phys. Soc. London A **65**, 203 (1952).

[31] B. E. Watt, Phys. Rev. **87**, 1037 (1952).

[32] R. K. Heaton, M.Sc. thesis, Queen's University at Kingston (1988).

[33] F. W. Walker, G. J. Kirouac, and F. M. Rourke, *Chart of Nuclides* (General Electric, 1977).

[34] C. M. Lederer and V. S. Shirley, *Tables of Isotopes* (John Wiley and Sons, 1978), Seventh edition.

[35] W. N. Hess, Annals of Physics **6**, 115 (1959).

[36] A. Smith and S. Flexser, "Radioactivities of Rock Samples from the SNO Cavity Excavation", LBL/LBF 10/10/93.

[37] M. Chen, M.Sc. thesis, Laurentian University (1995).

[38] P. Jagam (private communication).

[39] A. A. Pomansky, Nucl. Instrum. Methods, Sect. B **17**, 406 (1986).

[40] R. K. Heaton, Ph.D. thesis, Queen's University at Kingston (1994).

[41] M. Omori, G. Braoudakis, and L. S. Peak, Nucl. Instrum. Methods, Sect. A **329**, 183 (1993).

[42] A. Yates, Trans. Roy. Soc. Canada **33**, 151 (1938).

[43] The LVD Collaboration, Phys. Rev. D **58**, 2005 (1998).

[44] N. Tagg (private communication).

[45] S. Hayakawa, *Cosmic Ray Physics* (John Wiley and Sons, 1969).

[46] T. J. Radcliffe, "Fast Neutron from Muon Spallation in the SNO Detector", SNO-STR-93-023 (1993).

[47] Argonne National Laboratory, *Reactor Physics Constants*, second edition (1963), ANL-5800.

[48] D. J. Hughes and J. A. Harvey, *Neutron Cross Sections*, Brookhaven National Laboratory (1955), BNL-325.

[49] J. J. Duderstadt and L. J. Hamilton, *Nuclear Reactor Analysis* (John Wiley and Sons, 1976).

[50] N. West *et al.*, *The SNOMAN User's Manual, Version 3.02* (1998).

[51] M. D. Lay, D. L. Wark, and N. West, "It's Alive — the Birth of SNOMAN", SNO-STR-91-077 (1991).

[52] "MCNP — A General Monte Carlo N-Particle Transport Code", In edited by J. F. Briesmeister, *Proc. 4th Int. Solar Neutrino Conference.* Los Alamos National Laboratory report LA-12625-M (1997).

[53] G. McGregor (private communication).

[54] E. D. Earle and P. Y. Wong, "Shielding Calculations for the SNO Detector", In *Collection of Annexes in support of the main proposal, Annex-9.* National Research Consil Canada (1987).

[55] E. T. H. Clifford, "Background from the Walls and Floor of the SNO Cavity", SNO-STR-90-008 (1990).

[56] W. F. Davidson, E. D. Earle, E. D. Hallman, H.-B. Mak, and D. Sinclair, "Background Measurements in the Creighton Mine", In *Collection of Annexes in support of the main proposal, Annex-10.* National Research Consil Canada (1987).

[57] S. Elliott (private communication).

[58] A. Rindi, F. Celani, M. Lindozzi, and S. Miozzi, Nucl. Instrum. Methods, Sect. A **272**, 871 (1988).

[59] P. Belli, R. Bernabei, S. D'Angelo, M. P. D. Pascale, L. Paoluzi, R. Santonico, N. Taborgna, N. Iucci, and G. Villoresi, Nuovo Cimento A **101 A**, 959 (1989).

[60] S. R. Hashemi-Nezhad and L. S. Peak, Nucl. Instrum. Methods, Sect. A **357**, 524 (1995).

[61] V. Chazal, B. Chambon, M. D. Jesus, D. Drain, C. Pastor, L. Vagneron, R. Brissot, J. F. Cavaignac, A. Stutz, and Y. Giraud-Heraud, Astropart. Phys. **9**, 163 (1998).

[62] P. Skensved and B. C. Robertson, "Monte Carlo Simulation for Spherical SNO Detector with and without Reflectors", SNO-STR-88-126 (1988).

[63] W. R. Nelson, H. Hirayama, and D. W. O. Rogers, "The EGS4 Code System", In *Proc. 4th Int. Solar Neutrino Conference.* Stanford Linear Accelerator Center Report SLAC-265 (Stanford Calif.) (1985).

[64] P. Skensved and B. C. Robertson, "Extraction of Data in SNO for Various MSW Scenarios", SNO-STR-91-06 (1991).

[65] M. C. P. Isaac, Y. D. Chan, M. R. Dragowsky, D. L. Hurley, K. T. Lesko, M. E. Moorhead, E. B. Norman, A. R. Smith, D. L. Cluff, E. D. Hallman, J. Heise, and P. Jagam, "Gamma-Ray Background Measurements in the SNO Laboratory", submitted to Nucl. Instrum. Methods, Sect. A (1999).

[66] A. B. Smith, P. R. Fields, and A. M. Friedman, Phys. Rev. **104**, 699 (1956).

[67] G. F. Knoll, "Radioisotope Neutron Sources", In *Neutron Sources For Basic Physics and Applicatons* volume 2. Pergamon Press (1983).

[68] F. Ajzenberg-Selove and T. Lauritsen, Nucl. Phys. **11**, 1 (1959).

[69] M. C. Thompson, M. L. Hyder, and D. J. Reuland, J. Inorg. Nucl. Chem. **33**, 1553 (1971).

[70] "Thermal Neutron Capture Gammas by Target (Online)", http://www.nndc.bnl.gov/wallet/tnc/ngtblcontentbyn.shtml.

[71] E. A. Lorch, Int. J. of Applied Radiation and Isotopes **24**, 585 (1973).

[72] "National Nuclear Data Center (Online) — NuDat Database", http://www.nndc.bnl.gov/nndc/nudat/.

[73] J. J. Duderstadt and L. J. Hamilton, *Nuclear Reactor Analysis* (John Wiley and Sons, 1976).

[74] G. Doucas, S. Gil, N. A. Jelley, L. McGarry, M. E. Moorhead, N. W. Tanner, and C. E. Waltham, Nucl. Instrum. Methods, Sect. A **370**, 579 (1996).

[75] R. K. Heaton (private communication).

[76] T. Florkowski, T. Kostaka, and M. Kotas, Nucl. Geophys. **6**, 243 (1992).

Appendix A

Elemental Composition and Detailed Neutron Yield of Various Materials

The Following tables present the elemental composition of different materials as well as their detailed calculated neutron yields from the (α,n) reactions due to uranium and thorium decay chains (figure 2.4).

Element	Content (% wt.)	Neutron yield from U chain (year^{-1} g^{-1} ppm^{-1})	Neutron yield from Th chain year^{-1} g^{-1} ppm^{-1})
Hydrogen	0.15	0.000	0.000
Carbon	0.04	0.000	0.000
Oxygen	46.00	0.114	0.042
Sodium	2.23	0.273	0.137
Magnesium	3.29	0.175	0.081
Aluminum	8.95	0.382	0.204
Silicon	26.20	0.156	0.081
Phosphorus	0.12	0.000	0.000
Sulfur	0.20	0.000	0.000
Potassium	1.15	0.000	0.000
Calcium	5.22	0.000	0.000
Titanium	0.50	0.000	0.000
Iron	6.21	0.008	0.009
Totals	100.26	1.108	0.553

Table A.1: Norite (number obtained using program ALPCHN by Heaton [75]).

Element	Content (% wt.)	Neutron yield from U chain (year^{-1} g^{-1} ppm^{-1})	Neutron yield from Th chain year^{-1} g^{-1} ppm^{-1})
Hydrogen	1.10	0.000	0.000
Oxygen	56.00	0.128	0.297
Sodium	0.10	0.011	0.035
Magnesium	0.10	0.005	0.014
Aluminum	0.46	0.018	0.060
Silicon	36.54	0.200	0.647
Sulfur	0.20	0.000	0.000
Potassium	0.10	0.000	0.000
Calcium	8.80	0.000	0.000
Totals		0.362	0.169

Table A.2: Shotcrete (number obtained using program ALPCHN by Heaton [75]).

Element	Content (% wt.)	Neutron yield from U chain (year^{-1} g^{-1} ppm^{-1})	Neutron yield from Th chain year^{-1} g^{-1} ppm^{-1})
Oxygen	47.89	0.121	0.043
Carbon	11.45	0.060	0.024
Fluorine	0.03	0.013	0.005
Sodium	0.04	0.005	0.002
Magnesium	0.78	0.044	0.019
Aluminum	0.50	0.022	0.011
Silicon	1.10	0.007	0.003
Potassium	0.21	0.000	0.000
Calcium	37.10	0.012	0.008
Manganese	0.02	0.000	0.000
Iron	0.39	0.000	0.000
Totals	99.51	0.284	0.115

Table A.3: Limestone (rock at the Gran Sasso laboratory location — Composition and neutron yields taken from [76])

Element	Content (% wt.)
Chromium	19
Manganese	1.7
Iron	68
Nickel	10.5

Table A.4: Stainless Steel

Vita

Name:	Matthieu Dayon
Place and Year of birth:	Lachine, Canada, 1975
Education:	Bachelor of Science, Honours Physics McGill University, Montreal, Quebec, 1997
Experience:	Teaching Assistant (Physics Department) Queen's University, 1997 - 1999
	Laboratory Assistant (Physics Department) McGill University, Summer 1996
	Teaching Assistant (Engineering Department) McGill University, Spring 1995
	Teaching Assistant (Engineering Department) McGill University, Winter 1995
Awards:	Queen's Graduate Award, 1997 - 1999 Reinhardt Fellowship, 1997